Distribution Agreement

In presenting this thesis or dissertation as a partial fulfillment of the requirements for an advanced degree from Emory University, I hereby grant to Emory University and its agents the non-exclusive license to archive, make accessible, and display my thesis or dissertation in whole or in part in all forms of media, now or hereafter known, including display on the world wide web. I understand that I may select some access restrictions as part of the online submission of this thesis or dissertation. I retain all ownership rights to the copyright of the thesis or dissertation. I also retain the right to use in future works (such as articles or books) all or part of this thesis or dissertation.

Signature:

March 2, 2009

Daniel A. Hillesheim

Developing Oxidation Catalysts, Understanding Mechanisms of Polyoxometalate-based Oxidations, and Systems for Color-Change Detection Technology

By

Daniel A. Hillesheim
Doctor of Philosophy
Chemistry

_____

Craig L. Hill, Ph.D.
Advisor

_____

Karl S. Hagen, Ph.D.
Committee Member

_____

Vince P Conticello, Ph.D.
Committee Member

Accepted:

_____

Lisa A. Tedesco, Ph.D.
Dean of the Graduate School

_____

Date

Developing Oxidation Catalysts, Understanding Mechanisms of Polyoxometalate-based Oxidations, and Systems for Color-Change Detection Technology

By
Daniel A. Hillesheim
Bachelor of Science, Chemistry, N.C. State University, 2003

Advisor: Craig L. Hill, Ph.D.

An abstract of a dissertation submitted to the Faculty of the Graduate School of Emory University in partial fulfillment of the requirements for the degree of Doctor of Philosophy in Chemistry.

Chemistry

2009

Abstract

Developing Oxidation Catalysts, Understanding Mechanisms of Polyoxometalate-based Oxidations, and Systems for Color-Change Detection Technology

By Daniel A. Hillesheim

Transition-metal anionic clusters are studied for green oxidation catalysis. Particular attention is paid to understanding the active catalytic species and the mechanism of the reaction. The O_2-based oxidation of propane thiol by a gelating nonporous material is presented. The catalytic conversion 2-chloroethyl ethyl sulfide to the corresponding sulfoxide is presented for $Ag_2[(CH_3C(CH_2O)_3)_2V_6O_{13}]$ and a $[Fe(H_2O)PW_{11}O_{39}]^{4-}$ based material. A series of catalytic systems were developed and explored in an attempt to determine the key intermediate in the rapid and selective catalytic aerobic oxidation of sulfides to sulfoxides by nitrogen oxides and bromide Sources of nitrogen oxides and bromide anion were critical to catalysis. The tetra-*n*-butylammonium salt of $[\gamma\text{-}SiW_{10}O_{32}(OH)_4]^{4-}$ was shown to be the precursor of an active species that catalyzes oxygen transfer from aqueous H_2O_2 to olefins. An acid dependent H_2O_2-based reaction generates the active catalyst in solution via decomposition. A catalyst assembled in situ from monomeric components (TBA_2WO_4, $HClO_4$) exhibits similar properties. The work presented herein continues the pursuit to isolate and characterize palladium and platinum-oxo units stabilized by polyoxometalate ligands. The development, characterization and optimization of a readily deployable color-change detection sensor for the chemical warfare agent mustard is also described.

Developing Oxidation Catalysts, Understanding Mechanisms of Polyoxometalate-based Oxidations, and Systems for Color-Change Detection Technology

By
Daniel A. Hillesheim
Bachelor of Science, Chemistry, N.C. State University, 2003

Advisor: Craig L. Hill, Ph.D

A dissertation submitted to the Faculty of the Graduate School of Emory University in partial fulfillment of the requirements for the degree of Doctor of Philosophy in Chemistry

Chemistry

2009

Acknowledgments

When one undertakes an endeavor as complex as obtaining a Ph.D. one travels a long road, but never alone. Sometimes we have others beside us, sometimes we have those that will guide and pave the way, and sometimes there are those that would carry and support us through the difficult patches. My road has had many wonderful people of every kind.

My family has always been there with me. My mother, Marli Hillesheim, was my first "lab director." She taught me the joys of mixing and measuring and changing substances from just food into something more. My father, Raimundo Hillesheim, was the best example of work ethic any son could ask for. My brother, Patrick Hillesheim, was my first lab partner.

The science department at Westchester Academy left an indelible mark on me. Jane Bowie and Kim Meyerhoeffer recognized something in a teenager and provided the best possible environment to foster a love of science. Without their support I would not have interned at Novartis Crop protection. That opportunity made me chemist. It was through this job that I found a career.

North Carolina Sate University, and particularly the chemistry department, was full of exactly the kinds of colleagues and instructors and chance events that are so important for any education. I am unable to list them all, but a few will always stand out. Dr. "Buzz" Hentz was the instructor of my introductory chemistry courses. Dr. Charles Boss was the department head. Both of these great men epitomized stereotypical college professors: crazy stories, bad science jokes, and an unmistakable love of science and education. I want to extend a

special thanks to Dr. Bruce Eaton who gave me the opportunity to do research in his lab.

Outside the lab and class there were many friends who made college everything it was supposed to be, but none so much as Nick Kuklinski. I have never met a kinder and more giving person.

I would not have chosen to peruse an advanced degree if not for the folks at GlaxoSmithKline: Dr. William Hoekstra, Dr. William Zuercher, and Hari Patel. They taught me by example how a collaborative research environment can be both entertaining and productive.

I will be forever grateful to all that Dr. Craig Hill has taught me during my graduate career. His tireless dedication to his students is only matched by his exuberance for the work that he does. I want to thank the rest of the members of Hill Group, both past and present. Special thanks must be given to Dr. Yurii Geletii for his mentorship. His quiet and methodical approach to research is an inspiration.

"Thus says the LORD, 'Let not a wise man boast of his wisdom, and let not the mighty man boast of his might, let not a rich man boast of his riches; but let him who boasts boast of this, that he understands and knows Me, that I am the LORD who exercises loving kindness, justice and righteousness on earth; for I delight in these things,' declares the LORD." And so I boast not in my own accomplishment but in the strength given me by the Holy Spirit.

I close as I began, by thanking family. To Heather, whose love keeps me going… and sane.

Table of Contents

List of Figures

Chapter One

Figure 7. Tri functional organic linker. (a) thionyl chloride, reflux (b) trisamine, K_2CO_3, DMA, 80 °C.

Figure 8. Oxidation of PrSH (•) to PrSSPr (•), catalyzed by **5**. Reaction conditions: 230 mM propane thiol and 250 mM decane as an internal standard in 3.00 mL of acetonitrile with **5** as the catalyst sealed in a Schlenk flask with 1 atm of O_2 at 25 °C. The substrate:catalyst mole ratio was ~35790:1. The control reaction (•), was run simultaneously under identical conditions but without any catalyst present.

Figure 9. CEES (o) oxidation to CEESO (□) by 14.8 mM TBHP in acetonitrile at room temperature. Solid lines represent oxidation in the presence of 3.3 mM $Ag_2[(CH_3C(CH_2O)_3)_2V_6O_{13}]$ (**6**). Dashed lines represent the uncatalyzed background reaction. The dash-dot lines represent the background oxidation in the presence of 6.7 mM $AgClO_4$.[139]

Figure 10. UV-Vis absorbance at 530 nm. The oxidation of CEES to CEESO by TBHP catalyzed by **6** was monitored by UV-Vis spectroscopy. Changes in the UV-Vis spectra correspond roughly to similar changes in the catalyzed reactions themselves. Reaction conditions are described in Figure 9.[139]

Figure 11. Oxidation of CEES (□) to CEESO (O) catalyzed by the nitrate (4 mM $TBANO_3$) / proton (2 mM pTsH) / $TBA_4Fe(H_2O)PW_{11}O_{39}$ (0.8 mM) system in acetonitrile (5 mL) at 25° C and 1 atm O_2. The pressure drop of a pure oxygen headspace was monitored via digital manometer and plotted as mmol/2 of O_2 (◇).[95] Determination of CEESO via GC yields systematically smaller values than

actually present at low concentrations due to peak tailing. Coincident curves indicate equation 2 is correct as written.[123]

Figure 12. Comparison of M8 and HD-sensor responses. Column two shows M8 giving a false positive response. In contrast the HD-Sensor when exposed to oil before simulant challenge still detects CEES.

Figure 13. Reflectance spectrum of HD-sensor on paper. A hand-held spectrometer is used to quantify color changes of the HD-sensor. Circled areas represent sampled area. The sensor before exposure to CEES is much more reflective.

Figure 14. Absorbance curves at increasing bromide to cupric ion ratios. 640 (red); 520 (light blue); 430 (purple); 360 (green); 270 (dark blue)

Figure 15. From left to right the ratio of Cu^{2+} to Br^- increases. The unexposed solutions are in the background while the solutions exposed to simulant CEES are in the smaller vials. The color change is maximized for the second vial from the right, in which the mol ratio of Cu^{2+} : Br^- is 1 : 2.

Chapter Two

Figure 1. Oxidation of CEES (0.5 M) to CEESO catalyzed by nitrate (8 mM $TBANO_3$) / proton (42 mM *p*-TsOH) / bromide (8 mM TBABr) systems in acetonitrile at 30 °C and 1 atm O_2. Conversion (%) is calculated from the ratio of CEES to CEESO. The reactions when the following additional components are added to the reference catalytic system above (o) are shown: (■) plus 3.6 mM $TBA_4Fe(H_2O)PW_{11}O_{39}$, (□) plus $TBA_5Fe(H_2O)SiW_{11}O_{39}$, (◇) plus $TBA_6Cu(H_2O)SiW_{11}O_{39}$, (Δ) plus $CuClO_4$, (dashed line) reference system with no bromide, no POM.

Figure 2. Oxidation of CEES to CEESO by NO_x/Br system with different initial ratios of nitrosonium to bromide. Conversion (%) is calculated from the ratio of CEES to CEESO. Red: 5.0 mM $NOPF_6$, 2.5 mM TBABr; Blue: 5.0 mM $NOPF_6$, 5.0 mM TBABr; Green: 5.0 mM $NOPF_6$, 7.5 mM TBABr; Orange: 5.0 mM $NOPF_6$, 10 mM TBABr; Black: 5.0 mM $NOPF_6$, 20 mM TBABr. Conditions: 3 mL acetonitrile, 30 °C, 1 atm O_2, 100 μL CEES (0.86 mmoles, 286 mM), 100 μL 1,3-dichlorobenzene (DCB, 0.88 mmoles, 292 mM, internal standard).

Figure 3. Effects of aging and drying on NO_x/Br system. Conversion (%) is calculated from the ratio of CEES to CEESO. (◆) Fresh 2.5 mM $NOPF_6$, 5.0 mM TBABr; (□) 2.5 mM $NOPF_6$, 5.0 mM TBABr aged in acetonitrile; (□) 2.5 mM $NOPF_6$, 5.0 mM TBABr dried then reconstituted. Conditions: 3 mL of acetonitrile, 30 °C, 1 atm O_2, 100 μL CEES (0.86 mmoles, 286 mM), 100 μL 1,3-dichlorobenzene (DCB, 0.88 mmoles, 292 mM, internal standard).

Figure 4. UV-Visible absorption spectra of various NO_x/Br systems. Blue: 0.05 mM $NOPF_6$, 0.1 mM TBABr; Red: 0.05 mM $TBANO_2$, 0.1 mM TBABr, 0.1 mM *p*-TsOH; Black: 0.05 mM $TBANO_3$, 0.1 mM TBABr, 0.1 mM *p*-TsOH, fresh; Green: 0.05 mM $TBANO_3$, 0.1 mM TBABr, 0.1 mM *p*-TsOH, aged.

Figure 5. Dependence of stoichiometric reaction rate constant on TBABr concentration. Conditions: 0.5 mM $TBANO_2$; 4 mM *p*-TsOH; 202 mM CEES; 45 °C; Argon.

Figure 6. Apparent reaction rate constants for the reaction of NO_x/Br with CEES. Conditions: 0.5 mM $TBANO_2$; 2.0 mM TBABr; 2.0 mM *p*-TsOH; 45 °C; Argon.

Figure 7. Effect of the addition of acid to $NOPF_6$ / TBABr system. Conversion (%) is calculated from the ratio of CEES to CEESO. Blue: 5.0 mM $NOPF_6$, 10 mM TBABr; Red: 5.0 mM $NOPF_6$, 10 mM TBABr, 10 mM *p*-TsOH. Conditions: 3 mL acetonitrile, room temperature, 1 atm O_2, 100μL CEES (0.86 mmoles, 286 mM), 100 μL DCB (0.88 mmoles, 292 mM).

Figure 8. Dependence of reaction rate constant k for aerobic CEES oxidation on *p*-TsOH concentration. For each mole of acid added one mole of water was also introduced since the *p*-TsOH used was the monohydrate from. Conditions: 0.5 mM $TBANO_2$; 2.0 mM TBABr; 45 °C; Argon.

Figure 9. Effects of different nitrogen oxide sources on the catalytic conversion of CEES to CEESO by the NO_x/Br system. Yellow: 2.5 mM $NOPF_6$, 5.0 mM TBABr; Blue: 2.5 mM $TBANO_2$, 5.0 mM TBABr, 5.0 mM *p*-TsOH; Red: 2.5 mM

$TBANO_3$, 5.0 mM TBABr, 5 mM *p*-TsOH aged 12 hours. Conditions: 3 mL acetonitrile, 40 °C, 1 atm O_2, 100 µL CEES (0.86 mmoles, 286 mM), 100 µL DCB (0.88 mmoles, 292 mM).

Figure 10. Effects of different transition-metal halides as sources of bromide on the catalytic conversion of CEES to CEESO by the NO_x/Br system. Conversion (%) is calculated from the ratio of CEES to CEESO. Yellow: 2.5 mM $TBANO_3$, 2.5 mM $CuBr_2$, 10 mM *p*-TsOH; Blue: 2.5mM $TBANO_3$, 2.5 mM $NiBr_2$, 5.0 mM *p*-TsOH; Red: 2.5 mM $NOPF_6$, 2.5 mM $NiBr_2$, 10 mM *p*-TsOH; Green: 2.5 mM $TBANO_2$, 2.5 mM $CuBr_2$, 10 mM *p*-TsOH; Black: 2.5 mM $TBANO_3$, 1.3 mM $TBAFeBr_4$, 10 mM *p*-TsOH. Conditions: 3 mL acetonitrile, 100 µL CEES (0.86 mmoles, 286 mM), 100 µL DCB (0.88 mmoles, 292 mM), 1 atm O_2, room temperature.

Figure 11. Effects of different transition-metal halide combinations as sources of bromide on the catalytic conversion of CEES to CEESO by the NO_x/Br system. (Red ■): 1.0 mM $Cu(NO_3)_2$, 1.0 mM $TBAFeBr_4$, 2.0 mM, *p*-TsOH; (Blue ■): 0.67 mM $Fe(NO_3)_3$, 1.0 mM $CuBr_2$, 2.0 mM *p*-TsOH; (Red □): 1.0 mM $Cu(NO_3)_2$, 1.0 mM $TBAFeBr_4$; (Blue □): 0.67 mM $Fe(NO_3)_3$, 2.0 mM $CuBr_2$; Black x: 2.0 mM $TBANO_3$, 1.0 $TBAFeBr_4$, 2.0 mM *p*-TsOH; (Black ○): 0.67 $Fe(NO_2)_3$, 4.0 mM TBABr, 2.0 mM *p*-TsOH; (Green x): 2.0 mM $TBANO_3$, 2.0 $CuBr_2$, 2.0 mM *p*-TsOH; (Green ○): 1.0 mM $Cu(NO_3)_2$, 4.0 mM TBABr, 2.0 mM *p*-TsOH. Conditions: 3 mL acetonitrile, 1 atm O_2, 40 °C, 50 µL tetrahydrothiophene (THT, 0.57 mmoles, 189 mM), 50 µL DCB (0.38 mmoles, 128 mM).

Figure 12. Proposed catalytic cycle for the conversion of sulfides to sulfoxides by N_2O_4.

Chapter Three

Figure 1. Ball and stick model of $[\gamma\text{-}SiW_{10}O_{34}]^{4-}$. Tungsten in grey, oxygen in red, silicon in purple.

Figure 2. Aqueous titration of $[\gamma\text{-}SiW_{10}O_{36}]^{8-}$. The inset curves show reversibility, while the larger curve, obtained by extended exposure to acidic conditions, does not.

Figure 3. Typical gas chromatography trace. The *cis* and *trans* isomers of limonene oxide were distinguishable for both expoxide locations. Retention times in minutes are given for the respective peaks.

Figure 4. Kinetics of cis-cyclooctene epoxidation by hydrogen peroxide catalyzed by different tungsten-containing species: (○) 1.4 mM 1; (●) 0.84 mM TBA_2WO_4 and 2.2 mM $HClO_4$. Conditions: 365 mM *cis*-cyclooctene, 135 mM H_2O_2, ca. 0.25 M H_2O, 40.5 °C, acetonitrile.

Figure 5. Effects of addition of monomeric tungstate and acid on the activity of **1**: (o) no additions; (Δ) with both 0.24 mM TBA_2WO_4 and 0.4 mM $HClO_4$; (x) with 0.4 mM $HClO_4$; (□) with 0.24 mM TBA_2WO_4 only. Conditions: 365 mM *cis*-cyclooctene, 90 mM H_2O_2, 1.2 mM **1**, ca. 0.15 M H_2O, 40.5 °C, CH_3CN.

Figure 6. FT-IR of materials recovered after *cis*-cyclooctene epoxidation. **1** (blue); **1**/TBA_2WO_4/$HClO_4$ (black).

Figure 7. Changes in UV-vis spectra of a catalytic solution under reaction conditions. Conditions: 365 mM *cis*-cyclooctene, 90 mM H_2O_2, 1.2 mM 1, ca.

0.15 M H_2O, 40.5 °C, CH_3CN, 0.1 mL solution were withdrawn and added to 3 mL CH_3CN. Reaction time: 0, 2, 3, 4 and 6 hrs.

Figure S1. TGA plot of **1**. No loosely bound water molecules were observed.

Figure S2. TGA plot of 1. No loosely bound water molecules were observed. The anomaly at ~340 °C is attributed to explosive decomposition of the peroxide.

Figure S3. Acidification of monmeric tungstate. (o) TBA_2WO_4; (□) Na_2WO_4. No reversibility of the protonation was observed upon addition of base.

Figure S4. FT-IR spectra of $K_8[\gamma\text{-}SiW_{10}O_{36}]$ (black) and **1** (red) as isolated without recrystallization.

Figure S5. FT-IR spectra of **1** as isolated without recrystalization (red), **1** after one recrystalization (yellow), and **1** after two recrystalizations (blue). The black arrows indicate areas of most significant change.

Figure S6. FT-IR spectra of **1** after two recrystalizations (blue) and **2** as isolated from the reaction vessel by precipitation (green).

Chapter Four

Figure 1. Comparison of the infrared spectra of "(guanidinium)$_8$[$SiPt_2W_{10}O_{40}$]•$2H_2O$" ({$SiPt_2W_{10}$}; red spectrum), (guanidinium)$_8$[α-$SiW_{11}O_{39}$] ({SiW_{11}}; black spectrum on left), and (guanidinium)$_4$[α-$SiW_{12}O_{40}$] ({SiW_{12}}; black spectrum on right) in the spectral range relevant to metal oxygen vibrational modes.

Figure 2. Polyhedral representation of {$O{=}PdP_2W_{18}$}. The belt tungsten atoms are shown in ball-and-stick mode to accentuate the overlap of Pd and W (~20% Pd, 80% W present, as determined by X-ray crystallography). Tungsten octahedra in grey, phosphorus tetrahedra in blue, and palladium in light blue. Bound waters omitted for clarity.

Figure 3. Polyhedral representation of {$PdPhSnP_2W_{19}$}. Some atoms in the belt are shown in ball-and-stick mode to clarify positions. Tungsten octahedra are in grey, phosphorus tetrahedral are in blue, tin is a white sphere, and palladium is an aquamarine sphere. Bound waters, including one trans to the phenyl ring on the tin, are atom omitted for clarity.

Figure 4. Polyhedral representation of {$O{=}PdPhSnP_2W_{19}$} as seen from the crystallographically imposed C_2 axis. Some atoms in the belt are shown in ball-and-stick mode to clarify positions and accentuate the Pd/W positional disorder. Tungsten octahedra are in grey, phosphorus tetrahedral are in blue, the tin is a white sphere, and the palladium is an aquamarine sphere. Bound waters including one trans to the phenyl ring on the tin are atom hidden for clarity.

List of Tables

Chapter Two

Polyoxometalates, Organic-Inorganic Hybrid Materials, and Color-Change Agents for the Oxidative Decontamination and Detection of Sulfur-Containing Chemical Warfare Agents and Other Toxic Chemicals

Published in part in:

J. Mol. Catal. A Chem. **2006**, *246*, 11-17.

J. Mol. Catal. A Chem. **2006**, *251*, 234-238.

Comptes Rendus Chimie, **2007**, *10*, 305-312.

"Catalysts for Aerobic Decontamination of Chemical Warfare Agents Under Ambient Conditions," *Symposium on Polymers and Materials for Anti-terrorism and Homeland Defense*; American Chemical Society Symposium Series 980, Chapter 12, **2007**.

With:

Hill, C. L.; Geletii, Y. V.; Okun, N. O.; Tarr, J. C.

and Anderson, T. M.; Atalla, R. H.; Botar, B.; Cao, R.; Delannoy, L.; Duncan, D. C.; Han, J. W.; Hardcastle, K.; Morokuma, K.; Musaev, D. G.; Renneke, R. F.; Reiner, R. S.; Weinstock, I. A.; Zhang, L.

Abstract

The catalytic oxidative properties of inorganic compounds and inorganic-organic hybrid materials are presented. The reactivity of a gelating nonporous material based on a tris-triol amide linker and the hexavanadate isopolyanion toward the room temperature O_2-based oxidation of propane thiol was studied in detail. In order to expand the knowledge of this class of gelating nonporous materials the synthesis of a series of hybrid inorganic-organic materials all containing similar organic linkers, 4-{2-{3,5-bis[2-(4-carboxyphenyl)-1-ethynyl]phenyl}-1-ethynyl}benzoate derivatives, with varying inorganic components based on the initial gelating nonporous material was attempted. The catalytic conversion of the mustard (HD) simulant 2-chloroethyl ethyl sulfide (CEES) to the corresponding sulfoxide is presented for two unique systems: $Ag_2[(CH_3C(CH_2O)_3)_2V_6O_{13}]$ and a $[Fe(H_2O)PW_{11}O_{39}]^{4-}$ based material. The last part of the paper details the development, characterization and optimization of a readily deployable color-change detection sensor for the chemical warfare agent mustard.

Introduction

General polyoxometalate properties

Transition metal oxygen-anion clusters (polyoxometalates or "POMs") have been explored for their diverse chemical, structural, electronic, catalytic, and magnetic properties. POMs are discrete molecules formed by the assembly of d^0 metals such as V^V, Nb^V, Ta^V, Mo^{VI}, W^{VI} and others. The individual metals are surrounded by 5 or 6 oxo anions that can be shared with neighboring MO_x units. As the number of μ-oxo linkages increases via condensation, corner, edge, and face sharing of oxo anions is possible, as per Figure 1. Collections of MO_x units eventually reach a point where coulombic repulsion truncates further aggregation. Polymer formation is prevented as metal-metal repulsion causes the M-O bond distance to shorten and become double-bond like.[1-9] The assembly of MO_x units and the composition of the POM can be controlled mainly by stoichiometry, pH, and the choice of metals. Control of the reaction conditions can lead to a wide variety of functional characteristics associated with the individual structural and compositional variations of the POMs.[7]

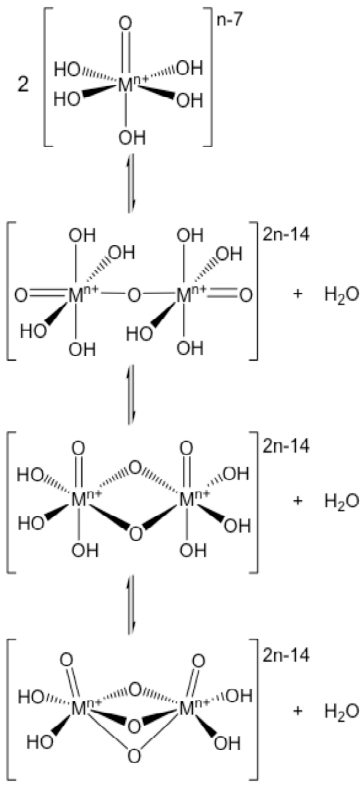

Figure 1. Condensation of MO_6 units with increasing numbers of μ-oxo linkages.[9]

POMs are oxidatively and thermally stable while being extremely modifiable. Some classes of

POMs are also hydrolytically stable in specific pH ranges.[4, 5, 10] Despite the overall negative charge of POM species, the oxidized clusters are generally electron acceptors and can exhibit a wide variety of redox reactions. Changes in a POM's oxidation state are rarely accompanied by changes in the overall structure of the cluster; yet more evidence for the overall stability of POMs.[11] Certain POM catalysts are also "dynamically stable" and can exist in equilibrium under turnover conditions. This property can be employed to produce POM structures in dynamic equilibrium that are active catalyst.[12-14] These properties have allowed POM-based catalysts to be deployed in several commercial processes involving homogeneous and heterogeneous acids under oxidative conditons.[7, 15-18]. The facile tuneablity of reactive properties combined with the oxidative stability of POMs make them ideal candidates for incorporation into functional multi-component materials.

Inorganic-organic hybrid and metal-organic framework materials

The synthesis of hybrid inorganic-organic materials has long been a goal for materials scientists. The marriage of inorganic substrates, their varied and controllable activities, with the easily tunable characteristics of organic compounds is collectively promising for creating functional materials. Herein the synthesis, characterization, and identification of the properties of two groups of inorganic-organic hybrid materials synthesized from the same inorganic subunit, $[V_6O_{19}]^{8-}$, is detailed. Both compounds utilizes a polyoxometalate-based unit, a bis(triester)hexavanadate, as the inorganic component, covalently bonded to the organic component through ester bonds.

In order to take advantage of the tunable properties of POMs it is critical to identify procedures by which these clusters can be successfully integrated into functional hybrid inorganic-organic materials. Identification of the connectivity between the POM and the organic portions of the material leads to two broad generalizations. In the first class of such materials, the POM subunits are weakly bound to the organic substrate. Electrochemical and electro-optical polymers with imbedded POMs,[19, 20] alternating layered films,[21-24] and POMs suspended in Sol-Gel matrixes[25-27] are good examples of this class of hybrid material. Materials formed of POMs covalently bonded to organic linkers form a second broad class. Class II compounds bearing V-O-C[28] linkages can be synthesized by surface modification, wherein the POM is functionalized after assembly[29] or, as in the case of the $NH_4C(CH_2O)_3V_6O_{13}$, prepared in situ.[30] Either preparation method can be used with the proper organic linkers to synthesize a variety of network polymeric inorganic-organic hybrid materials.

The minimal surface functionality of an inorganic component in a polymeric hybrid material must be two if the inorganic unit is to be incorporated as a building unit, and not just attached to a side chain of the polymer backbone. Prediction of the resultant material is dependant upon well-defined functional sites. Because of their tunable characteristics, and their relative ease of synthesis, POMs with the proper surface modifications are ideal candidates for use as secondary building units (SBUs); however certain limitations can arise. For example the Keggin[31] type POM (general formula $[XM_{12}O_{40}]^{n-}$, e.g. $[PW_{12}O_{40}]^{3-}$) can be functionalized by one of two methods: substitution of one or more d^0

metal centers with another transition metal or substitution of one of the terminal oxo groups with another ligand. d-Metal substitution of two positions often results in a mixture of inseparable isomers[32-36], and is therefore not an acceptable method for reticular synthesis.

The V_6 unit (general term for the hexavanadate group, "V_6O_{19}") is a particularly useful synthon for the rational development of functional hybrid inorganic-organic materials. The bis-capped V_6 unit is bifunctional, meaning it can be modified with organic groups in two locations, namely the three bridging oxygen atoms between the vanadium ions on the opposite faces of the complex. The degree of functionality (number of attachment points) of the organic linker determines the overall network topology of the material because the degree of functionality of the inorganic component is fixed as two for V_6. An organic compound with only one triol group of the type $RC(CH_2OH)_3$ will result in monomeric bis-capped V_6 POM compounds. Expansion of the functionality of the organic linker from 1 to 2, 3, or 4 allows for the possibility to synthesize rods, 2-D arrays, and 3-D lattices respectively (see Figure 2).

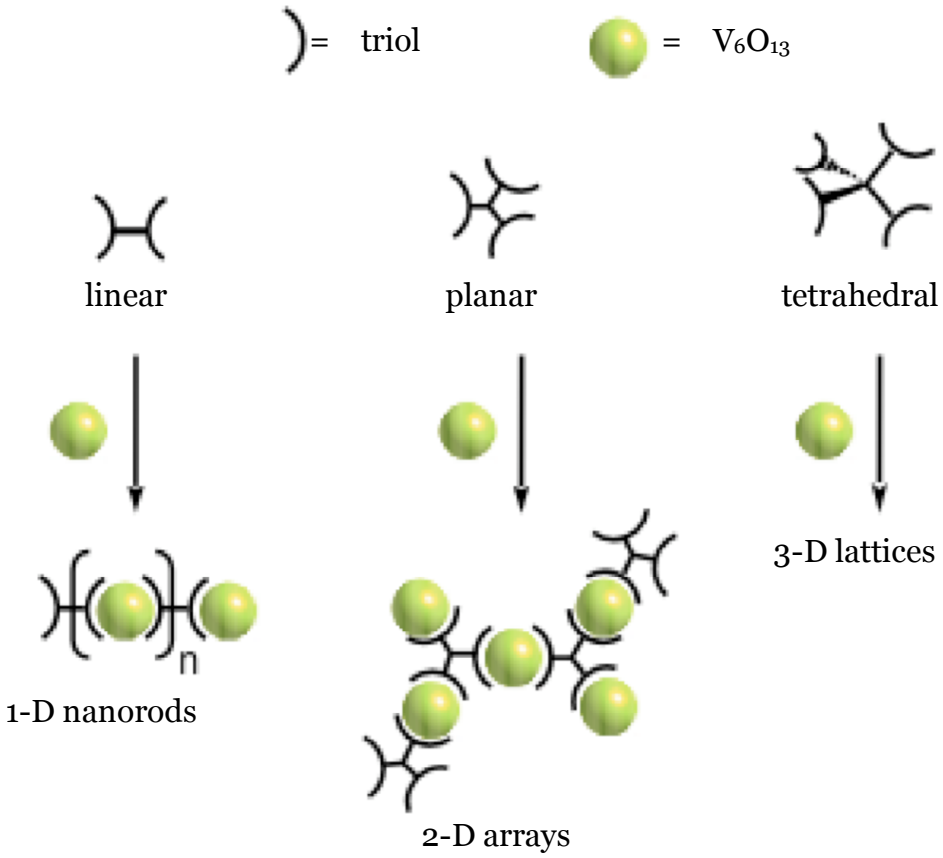

Figure 2. Increasing functionality of the organic linker leads to increasing dimensionality of the material.[9]

Directed control of the product hybrid material based on careful choice of organic and inorganic components is the basic concept of reticular synthesis. This method, applicable to organic-POM functional materials, was developed by Yaghi when referring to the design of coordination polymers.[37] The term coordination polymer refers to hybrid inorganic-organic materials wherein metal ions serve as bridges between organic linkers.[38] Often encountered linker functionalities bridging d-block transition metals are nitriles,[39-43] amines,[44-46] pyridines,[42, 47-54] and carboxylates.[55-60] A few examples of lanthanide based metal-organic frameworks also exist.[61-64]

Metal-organic framework (MOF) materials are often porous. Structurally, MOFs have been compared to zeolite materials. Figure 3 shows a typical MOF as reported by Yaghi et al.[37] Rigid linkers (organic), meet at precise angles and in well defined bonding schemes at the inorganic metal centers. Well defined and rigid secondary building units (hereafter SBUs) are critical to properly predict and control the 3-D structure of the MOF. Strong covalent metal-organic bonds ensure the stability of the system to stresses such as heat and evacuation.[29] MOFs can be classified by their increasing dimensionality. Zero dimensional materials are characterized by completely enclosed cavities. As the dimensionality increases channels, layers, and networks of intersecting channels are observed.[65]

MOFs characterized by networks of intersecting channels, a fully 3D

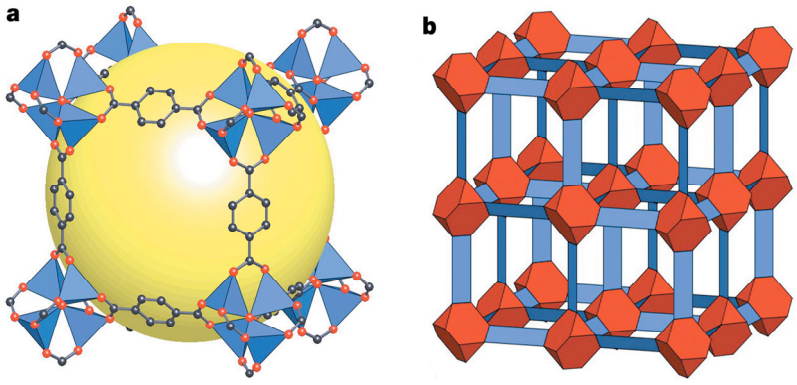

Figure 3. A typical MOF structure **a,** shown as ZnO_4 tetrahedra (blue polyhedra) joined by benzene dicarboxylate linkers (O, red and C, black) to give an extended 3D cubic framework **b**, An extended representation of the structure $(OZn_4)O_{12}$ clusters (red truncated tetrahedron) and benzene dicarboxylate (BDC) ion (blue slats).[37]

framework, are of particular interest in gas storage and catalytic applications. MOFs of the type shown in Figure 3 are capable of withstanding evacuation of the guest molecules contained in the spaces without the subsequent collapse of the structure.[37] Guest molecules can also be exchanged, such that the initial solvent molecules are replaced with the molecules of interest such as methane and hydrogen gas.[66-68] The material Zn_4O(1,4-benzenedicarboxylate) has been shown to adsorb up to 17.2 hydrogen molecules per formula unit at 78 Kelvin.[67] Many MOFs comprised mainly of Zn, Cu, Tb, Eu, La, and Ni as the metal joint and varying di, tri, and tetra carboxylates as the organic ligands, demonstrate large surface areas and structural integrity over a wide range of conditions.[63, 69-81]

A few MOFs have also been reported to show catalytic activity. The 2D MOF [Cd^{II}(4,4'-bipyridine)2)] was shown to catalyze the cyanosilylation of aldehyde[82] and the MOF reported by Han *et. al.* was shown to catalyze thiol oxidation.[64] Recently reported MOFs have been constructed of organic linkers that contain Lewis basic coordination sites within the walls of the compound. These polydentate Lewis basic sites are then filled with transition metals that often display open coordination sites. The possibility exits for accessing various catalytic functionalities by varying the coordinated metal.[65, 83, 84]

The hexavanadate unit

The particular POM explored herein to produce MOF-like inorganic-organic hybrid materials was first reported by Zubieta and coworkers; they subsequently explored a variety of synthetic methods and reported several crystal structures (Figure 4).[28, 85-91] Control of the synthetic conditions allowed for

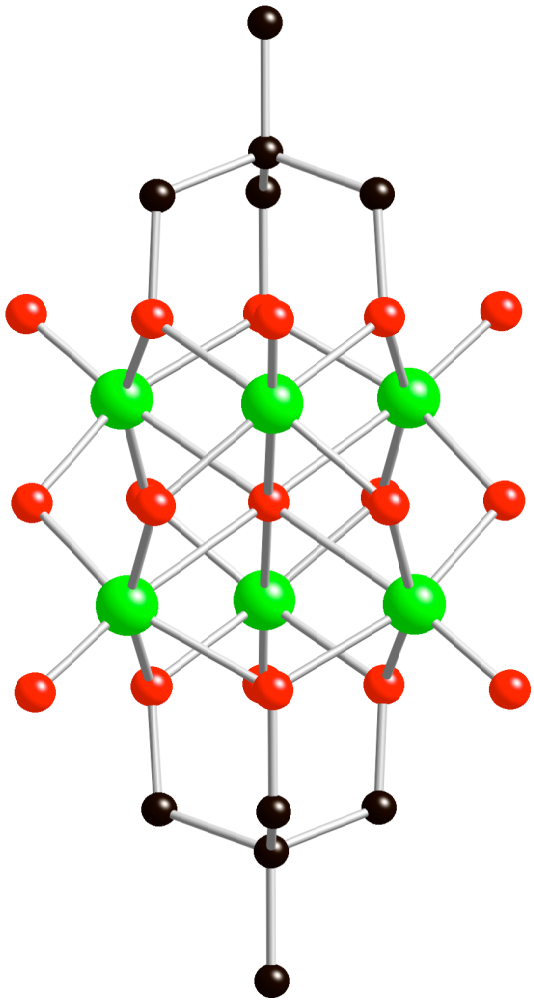

Figure 4. Ball and stick representation of the bis(triester) capped V_6O_{13} unit. Vanadium in green, oxygen in red, carbon in black, hydrogen omitted for clarity.[85]

assembly of the bis(triester)hexavanadate unit $[(RC(CH_2O)_3)_2V_6O_{13}]^{2-}$ (hereafter bis-capped V_6, R = organic ligand). The bis-capped V_6 precursor $H_3V_{10}O_{28}^{3-}$ is synthesized by acid titration of the simple metal source sodium orthovanadate.[92] Equation 1 shows the balanced reaction of organic triols that leads to the self assembly of the thermodynamically favorable and hydrolytically stable triester chelate bis-capped V_6 shown in Figure 4.[28, 29, 87, 93] Tri-esters of this type are

$$8\,[(n\text{-}C_4H_9)_4N]_3[H_3V_{10}O_{28}] + 18\,(HOCH_2)_3CR \longrightarrow 9\,[(n\text{-}C_4H_9)_4N]_2[V_6O_{13}\{(OCH_2)_3CR\}_2] + 2\,[(n\text{-}C_4H_9)_4N]_2[V_{13}O_{34}] + 39\,H_2O \quad (1)$$

notably stable to hydrolysis.[87, 93, 94]

The bis-capped V_6 POM itself has rich redox chemistry and undergoes color changes upon reduction. A series of e- transfers, along with the accompanying color change, was observed by isolation and characterization of the reduced forms. The reduced $2e^-$, $3e^-$, $4e^-$, and $6e^-$ forms have been reported and evidence shows that certain organic molecules can act as the reductant. Furthermore, vanadium containing POMs have been reported to be active oxidation catalysts. Green oxidants such as H_2O_2 and O_2 will reoxidize the V_6 POM unit to produce a catalytic cycle. Bis-capped V_6 compounds have been shown to catalyze the air-based oxidation of thiols to the corresponding disulfides at room temperature. [9, 29, 87, 93, 94]

Further attempts to identify suitable sulfoxidation catalysts led us to explore the bis(triester)hexavanadate POM Equation 1 shows the balanced reaction of organic triols that leads to the self assembly of the thermodynamically favorable and hydrolytically stable triester chelate bis-capped V_6 shown in Figure 4.[28, 29, 87, 93] We report herein that bis-capped V_6 units will also catalyze oxidations of sulfides with accompanying color change.[95]

Idealized POM catalysis

The V_6 unit presents a case study for the general method of designing and identifying POMs for oxidation catalysis. Figure 5 illustrates the general scheme. A POM in an oxidized rest state becomes reduced by a target molecule. In reduced POMs the d^1 electrons are delocalized and often produce dramatic colors

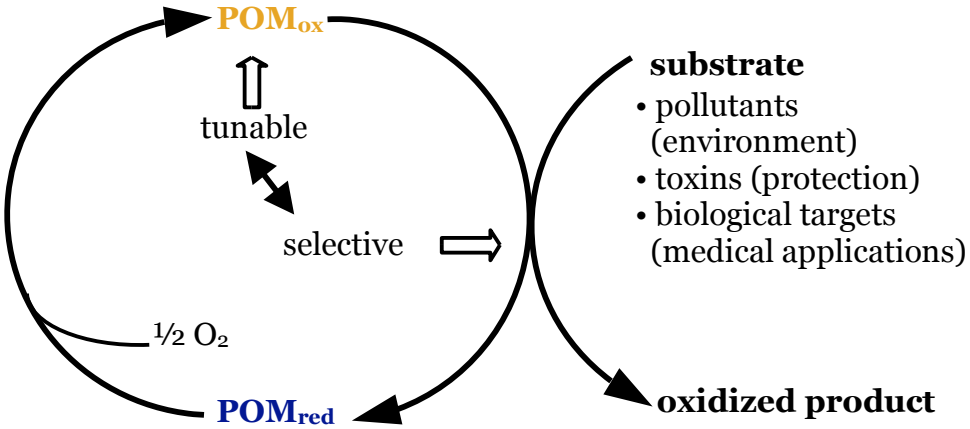

Figure 5. Idealized scheme for POM-based oxidation catalysis. Tuning the POM's redox properties to match the redox potential of the target compound is only half of the cycle; ensuring that the oxidant (ideally O_2) is able to reoxidize the catalyst is equally important.

as a result of very intense intervalence charge transfer (IVCT) transitions. This reduced POM is then reoxidized to complete the cycle.[11, 96-98] The success of this method depends on controlling the redox potential of the POM (via metal substitutions, changes charge density, varying the counterions, etc). The POM catalyst can also facilitate oxygen transfer. Instead of accepting an electron from the target the POM, the POM can bind or activate the oxidant (molecular oxygen, peroxide, etc), which then oxidizes the target.[99-103] Often it is helpful to separate the steps (POM reduction from POM reoxidation), testing order to identify stoichiometric oxidation of a target before focusing on reoxidizing the POM with an oxidant. Choosing the right target substrate to match the correct POM is also important.

Oxidation of sulfides, thiols, chemical warfare agents and odorous compounds

The selective aerobic oxidation of sulfides to sulfoxides has been of considerable interest for some time.[104-106] Chemical warfare agents, including mustard (HD, Equation 2) and VX as well as more commonly encountered toxic chemicals such as aldehydes, sulfur compounds, and nitrogen compounds are potential targets for oxidative decontamination by reaction with O_2.[107-109]. Mustard is not very reactive to oxidation (from electrophilic oxidants such as POMs), particularly when compared to other thioethers,[110] such as tetrahydrothiophene.[110-112]

Catalytic systems for O_2-based oxidations under mild conditions remain of considerable intellectual and practical interest.[15, 113-116] Those that function with air under ambient conditions are even more problematical to design and realize but have potential value not only in selective homogeneous catalytic oxidation (production of specialty chemicals, etc.) but also in nascent technologies including coatings, fabrics and other materials that catalyze air-based oxidative removal or decontamination of air pollutants, chemical warfare agents and other undesirable species.[117, 118]

The chemical warfare agent (CWA) mustard, bis(2-chloroethyl)sulfide or

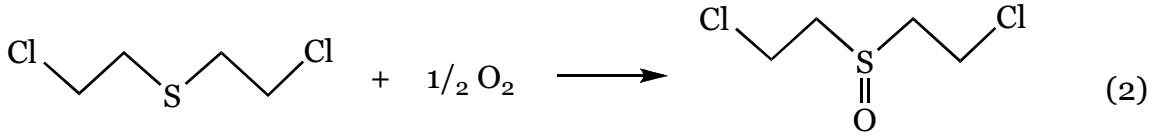

mustard (HD)
(toxic vesicant)

mustard sulfoxide (HDO)
(far less toxic than HD)

(2)

HD, was first used on the battle field in 1917. Since that time stockpiles of the material have been amassed and the compound remains a threat, both on the conventional battlefield and in unconventional theaters. The Chemical Weapons Convention (CWC) of 1997 seeks to eliminate all global stockpiles of chemical weapons. As of December 2002 the Organization for the Prohibition of Chemical Weapons (OPCW), charged with monitoring the progress of the CWC, reports a total combined world wide stockpile of over 3,800 metric tons of HD.[119] HD is a persistent chemical agent and harmful quantities of the vaporized agent can be encountered several days after initial deployment. HD is a vesicant and attacks the eyes, skin and mucous membranes. [120]

It has been shown that mustard is amenable to decontamination by oxidation.[107] Ideally such a process would be catalytic, operate under ambient conditions (~25 °C, air) and produce only non-toxic products. Ceric ammonium sulfate [121] and gold(III) nitrate complexes[105, 115, 122] were previously the best sulfide oxidation catalyts,[123] but these suffered from limitations of stringent conditions and expensive catalyst materials. For mustard the sulfoxide is significantly less toxic than the parent sulfide and so makes an attractive decontamination target.[124, 125] Selectivity and control of the oxidation reaction are of utmost importance as the sulfone (double oxidation) is far more toxic than the sulfoxide, although less toxic that the parent sulfide, HD.[120]

Sulfoxidation catalysts that operate under mild conditions (O_2/air, room temperature) are a topic of considerable interest. Several groups, including ours, have developed systems that can perform the decontamination reaction detailed

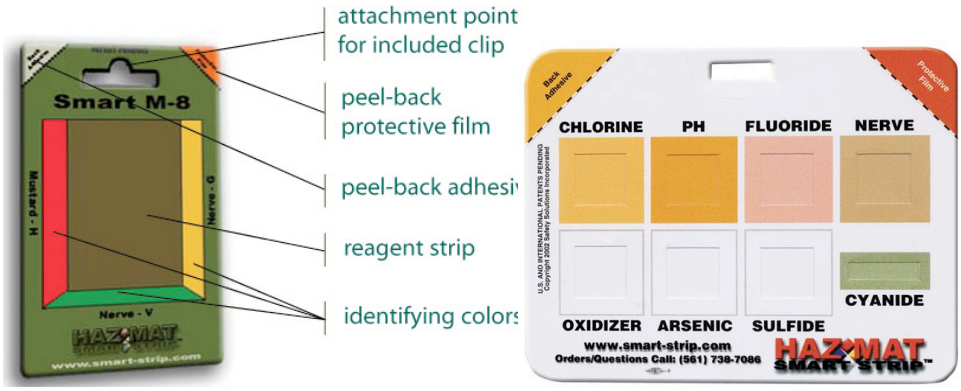

Figure 6. M8 and M9 chemical detection strips. The handheld cards are designed to be deployed in non-laboratory situations where information about unknown potentially toxic compounds is critical. Ease of use and unequivocal identification are only two of the many requirements for the design of effective testing strips.

in Equation 2.[105, 115, 117, 118, 122, 126-131] To date we have reported the most effective catalysts, which the data suggest contain a hydrogen dinitrate group associated with a d-electron-substituted polyoxometalate (POM), $Fe^{III}[H(ONO_2)_2]PW_{11}O_{39}]^{5-}$. The oxygen consumption study of this system is presented here. Furthermore a model system containing $[Fe(H_2O)PW_{11}O_{39}]^{4-}$ was explored and the results are given herein.

Paper-based CWA detection

In addition to decontamination of bulk quantities of HD, detection of this harmful agent in an operational environment is critically important. Currently the most widely used field detection technology are the M8 and M9 paper detectors (Figure 6). These materials contain reactive dyes that change color when exposed to CWAs. The technology is attractive for its ease of use and

transportability, but suffers from several major shortcomings. Namely, detector selectivity is quite poor and both M8 and M9 papers produce false positives when exposed to non-toxic agents such as oil, insecticides, solvent, fuel or other non-hazardous petroleum products. Some evidence has also been reported of false negatives, wherein the detector papers failed to give a response to a known CWA. Our goal is to develop a material that can overcome the selectivity concerns of the current technology while still maintaining the positive aspects of ease of use and transportability.[132]

Herein we show demonstrate a HD color-change detection system, deployed on a cellulosic support. The copper-bromide system undergoes rapid color-change upon exposure to the HD simulant CEES. The system is resistant to chemical interferents, does not give false positives and maintains a reasonable degree of color change response.

Experimental

Materials

All chemicals were commercially available reagent grade and used as received from commercial sources unless otherwise specified. All solvents were at least reagent grade and were used without further purification. The isopolyvanadates $[(n\text{-}C_4H_9)_4N]_3[H_3V_{10}O_{28}]$[92] and $[(n\text{-}(C_4H_9)_4N]_2[(CH_3C(CH_2O)_3)_2V_6O_{13}]$[85] were prepared according to literature procedures. The polyoxometalate $Fe(H_2O)PW_{11}O_{39}^{4-}$ was synthesized as the tetrabutylammonium salt as per literature methods.[123, 133, 134]

Instrumentation

Solution ^{1}H and ^{13}C NMR spectroscopic measurements were made on a Varian INOVA 400 MHz spectrometer and resonance signals were referenced to residual solvent signals. Elemental analyses were performed by Atlantic Microlabs Atlanta, GA (carbon, hydrogen, and nitrogen) and Kontilabs, Quebec, Canada (all elements). ^{51}V NMR spectra were acquired on a Varian 600MHz Unity spectrometer and externally referenced to 10 mM $H_4[PVMo_{11}O_{40}]$ in 0.6 M NaCl (δ = -533.6 ppm relative to neat $VOCl_3$).[135] Infrared spectra (3–5 wt. % in KBr) were recorded on a Thermo Electron Corporation Nicolet 6700 FT-IR spectrometer. Visible reflectance spectra were obtained using a HunterLab MiniScan XE Plus hand held spectrometer. Products of catalytic reactions identified using a Hewlett-Packard 5890 GC equipped with a HP-5 capillary column (poly(5% diphenyl/95% dimethylsiloxane) and HP-5971A quadrupole mass sensitive detector spectrometer. Catalytic reactions (reactant and product) were quantified using a Hewlett-Packard 5890 GC equipped with a HP-5 capillary column (poly(5% diphenyl/95% dimethylsiloxane) and an FID detector. UV-Vis spectra of the materials and reactions were acquired using a Hewlett-Packard 8452A diode array spectrophotometer. Consumption of oxygen was monitored using an Artisan RS-232 digital manometer.

*Preparation of 4-{2-{3,5-bis[2-(4-carboxyphenyl)-1-ethynyl]phenyl}-1-ethynyl}benzoic acid (**1**)*

An oven dried heavy-walled Schlenk tube equipped with a magnetic stirrer was charged with 1,3,5-triethynylbenzene, methyl 4-iodobenzoate, copper(I)

iodide, triphenylphosphine, bis-(triphenylphosphine)palladium(II) chloride, and diethyl amine. The flask was evacuated and backfilled with nitrogen, sealed with a Teflon cap, and stirred at 70 °C overnight. The mixture was allowed to cool and filtered through a glass fine fritted funnel. The filtrate was dried under reduced pressure and the product was isolated via column chromatography on silica gel (hexane:ethyl acetate, 4:1) to yield a yellow powder that was subsequently refluxed in pH 14 water for 3 hours. Acidification and filtration yielded a pale yellow solid: ^{1}H NMR (400 Mhz, DMSO-d_6) d 8.069 (d, 6H, *J* = 10.4 Hz), 7.694 (s, 3H), 7.591 (d, 6H, *J* = 10.8 Hz); FT-IR (2% KBr pellet) 2929 (s, w), 1694 (s, vb), 1605 (vs), 1606 (s), 1581 (m), 1559 (w), 1312 (s, b), 1278 (m, sh), 1175 (m), 1104 (m), 1017 (m), 874 (m), 770 (m) cm^{-1}; $C_{33}H_{18}O_6$ 510.5 g/mol.

*Preparation of 4-{2-{3,5-bis[2-(4-carboxyphenyl)-1-ethynyl]phenyl}-1-ethynyl}benzoic acid chloride (**2**)*

An oven-dried round-bottom flask equipped with a magnetic stirrer was charged with **1** (250 mg, 0.46 mmol) and 50 mL of thionyl chloride. The flask was equipped with a water condenser and the pale yellow solution was refluxed under a nitrogen atmosphere overnight. The solvent was removed under reduced pressure in a roto-vap to yield a yellow and white-flecked solid. Attempts to characterize the solid via ^{1}H NMR were hindered by water in the DMSO-d_6 solvent reacting with the acid chloride functional groups. FT-IR (2% KBr pellet) 3414 (vw, vb), 1770 (s), 1736 (m), 1692 (w, sh) 1597 (vs), 1556 (w), 1404 (m), 1204 (s), 1175 (s), 878 (s), 845 (m, sh), 740 (m) cm^{-1}.

*Preparation of tris(triol) benzamide (**3**)*

Fresh DMA was dried over activated 4 Å molecular sieves for 4 hours. A round-bottom flask equipped with a magnetic stirrer charged with tris(hydroxymethyl)aminomethane (75 mg, 0.613 mmol) and potassium carbonate (400 mg) was dried under reduced pressure in a vacuum oven for 3 hours. The flask was then filled with 100 mL of dry DMA via cannula transfer under argon atmosphere and gently heated to solvate the trisamine. The flask was cooled in an ice methanol bath and a solution of **2** (100 mg, 0.186 mmol) in 25 mL of DMA was added via cannula. The flask was equipped with a water condenser and the solution heated to 80 °C for three days under argon atmosphere. The solution was filtered to remove the solid carbonate species and evaporated to dryness under high vacuum.

*Preparation of bis-capped V_6 / **3** hybrid material (**4**) with K_2CO_3 as base*

A round-bottom flask equipped with a magnetic stirrer was charged with $[TBA]_2[(H_2NC(CH_2O)_3)_2V_6O_{13}]$ (340 mg, 0.27 mmol) and potassium carbonate (400 mg). The mixture was dissolved in 50 mL of dry DMA. A solution of **3** (100 mg, 0.186 mmol) in 25 mL of DMA was added via cannula. The flask was equipped with a water condenser and the solution heated to 80 °C for three days under argon atmosphere. No evidence of polymeric material was observed. Addition of diethyl ether caused precipitation of bis-capped V_6. Starting material **2** was not recovered.

*Preparation of bis-capped V_6 / **3** hybrid material (**4**) with $(CH_3CH_2)_3N$ as base*

A round bottom flask equipped with a magnetic stirrer was charged with $[(H_3NC(CH_2O)_3)_2V_6O_{13}]$ (480 mg, .31 mmol) and triethyl amine (0.1 mL, 0.7 mmol). The mixture was dissolved in 50 mL of dry DMA. A solution of **3** (100 mg, .186 mmol) in 25 mL of DMA was added via cannula. The flask was equipped with a water condenser and the solution heated to 80 °C for three days under argon atmosphere. No evidence of polymeric material was observed. Addition of diethyl ether caused precipitation of zwitterionic bis-capped V_6. Starting material **3** was not recovered.

*Oxidation of propane thiol to dipropyl disulfide, catalyzed by $[(n\text{-}C_4H_9)_4N]_{144}[(V_6O_{13})_{72}\{((OCH_2)_3CNHCO)_3C_6H_3\}_{36}\{((OCH2)_3CNHCO)_2((HOCH_2)_3CN\,HCO)C_6H_3\}_{18}]$ (**5**)*

Catalytic reactions were carried out at room temperature using pure O_2 as the oxidant. The reactions were performed in 3.00 mL of acetonitrile with 230 mM propane thiol and 250 mM 1,3-dichlorobenzene as an internal standard. The reaction mixture was sealed in a Schlenk flask equipped with a magnetic stirrer with 1 atm of O_2 at 25 °C. The mole ratio of substrate to catalyst was 35790:1. The mole ratio was calculated based on percent weight of bis-capped V_6 units. The catalyzed and control reactions were run simultaneously under identical conditions with no catalyst present in the control reaction vials. The substrate, propane thiol, and its corresponding oxidation product, dipropyl disulfide, were quantified by GC. No other products were detected by GC.

*Synthesis of $Ag_2[(CH_3C(CH_2O)_3)_2V_6O_{13}]$ (**6**)*

To a solution of $[(n\text{-}(C_4H_9)_4N]_2[(CH_3C(CH_2O)_3)_2V_6O_{13}]$ (0.121 g) in acetonitrile (6 mL) was added an excess amount of $NaClO_4$ (0.5 g). A precipitate formed upon shaking and was isolated via filtration and dried *in vacuo*. The precipitate was redissolved in water and three molar equivalents of $AgNO_3$ were added. The resulting red-orange precipitate was separated by filtration, washed with cold water, then ether, then dried *in vacuo*. Pure crystals were obtained by ether diffusion into a concentrated acetonitrile solution. ^{1}H NMR (400 MHz, CD_3CN): δ = 4.897 (s), 0.767 (s). ^{51}V NMR (600 MHz, CD_3CN): δ = -498.494 (s). FT-IR (Diamond ATR): 2955, 2923, 1614 (weak broad), 1452, 1394, 1369 (weak), 1204 (weak), 1122, 1013 (very strong), 967 (very strong), 952 (very strong), 932 (shoulder), 784 (broad), 684 (broad) cm^{-1}.

*Reactions Catalyzed by **6***

A solution of CEES (13.7 mM), 1,3-dichlorobenzene (internal standard, 14 mM), and TBHP (14.8 mM) in acetonitrile was prepared. Three septum-capped scintillation vials were equipped with magnetic stirrers and charged with 3 mL each of the prepared solution. Nothing else was added to vial 1. To vial 2 was added 10 mg (0.010 mmol) of $Ag_2[(CH_3C(CH_2O)_3)_2V_6O_{13}]$, **6**. To vial 3 was added 4 mg $AgClO_4$ (0.020 mmol). The mixtures were stirred at 300 rpm at room temperature. Reactions were monitored via GC and concentrations of CEES and CEESO were calculated using internal standard techniques.

Reactive catalyst for aerobic sulfide oxidation.

A 25-mL round bottom flask with side arm was charged with $TBANO_3$ (0.0105 mmol), *p*-toluenesulfonic acid (0.0108 mmol), $TBA_4Fe(H_2O)PW_{11}O_{39}$ (0.0045 mmol), 1,3-dichlorobenzene (0.83 mmol), and 2-chloroethyl ethyl sulfide (CEES) (0.86 mmol). Dry acetonitrile was added to give a total volume of 5 mL. The apparatus was flushed with O_2 (total volume 40 mL) and equipped with a magnetic stir bar, gas tight septum, and a digital manometer. This apparatus was then placed in a water bath at ambient temperature

Preparations of HD-agent Sensors

In a typical experiment a stock solution of a 0.1 to 0.6 M Cu^{2+} salt ($CF_3SO_3^-$, $CH_3CO_2^-$, Br^-, ClO_4^-) in dry acetonitrile was prepared. A 0.01 to 0.02 M stock solution of Br^- ($C_6H_5O(CH_2)_2N(CH_3)_2(CH_2)_{11}CH_3^+$, ($n$-$CH_3(CH_2)_3)_4N^+$ = tetrabutylammonium (TBA), or Li^+ salt) in dry acetonitrile was prepared. The stock solutions were mixed to yield sensor solutions with known mole ratios of Cu^{2+} : Br^- (ratios range from 1 : 0.5 to 1 : 20). Sensor strips were made by treating various cellulosic supports (e.g. paper, cotton) with the Cu^{2+} : Br^- sensor solution. Typically the paper swatches were submersed in a Petri dish containing the sensor solution for 10 seconds to allow for even coverage. The wet treated swatches were then suspended vertically and allowed to dry to constant weight under ambient conditions. The sensor (Cu^{2+} : Br^- / support) was then exposed to liquid or vaporous HD simulant (CEES). Liquid-liquid challenges of the stock sensor solutions were also performed.

Preparations of Coated HD-agent Sensor Strip

To 10 mL of a 0.55 M solution of $Cu(CF_3SO_3^-)_2$ (20 g in 100 mL of acetonitrile) were added 3 mL of a 0.12 M domiphen bromide (5 g in 100 mL of acetonitrile). The solution was placed in a Petri dish and a sample of KX Industries nano-fiber paper was placed in the solution. The paper was suspended vertically and allowed to dry to constant weight. A suspension of 5 grams of poly-*n*-butylcyanoacrylate in 15 mL of acetonitrile was applied via pipette to both sides of the sensor, sequentially. Again the swatches were dried by vertical hanging to yield the completed sensor materials.

Results and Discussion

Attempted syntheses of gelating nanoarrays

Reticular synthesis is a bottom up material design concept that employs well defined reactions and rigid components to control the creation of hybrid materials. Bonding between the inorganic junctions and the organic linkers must be stable and directional.[37] The linker compound **1** (Figure 7) was prepared by literature methods via a Suzuki coupling of 1,3,5-triethynylbenzene with methyl 4-iodobezoate followed by base hydrolysis.[136, 137] This material was found to be insoluble in all but the high boiling polar aprotic solvents such as DMF, DMA, and DMSO. ^{1}H NMR and FT-IR spectra were in line with expected values for compound **1**. The acid functionalities of **1**, required conversion to triol groups in order to form a bis-capped tri-ester of the V_6 POM. The obvious route was a reaction of the readily available tris(hydroxymethyl)aminomethane (trisamine) with the acid form of **1** to produce a tris(triol) **3**. To such end **1** was refluxed in thionyl chloride, the FT-IR of compound **2** showed a shift in the carbonyl peak

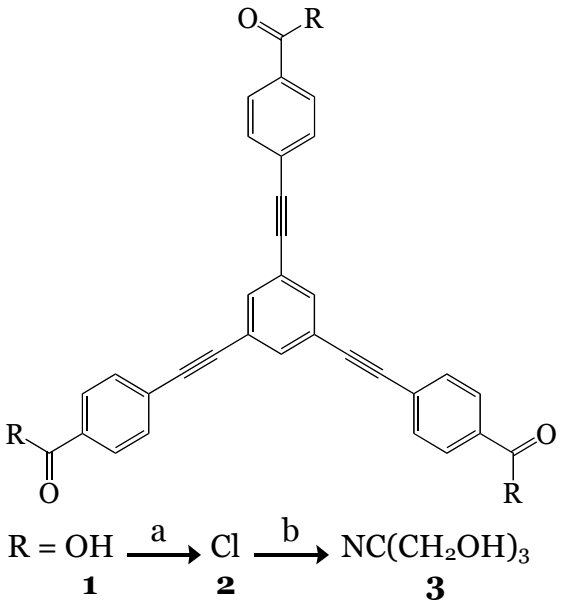

Figure 7. Tri functional organic linker. (a) thionyl chloride, reflux (b) trisamine, K_2CO_3, DMA, 80 °C.

and significant reduction in the O-H stretching region. Reaction of **2** with a solution of trisamine in DMA proved unsuccessful. DMA is tenaciously hygroscopic and as such great pains were taken to dry the solvent, however in all attempts only the starting material was recovered.

Thiol oxidation catalyzed by gelating nanoarray

The bis-capped V_6 unit is an example of oxo-ligand substitution that yields a well-defined and controllable product.[9, 28, 85-91, 94, 138] Control of the attachment of an organic triol ligand to the inorganic V_6 POM is effected via *in situ* synthetic methods. The organic solvent soluble isopolyanion $[(n\text{-}C_4H_9)_4N]_2[H_3V_{10}O_{28}]$ is the synthetic precursor of bis-capped V_6. Preparation of the precursor via literature procedures[92] proceeded well and both ^1H NMR and FT-IR spectra compared with previous data. Reaction Equation 1 shows the balanced reaction while Figure 2 illustrates the thermodynamically favorable and hydrolytically stable triester chelate.[29] In an effort to asses possible synthetic condition for the reaction of $[(n\text{-}C_4H_9)_4N]_3[H_3V_{10}O_{28}]$ with **3**, both the zwitterionic $[(H_3NC(CH_2O)_3)_2V_6O_{13}]$ and the TBA salt of $[(H_2NC(CH_2O)_3)_2V_6O_{13}]^{2-}$ were synthesized. In an attempt to circumvent the issues with the synthesis of **3**, the acid chloride **2** was reacted with both forms of the bis-capped V_6 unit in DMA in the presence of a base. No reaction was observed in either case.

Unpublished work by Zeng[94] and Neiwert[9] has shown that materials synthesized from rigid tris(triol) organic linkers and the bis(triester) capped V_6 unit exhibit a range of interesting and potentially useful properties. The porous network nanoarray material with $C_6H_3(CONHC(CH_2OH)_3)_3$ as the organic linker

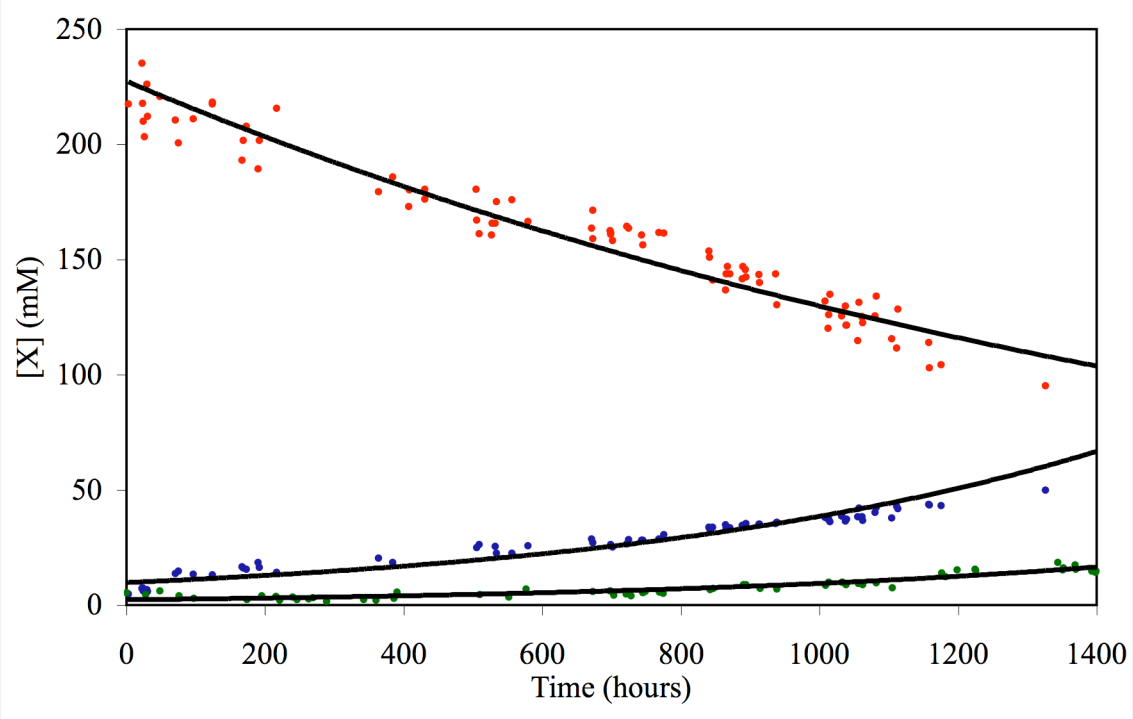

Figure 8. Oxidation of PrSH (•) to PrSSPr (•), catalyzed by **5**. Reaction conditions: 230 mM propane thiol and 250 mM decane as an internal standard in 3.00 mL of acetonitrile with **5** as the catalyst sealed in a Schlenk flask with 1 atm of O_2 at 25 °C. The substrate:catalyst mole ratio was ~35790:1. The control reaction (•), was run simultaneously under identical conditions but without any catalyst present.

and bis(triester) capped V_6 units was shown to have gelating properties, particularly with DMF. The material was also shown to have catalytic properties. Figure 8 shows the room temperature O_2–based oxidation of propane thiol to the respective disulfide, catalyzed by this material. As the reaction proceeded a color change was observed, from rusty red to a dark green indicating a reduced vanadium species. The accumulation of a reduced vanadium species, as indicated by the color change, leads to the speculation that reoxidation of the V_6 unit is the

rate limiting step. The reaction proceeds with a turnover frequency (TOF) of ~60 h^{-1}. Despite the slow reaction rate the turnover number (TON) for this material was an impressive >9900 (moles product/moles catalyst). The catalyst did not appear to be poisoned by the great excess of target compound, propane thiol. Figure 8 also shows that, despite the detection error presented by the analysis of the disulfide, the reaction proceeds via the predicted Equation 3.

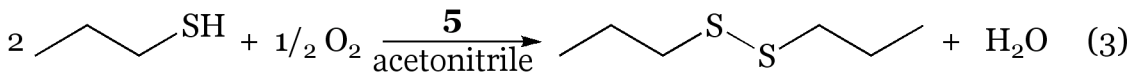

(3)

CEES sulfoxidation catalyzed by $Ag_2[(CH_3C(CH_2O)_3)_2V_6O_{13}]$

Bis(triester)V_6 units are known to catalyze the aerobic oxidation of thiols, as per Equation 4, under ambient conditions[9, 94] but sulfoxidation had not been addressed prior to our work. Previous results indicate that aerobic sulfoxidation of CEES catalyzed by **6** is probably too slow under ambient conditions to be of interest.[139] We selected *tert*-butyl hydroperoxide (TBHP) as an oxidant for CEES because it is inexpensive, easily handled, has a high oxygen content, and quite safe.

Sulfoxidation by TBHP catalyzed by **6**, Equation 4, shows an induction

(4)

period. However, once Equation 4 starts, it proceeds rapidly at 25 °C to completion. Representative kinetics are shown in Figure 9. ^{51}V NMR, electronic

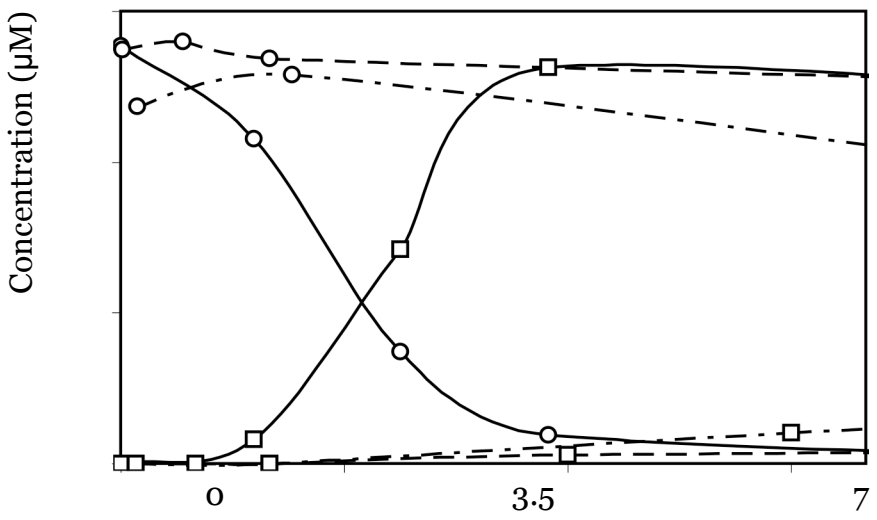

Figure 9. CEES (o) oxidation to CEESO (□) by 14.8 mM TBHP in acetonitrile at room temperature. Solid lines represent oxidation in the presence of 3.3 mM $Ag_2[(CH_3C(CH_2O)_3)_2V_6O_{13}]$ (**6**). Dashed lines represent the uncatalyzed background reaction. The dash-dot lines represent the background oxidation in the presence of 6.7 mM $AgClO_4$.[139]

absorption spectroscopy, and gas chromatography can be used to follow the progress of the reaction.

In compound **6**, all the vanadium centers are equivalent by symmetry and can be characterized by a single singlet peak in the ^{51}V NMR spectrum at the outset of the reaction. In parallel with the catalytic activity this signal decreases and multiple signals increase. The electronic absorption spectra also exhibit a time dependence (Figure 10). These changes in the ^{51}V NMR and UV-visible spectra are not seen if any one of the components of the reaction is missing. That is, incubating **6** in acetonitrile with each of the individual components (sulfide or

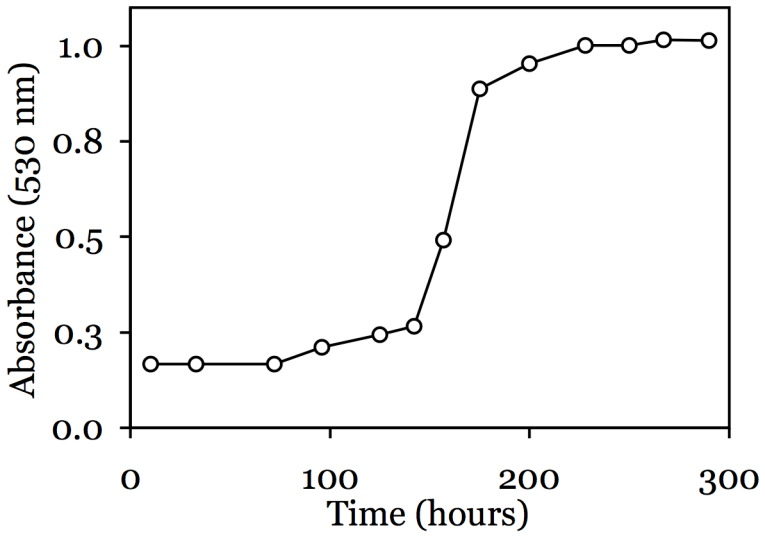

Figure 10. UV-Vis absorbance at 530 nm. The oxidation of CEES to CEESO by TBHP catalyzed by **6** was monitored by UV-Vis spectroscopy. Changes in the UV-Vis spectra correspond roughly to similar changes in the catalyzed reactions themselves. Reaction conditions are described in Figure 9.[139]

oxidant or solvent) affords no change in spectra or any evidence of the oxidation product (CEESO).

The spectral changes are consistent with but do not prove the formation of a transient alkylhydroperoxide derivative of the V_6 cage (replacement of a μ-oxo bridge with an alkyl hydroperoxo group), which could well be an important intermediate in the principle catalytic cycle. While only 4 turnovers are observed, the reaction is evidently catalytic, as the reaction does not proceed in the absence of catalyst on the same time scale.

As the reaction proceeds a color change from rusty red to a dark green is observed, indicating a reduced vanadium species. The buildup of reduced vanadium species, as indicated by the color change, leads to the speculation that

reoxidation of the V_6 unit is the rate limiting step. The color changes were monitored by UV-Vis spectroscopy (Figure 10).

Identification of O_2 stoichiometry for a aerobic sulfoxide oxidation reaction catalyzed by an Fe-containing POM

An unusually reactive catalyst for aerobic oxidation of sulfides to sulfoxides, as per Equation 2, a POM with a hydrogen dinitrate group associated with a d-electron-substituted POM, $Fe^{III}[H(ONO_2)_2]PW_{11}O_{39}^{5-}$ was reported by our group.[123] The organic solvent soluble salt, $[(n\text{-}CH_3(CH_2)_3)_4N]_3H_2Fe^{III}[H(ONO_2)_2]PW_{11}O_{39}]$, under aerobic conditions converted 92.8% of CEES to the corresponding sulfoxide with complete selectivity (no sulfone was detected via GC-MS).[95, 123, 139] During the peer review process the validity of the of the reported reaction stoichiometry in that publication, namely RSR + ½ O_2 -> RS(O)R was called into question.

To unequivocally confirm the stoichiometry to of this equation a model system ($TBANO_3$ and *p*-toluenesulfonic acid in the presence of $TBA_4Fe(H_2O)PW_{11}O_{39}$ in acetonitrile solvent) was analyzed because it afforded more strict control the relative ratios of nitrate, proton, and Fe-POM (ca. 2:2:1 equivalents, respectively). The model system converts ~70% of the sulfide, 2-chloroethyl ethyl sulfide, CEES (a mustard simulant) to the corresponding sulfoxide, CEESO, with effectively 100% selectivity. No sulfone or other organic product is detected via gas chromatographic (GC) analysis. This corresponds to ~150 turnovers with a turnover frequency of ~40 h^{-1}.

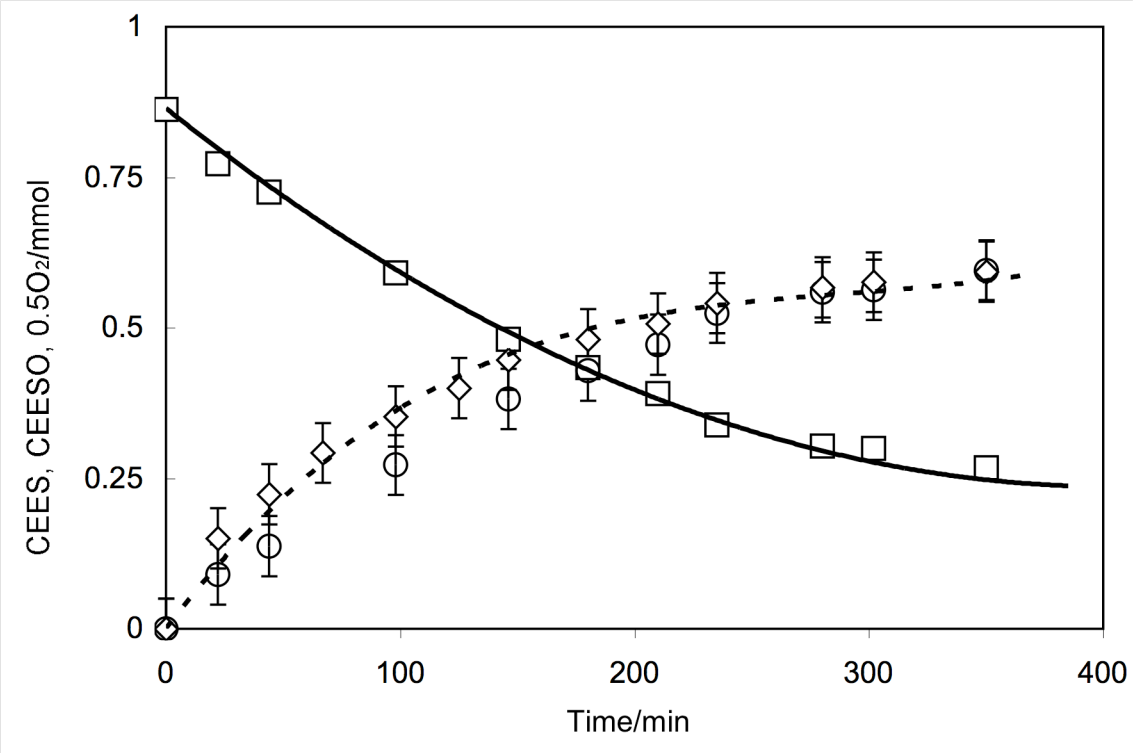

Figure 11. Oxidation of CEES (□) to CEESO (O) catalyzed by the nitrate (4 mM $TBANO_3$) / proton (2 mM pTsH) / $TBA_4Fe(H_2O)PW_{11}O_{39}$ (0.8 mM) system in acetonitrile (5 mL) at 25° C and 1 atm O_2. The pressure drop of a pure oxygen headspace was monitored via digital manometer and plotted as mmol/2 of O_2 (◇).[95] Determination of CEESO via GC yields systematically smaller values than actually present at low concentrations due to peak tailing. Coincident curves indicate equation 2 is correct as written.[123]

In order to monitor both consumption of CEES and O_2 simultaneous with production of CEESO we employed two separate instruments. Gas chromatography was used for CEES and CEESO values and the catalytic oxidation reaction was carried out in a sealed vessel equipped with a digital manometer to record the pressure drop. Pure oxygen was used as the headspace

gas. The moles of O_2 present were determined from the ideal gas equation (with R adjusted to room temperature). When there were low quantities of CEESO in the reaction solution, it was problematical to achieve mass balance. Determination of CEESO via GC yields systematically lower values than actually present at low concentrations due to peak tailing. Despite this the reaction proceeded quickly and when consumption of 0.5 O_2 was plotted on the same axis as production of CEESO, the curves were nearly coincidental as per Figure 11. The reaction operates under the atom efficient dioxygenase stoichiometry as shown by the coincident curves of moles of CEESO and ½ O_2.[95, 123]

Color-change detection of mustard

A paper-supported color-change system for the detection of mustard (HD) was developed by our group. The system consisted of a trinary mixture of Cu(triflate)$_2$, domiphen bromide and polydialkyldiallylammonium chloride (10,000 - 20,000 M.W., 20% solution in water) in acetonitrile. The mixture was coated onto paper supports via brush application.[132] Treating the cellulosic

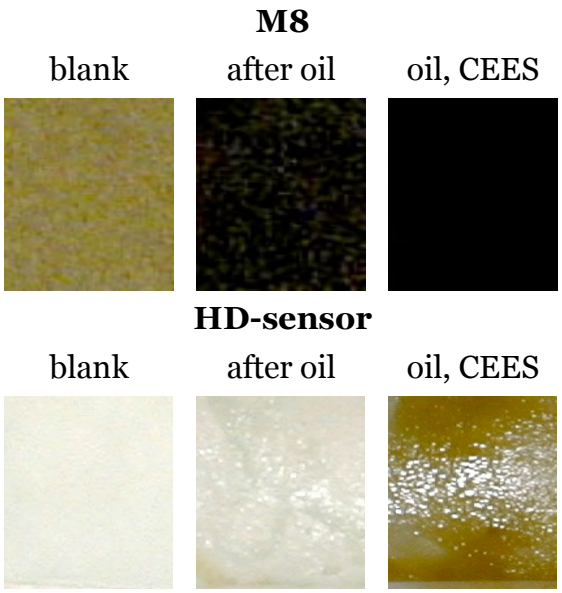

Figure 12. Comparison of M8 and HD-sensor responses. Column two shows M8 giving a false positive response. In contrast the HD-Sensor when exposed to oil before simulant challenge still detects CEES.

supports with the sensor solutions in acetonitrile afforded a color change detection material that gave a rapid and reliable response when exposed to simulant (CEES). Side-by-side comparative tests of our material to the commonly used M8 detector paper further demonstrated that our sensor is superior in selectivity and does not give rise to false positives when exposed to oils unlike M8 paper (Figure 12). While most color changes are recorded via digital photography and optimized for maximum detectable visual changes, the color change can also be quantified satisfactorily via reflectance spectroscopy (see Figure 13).

The system was difficult to reproduce and sensitive to atmospheric water. Attempts proceeded to characterize the active species and optimize the sensor system performance. A simplified system was developed ($Cu(ClO_4)_2$ and TBABr) in dry acetonitrile was studied via UV-Vis spectroscopy. The concentration of Cu^{2+} was maintained while the ratio of Cu^{2+} to Br^- was varied. Overlapping peaks were extracted by the use of OmniLab's peak simulation program (Figure 12). The changes in the UV-Vis spectra matched similar experiments performed by Chmurzynski *et. al.*[140] Analysis indicated that the copper-bromide complex(es) in acetonitrile solution is concentration dependent. The low Cu^{2+}-to-Br^--ratio complex is likely a tetragonally distorted octahedral $CuBr(acetonitrile)_5^+$ or $CuBr_2(acetonitrile)_4$.[140] As the ratio and the concentration of bromide increases, the system undergoes a change to flattened tetrahedral complexes $CuBr_3(acetonitrile)^-$ and $CuBr_4^{2-}$.[141] The change in color is due to the change in

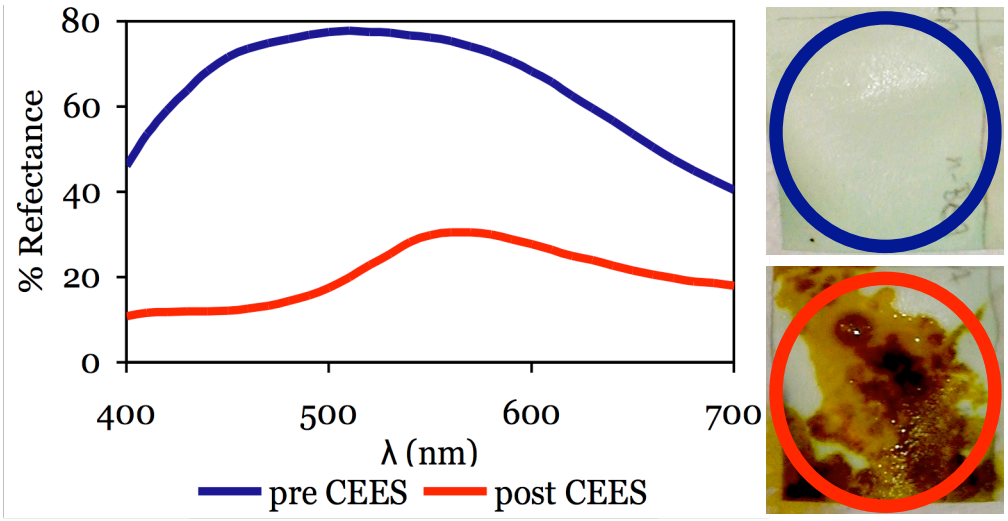

Figure 13. Reflectance spectrum of HD-sensor on paper. A hand-held spectrometer is used to quantify color changes of the HD-sensor. Circled areas represent sampled area. The sensor before exposure to CEES is much more reflective.

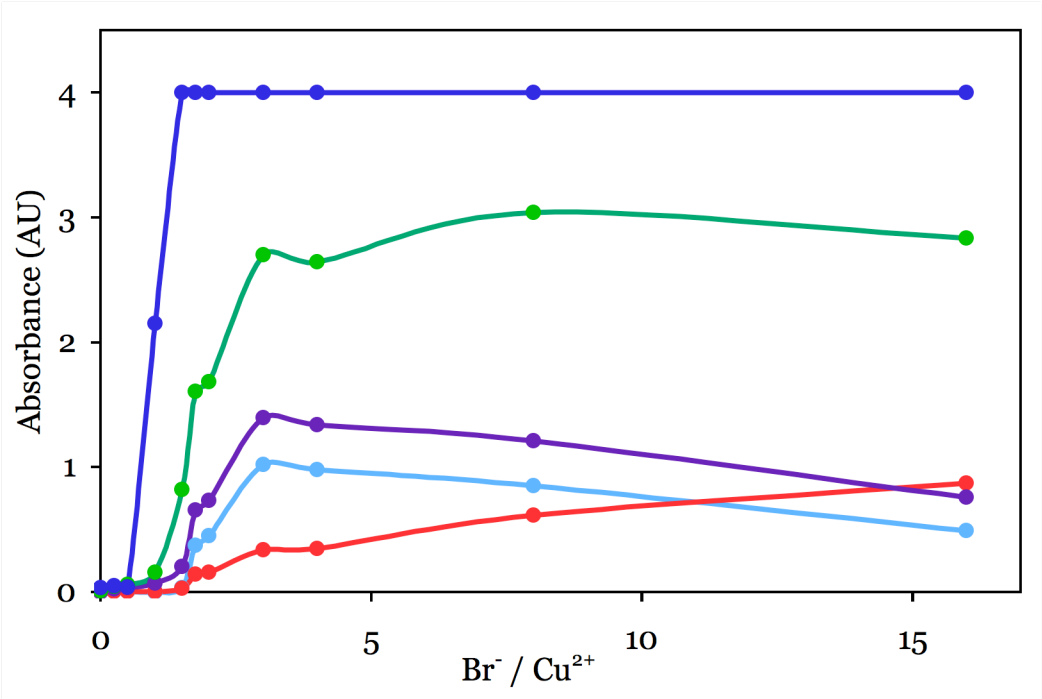

Figure 14. Absorbance curves at increasing bromide to cupric ion ratios. 640 (red); 520 (light blue); 430 (purple); 360 (green); 270 (dark blue)

absorption transitions, from a $^2E_g(D) \rightarrow {}^2T_{2g}(D)$ transition for the octahedral species[142] to a $^2T_2(D) \rightarrow {}^2E(D)$ transition for the tetrahedral species.[143] As the tetrahedral complexes are already darkly colored, and thus show little change upon addition of CEES, the mole ratio of Cu^{2+} : Br^- for optimal color change in a liquid-liquid CEES challenge was determined to be 1 : 2.

We have attempted to address the only apparent significant problem associated with this color-change sensor system, namely sensitivity to H_2O, by two routes: use of barrier-coating agents to prevent water contact with the impregnated sensor components, and hydrophobization of both the sensor solutions and the support material. In order to hydrophobize the sensor mixtures themselves a variety of counter ions to both Cu^{2+} and Br^- were screened. However, because all the compounds investigated were ionic salts, the effort proved unsuccessful. Attempts to apply a sensor solution to laminated hydrophobic paper succeeded, but were unable to address the moisture sensitivity of the sensor strips. It was later revealed that the lamination process used by our collaborators, KX Industries, is incapable of producing a truly

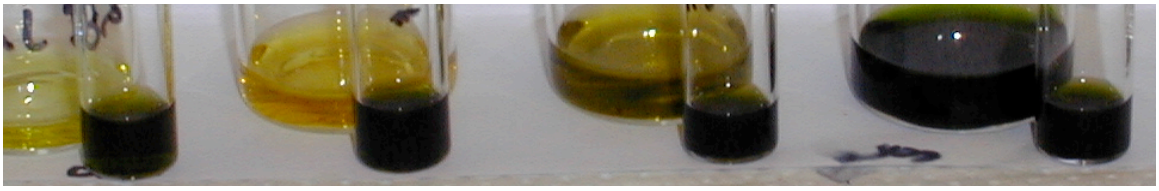

Figure 15. From left to right the ratio of Cu^{2+} to Br^- increases. The unexposed solutions are in the background while the solutions exposed to simulant CEES are in the smaller vials. The color change is maximized for the second vial from the right, in which the mol ratio of Cu^{2+} : Br^- is 1 : 2.

hydrophobic material for our sensor solutions. Our efforts turned instead to an application of a barrier-coating agent to the prepared sensor strips. The coatings were designed to exclude vaporous water while still allowing the target molecule (CEES) to penetrate to the sensor. Several cyanoacrylates of varying molecular weights were analyzed. Results were encouraging as the reduction in water sensitivity was directly proportional to the thickness of the cyanoacrylate coating. It was found that pre-polymerized *n*-butylcyanoacrylate suspended in acetonitrile produced an optimal coating. Unfortunately, the coating, while protecting the sensor mixture from water, also inhibited rapid color change, most likely due to slowed penetration of CEES into the sensor material. The objective is a significant color change in 10 seconds or less after exposure to HD simulant. Current work is proceeding to finalize a sensor material for commercial production in collaboration with Materials Technology Corporation.

References

1. Pope, M. T.; Müller, A., Chemistry of polyoxometallates. Actual variation on an old theme with interdisciplinary references. . *Angew. Chem. Int. Ed.* **1991,** 30, (1), 34-48.
2. Pope, M. T., Isopolyanions and Heteropolyanions. In *Comprehensive Coordination Chemistry*, Wilkinson, G.; Gillard, R. D.; McCleverty, J. A., Eds. Pergamon Press: New York, 1987; Vol. 3, p Chapter 38.
3. Pope, M. T., Polyoxo Anions: Synthesis and Structure. In *Comprehensive Coordination Chemistry II: From Biology to Nanotechnology*, Wedd, A. G., Ed. Elsevier Ltd.: Oxford, UK, 2004; Vol. 4, pp 635-678.
4. Yamase, T.; Pope, M. T., *Polyoxometalate Chemistry for Nano-Composite Design*. Kluwer Academic/Plenum Publishers: New York, 2002; Vol. 2, p 235.
5. Pope, M. T.; Müller, A., *Polyoxometalate Chemistry From Topology via Self-Assembly to Applications*. Kluwer Academic Publishers: Dordrecht, Netherlands, 2001; p 427.
6. Pope, M. T.; Müller, A., *Polyoxometalates: From Platonic Solids to Anti-retroviral Activity*. Kluwer Academic Publishers: Dordrecht, Netherlands, 1993; Vol. 10.
7. Hill, C. L., Polyoxometalates: Reactivity. In *Comprehensive Coordination Chemistry-II: From Biology to Nanotechnology*, Wedd, A. G., Ed. Elsevier Ltd.: Oxford, UK, 2004; Vol. 4, pp 679-759.
8. Hill, C. L., Stable, Self-Assembling, Equilibrating Catalysts for Green Chemistry. *Angew. Chem. Int. Ed.* **2004,** 43, 402-404.

9. Neiwert, W. A. Polyoxometalates as Nanoscale Building Blocks for the Formation of Fundamentally New Materials. Emory University, Atlanta, 2004.

10. Borrás-Almenar, J. J.; Coronado, E.; Müller, A.; Pope, M. T., *Polyoxometalate Molecular Science*. Kluwer Academic Publishers: Dordrecht, 2003; Vol. 98.

11. Weinstock, I. A., Homogeneous-Phase Electron-Transfer Reactions of Polyoxometalates. *Chem. Rev.* **1998,** 98, (1), 113-170.

12. Weinstock, I. A.; Atalla, R. H.; Reiner, R. S.; Moen, M. A.; Hammel, K. E.; Houtman, C. J.; Hill, C. L.; Harrup, M. K., A New Environmentally Benign Technology for Transforming Wood Pulp Into Paper. Engineering Polyoxometalates As Catalysts for Multiple Processes. *J. Mol. Catal. A: Chem.* **1997,** 116, 59-84.

13. Weinstock, I.; Atalla, R. H.; Reiner, R. S.; Houtman, C. J.; Hill, C. L., Selective transition-metal catalysis of oxygen delignification using water-soluble salts of polyoxomeralate (POM) anions. Part I. Chemical principles and process concepts. *Holz Forschung* **1998,** 52, 304-310.

14. Weinstock, I. A.; Barbuzzi, E. M. G.; Wemple, M. W.; Cowan, J. J.; Reiner, R. S.; Sonnen, D. M.; Heintz, R. A.; Bond, J. S.; Hill, C. L., Equilibrating Metal-oxide Cluster Ensembles for Oxidation Reactions Using Oxygen in Water. *Nature* **2001,** 414, (6860), 191-195.

15. Hill, C. L.; Prosser-McCartha, C. M., Homogeneous catalysis by transition metal oxygen anion clusters. *Coord. Chem. Rev.* **1995,** 143, 407-455.

16. Okuhara, T.; Mizuno, N.; Misono, M., Catalytic Chemistry of Heteropoly Compounds. *Advances in Catalysis* **1996,** 41, 113-252.

17. Mizuno, N.; Misono, M., Heterogeneous Catalysis. *Chem. Rev.* **1998,** 98, (1), 199-218.

18. Neumann, R., Polyoxometalate Complexes in Organic Oxidation Chemistry. *Prog. Inorg. Chem.* **1998,** 47, 317-370.

19. Katsoulis, D. E., A Survey of Applications of Polyoxometalates. *Chem. Rev.* **1998,** 98, (1), 359-388.

20. Otero, T. F.; Cheng, S. A.; Huerta, F., Hybrid Materials Polypyrrole/PW12O403-. 1. Electrochemical Synthesis, Kinetics and Specific Charges. *J. Phys. Chem. B.* **2000,** 104, (45), 10522-10527.

21. Clemente-León, M.; Mingotaud, C.; Agricole, B.; Gómez-Garcia, C. J.; Coronado, E.; Delhaès, P., Application of the Langmuir-Blodgett Technique to Polyoxometalates: Towards New Magnetic Films. *Angew. Chem. Int. Ed.* **1997,** 36, (10), 1114-1116.

22. Caruso, F.; Kurth, D. G.; Volkmer, D.; Koop, M. J.; Müller, A., Ultrathin Molybdenum Polyoxometalate- Polyelectrolyte Multilayer Films. *Langmuir* **1998,** 14, (13), 3462-3465.

23. Cheng, L. N., L.; Gong, J.; Dong, S., Electrochemical Growth and Characterization of Polyoxometalate-Containing Monolayers and Multilayers on Alkanethiol Monolayers Self-Assembled on Gold Electrodes. *Chem. Mater.* **1999,** 11, (6), 1465-1475.

24. Tang, Z.; Liu, S.; Wang, E.; Dong, S.; Wang, E., Preparation, Structures, and Electrochemistry of a New Polyoxometalate-Based Organic/Inorganic Film on Carbon Surfaces. *Langmuir* **2000,** 16, (13), 5806-5813.

25. Stein, A.; Fendorf, M.; Jarvie, T. P.; Müller, K. T.; Benesi, A. J.; Mallouk, T. E., Salt gel synthesis of porous transition-metal oxides. *Chem. Mater.* **1995,** 7, (2), 304-313.

26. Yun, S. K.; Maier, J., Synthesis and Ionic Conductivity of Supramolecular Layered Silicate Hybrids of Phosphotungstates and Poly(ethylene glycol) Dicarboxylates. *Chem. Mater.* **1999,** 11, 1644-1647.

27. Guo, Y.; Wang, Y.; Hu, C.; Wang, Y.; Wang, E.; Zhou, Y.; Feng, S., Microporous Polyoxometalates POMs/SiO_2: Synthesis and Photocatalytic Degradation of Aqueous Organocholorine Pesticides. *Chem. Mater.* **2000,** 12, (11), 3501-3508.

28. Chen, Q.; Zubieta, J., Synthesis and structural characterization of a polyoxovanadate coordination complex with a hexametalate core: $[(n\text{-}C_4H_9)_4N]_2[V_6O_{13}\{O_2NC(CH_2O)_3\}_2$. *Inorg. Chem.* **1990,** 29, (8), 1456-1458.

29. Zeng, H.; Newkome, G. R.; Hill, C. L., Poly(polyoxometalate) Dendrimers: Molecular Prototypes of New Catalytic Materials. *Angew. Chem. Int. Ed.* **2000,** 39, (10), 1771-1774.

30. Khan, M. I.; Chen, Q.; Goshorn, D. P.; Hope, H.; Parkin, S.; Zubieta, J., Polyoxo Alkoxides of Vanadium: The Structures of the Decanuclear Vanadium (IV) Clusters $[V_{10}O_{16}\{CH_3CH_2C(CH_2O)_3\}_4]^{4-}$ and $[V_{10}O_{13}\{CH_3CH_2C(CH_2O)_3\}_5]^{4-}$. *J. Am. Chem. Soc.* **1992,** 114, 3341-3346.

31. Keggin, J. F., Structure of the Molecule of i2-Phosphotungstic. *Nature* **1933,** 131, 908-909.

32. Baker, L. C. W.; Figgis, J. S., A New Fundamental Type of Inorganic Complex: Hybrid between Heteropoly and Conventional Coordination Complexes. Possibilities for Geometrical Isomerisms in 11-, 12-, 17-, and 18-Heteropoly Derivatives. *J. Am. Chem. Soc.* **1970,** 92, (12), 3794-3797.

33. Weakley, T. J. R., Heteropolyanions Containing Two Different Heteroatoms. Part III. Cobalto(II)undecatungstophosphate and Related Anions. *J. Chem. Soc., Dalton Trans. Inorg. Chem.* **1973,** 3, 341-346.

34. Zonnevijlle, F.; Tourné, C. M.; Tourné, G. F., Ligand- and Metal-Exchange Reactions on Substituted Lacunary Heteropolytungstates. *Inorg. Chem.* **1983,** 22, (8), 1198-1202.

35. Katsoulis, D. E.; Pope, M. T., New Chemistry for Heteropolyanions in Anhydrous Nonpolar Solvents. Coordinative Unsaturation of Surface Atoms. Polyanion Oxygen Carriers. *J. Am. Chem. Soc.* **1984,** 106, (9), 2737-2738.

36. Bi, L.-H.; Wang, E.-B.; Peng, J.; Huang, R.-D.; Xu, L.; Hu, C.-W., Crystal Structure and Replacement Reaction of Coordinated Water Molecules of the Heteropoly Compounds of Sandwich-Type Tungstoarsenates. *Inorg. Chem.* **2000,** 39, (4), 671-679.

37. Yaghi, O. M.; O'Keeffe, M.; Ockwig, N. W.; Chae, H. K.; Eddaoudi, M.; Kim, J., Reticular synthesis and the design of new materials. *Nature* **2003,** 423, 705.

38. Bailar, J. C., Jr., *Prep. Inorg. React.* **1964,** 1, 1-27.

39. Kinoshita, Y.; Matsubara, I.; Higuchi, T.; Saito, Y., The Crystal Structure of Bis(adiponitrilo)copper(I) Nitrate. *Bull. Chem. Soc. Jpn.* **1959,** 32, (11), 1221-1226.

40. Hirsch, K. A.; Venkataraman, D.; Wilson, S. R.; Moore, J. S.; Lee, S., Crystallization of 4,4-biphenyldicarbonitrile with silver(I) salts: a change in topology concomitant with a change in counterion leading to a ninefold diamondoid network. *Chem. Commun.* **1995,** 21, 2199 - 2200.

41. Hoskins, B. F.; Robson, R., Infinite polymeric frameworks consisting of three dimensionally linked rod-like segments *J. Am. Chem. Soc.* **1989,** 111, (15), 5962-5964.

42. Aumüller, A.; Erk, P.; Klebe, G.; Hünig, S.; Schütz, J. U. v.; Werner, H.-P., A Radical Anion Salt of 2,5-Dimethyl-N,N-dicyanoquinonediimine with Extremely High Electrical Conductivity. *Angew. Chem. Int. Ed.* **1996,** 25, (8), 740-741.

43. Kiang, Y.-H.; Gardner, G. B.; Lee, S.; Xu, Z.; Lobkovsky, E. B., Variable Pore Size, Variable Chemical Functionality, and an Example of Reactivity within Porous Phenylacetylene Silver Salts. *J. Am. Chem. Soc.* **1999,** 121, (36), 8204-8215.

44. Carlucci, L.; Ciani, G.; Gudenberg, D. W. v.; Proserpio, D. M.; Sironi, A., Self-assembly of a three-dimensional network from two-dimensional layers via metallic spacers: the (3,4)-connected frame of $[Ag_3(hmt)_2][ClO_4]_3 \cdot 2H_2O$ (hmt = hexamethylenetetramine). *Chem. Commun.* **1997,** 6, 631-632.

45. Pyun, J.; Matyjaszewski, K., The Synthesis of Hybrid Polymers Using Atom Transfer Radical Polymerization: Homopolymers and Block Copolymers from Polyhedral Oligomeric Silsesquioxane Monomers *Macromolecules* **2000,** 33, (1), 217-220.

46. Fu, B. X.; Hsiao, B. S.; Pagola, S.; Stephens, P.; White, H.; Rafailovich, M.; Sokolov, J.; Mather, P. T.; Jeon, H. G.; Phillips, S.; Lichtenhan, J.; Schwab, J., Structural development during deformation of polyurethane containing polyhedral oligomeric silsesquioxanes (POSS) molecules. *Polymer* **2001,** 42, (2), 599-611.

47. Simard, M.; Su, D.; Wuest, J. D., Use of hydrogen bonds to control molecular aggregation. Self-assembly of three-dimensional networks with large chambers. *J. Am. Chem. Soc.* **1991,** 113, (12), 4696-4698.

48. Lu, J.; Paliwala, T.; Lim, S. C.; Yu, C.; Niu, T.; Jacobson, A. J., Coordination Polymers of $Co(NCS)_2$ with Pyrazine and 4,4'-Bipyridine: Syntheses and Structures. *Inorg. Chem.* **1997,** 36, (5), 923-929.

49. Kitagawa, S.; Kondo, M., Functional Micropore Chemistry of Crystalline Metal Complex-Assembled Compounds. *Bull. Chem. Soc. Jpn.* **1998,** 71, (8), 1739-1753.

50. Hagrman, D.; Hagrman, P. J.; Zubieta, J., Solid-State Coordination Chemistry: The Self-Assembly of Microporous Organic - Inorganic Hybrid Frameworks Constructed from Tetrapyridylporphyrin and Bimetallic Oxide Chains or Oxide Clusters. *Angew. Chem. Int. Ed.* **1999,** 38, (21), 3165-3168.

51. Pamela J. Hagrman; Hagrman, D.; Zubieta, J., Organic-Inorganic Hybrid Materials: From Simple Coordination Polymers to Organodiamine-Templated Molybdenum Oxides. *Angew. Chem. Int. Ed.* **1999,** 38, (18), 2638-2684.

52. Kondo, M.; Shimamura, M.; Noro, S.-i.; Minakoshi, S.; Asami, A.; Seki, K.; Kitagawa, S., Microporous Materials Constructed from the Interpenetrated Coordination Networks. Structures and Methane Adsorption Properties. *Chem. Mater.* **2000,** 12, (5), 1288-1299.

53. Moulton, B.; Zaworotko, M. J., From Molecules to Crystal Engineering: Supramolecular Isomerism and Polymorphism in Network Solids. *Chem Rev.* **2001,** 101, (6), 1629-1658.

54. Zaworotko, M. J., Superstructural diversity in two dimensions: crystal engineering of laminated solids. *Chem. Commun.* **2001,** 1, 1-9.

55. Yaghi, O. M.; Li, H.; Groy, T. L., Construction of Porous Solids from Hydrogen-Bonded Metal Complexes of 1,3,5-Benzenetricarboxylic Acid. *J. Am. Chem. Soc.* **1996,** 118, (38), 9096-9101.

56. Chui, S. S.-Y.; Siu, A.; Feng, X.; Zhang, Z. Y.; Mak, T. C. W.; Williams, I. D., Hydrothermal synthesis of three new 3-D framework rare-earth mellitates. *inorg. Chem. Commun.* **2001,** 4, (9), 467-470.

57. Eddaoudi, M.; Moler, D. B.; Li, H.; Chen, B.; Reineke, T. M.; O'Keeffe, M.; Yaghi, O. M., Modular Chemistry: Secondary Building Units as a Basis for the Design of Highly Porous and Robust Metal-Organic Carboxylate Frameworks. *Acc. Chem. Res.* **2001,** 34, 319 - 330.

58. Gutschke, S. O. H.; Price, D. J.; Powell, A. K.; Wood, P. T., Hydrothermal Synthesis, Structure, and Magnetism of $[Co_2(OH)\{1,2,3\text{-}(O_2C)_3C_6H_3\}(H_2O)]H_2O$ and $[Co_2(OH)\{1,2,3\text{-}(O_2C)_3C_6H_3\}]$: Magnetic - Chains with Mixed Cobalt Geometries. *Angew. Chem. Int. Ed.* **2001,** 40, (10), 1920-1923.

59. Prior, T. J.; Rosseinsky, M. J., Crystal engineering of a 3-D coordination polymer from 2-D building blocks. *Chem. Commun.* **2001,** 5, 495 - 496.

60. Kumagai, H.; Arishima, M.; Kitagawa, S.; Ymada, K.; Kawata, S.; Kaizaki, S., New Hydrogen Bond-Supported 3-D Molecular Assembly from Polyoxovanadate and Tetramethylbiimidazole. *Inorg. Chem.* **2002,** 41, (7), 1989-1992.

61. Kiritsis, V.; Michaelides, A.; Skoulika, S.; Ouahab, L.; Golhen, S., Assembly of a Porous Three-Dimensional Coordination Polymer: Crystal Structure of $\{[La_2(adipate)_3(H_2O)_4]_6H_2O\}_n$. *Inorg. Chem.* **1998,** 37, (13), 3407-3410.

62. Reineke, T. M.; Eddaoudi, M.; Fehr, M.; Kelley, D.; Yaghi, O. M., From Condensed Lanthanide Coordination Solids to Microporous Frameworks Having Accessible Metal Sites. *J. Am. Chem. Soc.* **1999,** 121, (8), 1651-1657.

63. Reineke, T. M.; Eddaoudi, M.; O'Keeffe, M.; Yaghi, O. M., A Microporous Lanthanide-Organic Framework. *Angew. Chem. Int. Ed.* **1999,** 37, (17), 2590-2594.

64. Han, J. W.; Hill, C. L., A coordination network that catalyzes O_2-based oxidations. *J. Am. Chem. Soc.* **2007,** 129, 15094-15095.

65. Kitagawa, S.; Kitaura, R.; Noro, S.-i., Functional Porous Coordination Polymers. *Angew. Chem. Int. Ed.* **2004,** 43, 2334 –2375.

66. Eddaoudi, M.; Kim, J.; Rosi, N.; Vodak, D.; Wachter, J.; O'Keeffe, M.; Yaghi, O. M., Systematic Design of Pore Size and Functionality in Isoreticular MOFs and Their Application in Methane Storage. *Science* **2002,** 295, (5554), 469-472.

67. Rosi, N. L.; Eckert, J.; Eddaoudi, M.; Vodak, D. T.; Kim, J.; O'Keeffe, M.; Yaghi, O. M., Hydrogen Storage in Microporous Metal-Organic Frameworks. *Science* **2003,** 300, 1127-1129.

68. Rowsell, J. L. C.; Millward, A. R.; Park, K. S.; Yaghi, O. M., Hydrogen Sorption in Functionalized Metal-Organic Frameworks *J. Am. Chem. Soc.* **2004,** 126, (18), 5666-5667.

69. Chui, S. S.-Y.; Lo, S. M.-F.; Charmant, J. P. H.; Orpen, A. G.; Williams, I. D., A Chemically Functionalizable Nanoporous Material $[Cu_3(TMA)_2(H_2O)_3]_n$. *Science* **1999,** 283, 1148-1150.

70. Seki, K.; Takamizawa, S.; Mori, W., Design and Gas Adsorption Property of a Three-Dimensional Coordination Polymer with a Stable and Highly Porous Framwork. *Chem. Lett.* **2001,** 30, (4), 332-333.

71. Li, H.; Eddaoudi, M.; O'Keeffe, M.; Yaghi, O. M., Design and synthesis of an exceptionally stable and highly porous metal-organic framework. *Nature* **1999,** 402, (6759), 276-279.

72. Yaghi, O. M.; O'Keeffe, M.; Kanatzidis, M., Design of Solids from Molecular Building Blocks: Golden Opportunities for Solid State Chemistry. *Journal of Solid State Chemistry* **2000,** 152, (1), 1-2.

73. Eddaoudi, M.; Li, H.; Yaghi, O. M., Highly Porous and Stable Metal-Organic Frameworks: Structure Design and Sorption Properties. *J. Am. Chem. Soc.* **2000,** 122, (7), 1391-1397.

74. Chen, B.; Eddaoudi, M.; Hyde, S. T.; O'Keeffe, M.; Yaghi, O. M., Interwoven Metal-Organic Framework on a Periodic Minimal Surface with Extra-Large Pores. *Science* **2001,** 291, 1021-1023.

75. Noro, S.-i.; Kitagawa, S.; Kondo, M.; Seki, K., A New, Methane Adsorbent, Porous Coordination Polymer [{$CuSiF_6$(4,4-bipyridine)$_2$}$_n$]. *Angew. Chem. Int. Ed.* **2000,** 39, (12), 2081-2084.

76. Biradha, K.; Hongo, Y.; Fujita, M., Open Square-Grid Coordination Polymers of the Dimensions 20×20 Å: Remarkably Stable and Crystalline Solids Even after Guest Removal. *Angew. Chem. Int. Ed.* **2000,** 39, (21), 3843-3845.

77. Davis, M. E., Ordered porous materials for emerging applications. *Nature* **2002,** 417, 813 - 821.

78. Mark E. Davis, C. M., Paul E. Hathaway, Juan P. Arhancet, Dennis L. Hasha, Juan M. Garces, Physicochemical properties of VPI-5. *J. Am. Chem. Soc.* **1989,** 111, (11), 3919-3924.

79. Millange, F.; Serre, C.; Férey, G., Synthesis, structure determination and properties of MIL-53as and MIL-53ht: the first CrIII hybrid inorganic–organic microporous solids: $Cr^{III}(OH)\cdot\{O_2C–C_6H_4–CO_2\}\cdot\{HO_2C–C_6H_4–CO_2H\}_x$. *Chem. Commun.* **2002,** 8, 822 - 823.

80. Yaghi, O. M.; Li, H.; Davis, C.; Richardson, D.; Groy, T. L., Synthetic Strategies, Structure Patterns, and Emerging Properties in the Chemistry of Modular Porous Solids. *Acc. Chem. Res.* **1998,** 31, (8), 474-484.

81. Stein, A.; Keller, S. W.; Mallouk, T. E., Turning Down the Heat: Design and Mechanism in Solid-State Synthesis. *Science* **1993,** 259, (1558-1564), 1558.

82. Fujita, M.; Kwon, Y. J.; Washizu, S.; Ogura, K., Preparation, Clathration Ability, and Catalysis of a Two-Dimensional Square Network Material Composed of Cadmium(11) and 4,Y-Bipyridine. *J. Am. Chem. Soc.* **1994,** 116, 1151-1152.

83. Sheldon, R. A.; Kochi, J. K., *Metal-Catalyzed Oxidations of Organic Compounds*. Academic Press: New York, 1981; p Chapter 5.

84. Ito, Y. N.; Katsuki, T., Asymmetric Catalysis of New Generation Chiral Metallosalen Complexes. *Bull. Chem. Soc. Jpn.* **1999,** 72, (4), 339-345.

85. Chen, Q.; Goshorn, D. P.; Scholes, C. P.; Tan, X. L.; Zubieta, J., Coordination Compounds of Polyoxovanadates with a Hexametalate Core. Chemical and Structural Characterization of $[V^{V}_{6}O_{13}\{(OCH_2)_3CR\}_2]^{2-}$, $[V^{V}_{6}O_{11}(OH)_2\{(OCH_2)_3CR\}_2]$, $[V^{IV}_{4}V^{V}_{2}O_9(OH)_4\{(OCH_2)_3CR\}_2]^{2-}$, and $[V^{IV}_{6}O_7(OH)_6\{(OCH_2)_3CR\}_2]^{2-}$. *J. Am. Chem. Soc.* **1992,** 114, (12), 4667-4681.

86. Chen, Q.; Zubieta, J., Structural investigations of the hexavanadium core (V_6O_{19}) in Oxidized, mixed valence and reduced Clusters of the Type $(V_{6-n}^{(V)}V_n^{(IV)}O_{13-n}(OH)_n((OCH_2)_3Cr)_2)^{2-}$, n=0, 3, and 6. *Inorganica Chimica Acta* **1992,** 200, 95-110.

87. Chen, Q.; Zubieta, J., Coordination Chemistry of Soluble Metal Oxides of Molybdenum and Vanadium. *Coord. Chem. Rev.* **1992,** 114, (2), 107-167.

88. Khan, M. I.; Chang, Y.; Chen, O.; Hope, H.; Parking, S.; Goshorn, D. P.; Zubieta, J., (Organoarsonato)polyoxovanadium Clusters - properties and Structures of the V(V) Cluster $(V_{10}O_{24}(O_3AsC_6H_4\text{-}4\text{-}NH_2)^{4-}$ and the V(IV)/V(V) Cluster $(H_2(V_6O_{10}(O_3AsC_6H_5)_6)^{2-}$. *Angew. Chem. Int. Ed.* **1992,** 31, 1197-1200.

89. Khan, M. I.; Chen, Q.; Zubieta, J.; Goshorn, D. P., Hexavanadium polyoxo Alkoxide Anion Clusters - Structures of the Mixed-valence Species $(M_3NH)(V^{(IV)}_5V^{(V)}O_7(OH)_3(CH_3C(CH_2O)_3)_3)$ and of the reduced complex $Na_2(V^{(IV)}_6O_7(CH_3CH_2C(CH_2O)_3)_4$. *Inorg. Chem.* **1992,** 31, 1556-1558.

90. Chen, Q.; Zubieta, J., A novel hexavanadate core: synthesis and structure of the mixed valence cluster $[V_6O_8\{(OCH_2)_3CE_t\}_2\{(OCH_2)_2C(CH_2OH)(Et)\}_4]^{2-}$ and a comparison with the hexametallate core of $[V_6O_{13}(OMe)_3\{(OCH_2)_3CCH_2OH\}]^{2-}$. *J. Chem. Soc., Chem. Comm.* **1993**, (15), 1180-1182.

91. Khan, M. I.; Chen, Q.; Hope, H.; Parkin, S.; Oconnor, C. J.; Zubieta, J., Hydrothermal Synthesis and Characterization of Hexavanadium polyoxo Alkoxide Anion Clusters - Crystal Structures of the Vanadium (IV) Species $Ba[V_6O_7(OH)_3((OCH_2)_3CCH_3)_3]\bullet 3H_2O$ and $Na_2[V_6O_7((OCH_2)_3CCH_2CH_3)_4]$, of the Mixed-Valence Complex $(Me_3NHo[V(IV)_5V(V)O_7(OH)_3((OCH_2)_3CCH_3)_3]$, and of the fluoro Derivative $Na[V_6O_6F(OH)_{399}OCH_2)_3CCH_3)_3]\bullet 3H_2O$. *Inorg. Chem.* **1993,** 32, 2929-2937.

92. Day, V. W.; Klemperer, W. G.; Maltbie, D. J., Where Are the Protons in $H_3V_{10}O_{28}^{3-}$? *J. Am. Chem. Soc.* **1987,** 109, 2991-3002.

93. Hou, Y.; Hill, C. L., Hydrolytically stable organic triester capped polyoxometalates with catalytic oxygenation activity of formula $[RC(CH_2O)_3V_3P_2W_{15}O_{59}]^{6-}$ (R = CH_3, NO_2, CH_2OH). *J. Am. Chem. Soc.* **1993,** 115, (25), 11823-11830.

94. Zeng, H. Toward Functional Supramolecular Poly(Polyoxometalate)s and Materials. Emory University, Atlanta, 2004.

95. Hill, C. L.; Anderson, T. M.; Han, J.; Hillesheim, D. A.; Geletii, Y. V.; Okun, N. M.; Cao, R.; Botar, B.; Musaev, D. G.; Morokuma, K., New complexes and materials for O_2-based oxidations. *J. Mol. Catal. A: Chem.* **2006,** 251, 234-238.

96. Khenkin, A. M.; Weiner, L.; Wang, Y.; Neumann, R., Electron and Oxygen Transfer in Polyoxometalate, $H_5PV_2Mo_{10}O_{40}$, Catalyzed Oxidation of Aromatic and Alkyl Aromatic Compounds: Evidence for Aerobic Mars-van Krevelen-Type Reactions in the Liquid Homogeneous Phase. *J. Am. Chem. Soc.* **2001,** 123, (35), 8531-8542.

97. Geletii, Y. V.; Gueletii, A.; Weinstock, I. A., Electron capture and transport by heteropolyanions: Multi-functional electrolytes for biomass-based fuel cells. *J. Mol. Catal. A: Chem.* **2007,** 262, 59-66.

98. Hill, C. L.; Delannoy, L.; Duncan, D. C.; Weinstock, I. A.; Renneke, R. F.; Reiner, R. S.; Atalla, R. H.; Han, J. W.; Hillesheim, D. A.; Cao, R.; Anderson, T. M.; Okun, N. M.; Musaev, D. G.; Geletii, Y. V., Complex

catalysts from self-repairing ensembles to highly reactive air-based oxidation systems. *C.R. Chimie* **2007,** 10, 305-312.

99. Duncan, D. C.; Chambers, R. C.; Hecht, E.; Hill, C. L., Mechanism and Dynamics in the $H_3[PW_{12}O_{40}]^-$ Catalyzed Selective Epoxidation of Terminal Olefins by H_2O_2. Formation, Reactivity, and Stability of $\{PO_4[WO(O_2)_2]_4\}^{3-}$. *J. Am. Chem. Soc.* **1995,** 117, (2), 681-691.

100. Kamata, K.; Yonehara, K.; Sumida, Y.; Yamaguchi, K.; Hikichi, S.; Mizuno, N., Efficient Epoxidation of Olefins with >99% Selectivity and Use of Hydrogen Peroxide. *Science* **2003,** 300, (5621), 964-966.

101. Kamata, K.; Kotani, M.; Yamaguchi, K.; Hikichi, S.; Mizuno, N., Olefin Epoxidation with Hydrogen Peroxide Catalyzed by Lacunary Polyoxometalate $[\gamma\text{-}SiW_{10}O_{34}(H_2O)_2]^{4-}$. *Chem. Eur. J.* **2007,** 13, (2), 639-648.

102. Nakagawa, Y.; Mizuno, N., Mechanism of $[\gamma\text{-}H_2SiV_2W_{10}O_{40}]^{4-}$Catalyzed Epoxidation of Alkenes with Hydrogen Peroxide. *Inorg. Chem.* **2007,** 46, (5), 1727-1736.

103. Prabhakar, R.; Morokuma, K.; Geletii, Y. V.; Hill, C. L.; Musaev, D. G., Insights into the Mechanism of H_2O_2-based Olefin Epoxidation Catalyzed by the Lacunary $[\gamma\text{-}(SiO_4)W_{10}O_{32}H_4]^{4-}$ and di-V-substituted-γ-Keggin $[\gamma\text{-}1,2\text{-}H_2SiV_2W_{10}O_{40}]^{4-}$ Polyoxometalates. A Computational Study. In *Computational Modeling for Homogenous and Enzymatic Catalysis*, Morokuma, K.; Musaev, D. G., Eds. Wiley: New York, 2008; pp 215-230.

104. Ozaki, S.-i.; Ortiz de Montellano, P. R., Molecular Engineering of Horseradish Peroxidase: Thioether Sulfoxidation and Styrene Epoxidation

by Phe-41 Leucine and Threonine Mutants. *J. Am. Chem. Soc.* **1995,** 117, 7056-7064.

105. Boring, E.; Geletii, Y.; Hill, C. L., Catalysts for Selective Aerobic Oxidation under Ambient Conditions. Thioether Sulfoxidation Catalyzed by Gold Complexes. In *Catalytic Activation of Dioxygen*, Simandi, L. I., Ed. Kluwer: Dordrecht, 2001.

106. Sigman, M. S.; Jensen, D. R.; Rajaram, S., Catalytic enantioselective oxidations using molecular oxygen. *Current Opinion in Drug Discovery & Development* **2002,** 5 (6), 860-869.

107. Yang, Y. C.; Baker, J. A.; Ward, J. R., Decontamination of Chemical Warfare Agents. *Chem. Rev.* **1992,** 92, (8), 1729-1743.

108. Harrison, R. M., Setting Health-based Air Quality Standards. In *Air Pollution and Health*, Hester, R. E.; Harrison, R. M., Eds. Royal Society of Chemistry: Cambridge, 1998; Vol. 10, pp 101-126.

109. Salthammer, T., *Organic Indoor Air Pollutants: Occurrence-Measurement-Evaluation*. Wiley-VCH: Weinheim, 1999.

110. Gall, R. D.; Faraj, M.; Hill, C. L., Role of Water in Polyoxometalate-Catalyzed Oxidations in Nonaqueous Media. Scope, Kinetics, and Mechanism of Oxidation of Thioether Mustard (HD) Analogs by *tert*-Butyl Hydroperoxide Catalyzed by $H_5PV_2Mo_{10}O_{40}$. *Inorg. Chem.* **1994,** 33, (22), 5015-5021.

111. Gall, R. D.; Hill, C. L.; Walker, J. E., Carbon Powder and Fiber-Supported Polyoxometalate Catalytic Materials. Preparation, Characterization, and

Catalytic Oxidation of Dialkyl Sulfides as Mustard (HD) Analogues. *Chem. Mater.* **1996,** 8, (10), 2523-2527.

112. Gall, R. D.; Hill, C. L.; Walker, J. E., Selective oxidation of thioether mustard (HD) analogs by *tert*-butylhydroperoxide catalyzed by $H_5PV_2Mo_{10}O_{40}$ supported on porous carbon materials. *J. Catal.* **1996,** 159, (2), 473-478.

113. Brink, G.-J.; Arends, I. W. C. E.; Sheldon, R. A., Green, Catalytic Oxidation of Alcohols in Water. *Science* **2000,** 287, (5458), 1636-1639.

114. Sheldon, R. A.; Arends, I. W. C. E., Catalytic oxidations of alcohols. In *Advances in Catalytic Activation of Dioxygen by Metal Complexes*, Simandi, L. I., Ed. Kluwer Academic Publishers: Dordrecht, 2003; Vol. 26, pp 123-156.

115. Boring, E.; Geletii, Y. V.; Hill, C. L., A Homogeneous Catalyst for Selective O_2 Oxidation at Ambient Temperature. Diversity-Based Discovery and Mechanistic Investigation of Thioether Oxidation by the $Au(III)Cl_2NO_3$(thioether)/O_2 System. *J. Am. Chem. Soc.* **2001,** 123, (8), 1625-1635.

116. Ben-Daniel, R.; Alsters, P.; Neumann, R., Selective Aerobic Oxidation of Alcohols with a Combination of a Polyoxometalate and Nitroxyl Radical as Catalysts. *Journal of Organic Chemistry* **2001,** 66, (25), 8650-8653.

117. Okun, N. M.; Anderson, T. M.; Hill, C. L., $[(Fe^{III}(OH_2)_2)_3(A\text{-}\alpha\text{-}PW_9O_{34})_2]^{9-}$ on Cationic Silica Nanoparticles, a New Type of Material and Efficient Heterogeneous Catalyst for Aerobic Oxidations. *J. Am. Chem. Soc.* **2003,** 125, (11), 3194-3195.

118. Okun, N. M.; Anderson, T. M.; Hardcastle, K. I.; Hill, C. L., Cupric Decamolybdodivanadophosphate. A Coordination Polymer Heterogeneous Catalyst for Rapid, High Conversion, High Selectivity Sulfoxidation Using the Ambient Environment. *Inorg. Chem.* **2003,** 42, (21), 6610-6612.

119. Media and Public Affairs Branch, T. S., OPCW The Chemical Weapons Ban: Facts and Figures. http://www.opcw.org/

120. Marrs, T. C.; Maynard, R. L.; Sidell, F. R., In *Chemical Warfare Agents: Toxicology and Treatment*, Wiley & Sons: Chichester, New York, 1996; p 141.

121. Riley, D. P.; Smith, M. R.; Correa, P. E., Selective Molecular Oxygen Oxidation of Thioethers to Sulfoxides Catalyzed by Ce(IV). *J. Am. Chem. Soc.* **1988,** 110, (1), 177-180.

122. Boring, E.; Geletii, Y.; Hill, C. L., Catalytic aerobic oxidation of 2-chloroethyl ethyl sulfide (CEES), an HD simulant, under ambient conditions. Effect of solvents, ligands, and transition metals on reactivity. *J. Mol. Catal. A: Chem.* **2001,** 176, 49-63.

123. Okun, N. M.; Tarr, J. C.; A., H. D.; Zhang, L.; Hardcastle, K. I.; Hill, C. L., Highly Reactive Catalysts for Aerobic Thioether Oxidation. The Fe-substituted Polyoxometalate/hydrogen Dinitrate System. *J. Mol. Catal. A. Chem.* **2006,** 246, 11-17.

124. Hirade, J.; Ninomiya, A., Effects of the Oxidation of Vesicants on Their Blistering Capacity. *J. Biochem. (Tokyo)* **1950,** 37, 19-26.

125. Anslow, J., W. P.; Karnofsky, D. A.; Val Jager, B.; Smith, H. W., *J. Pharmacol. Exp. Ther.* **1948,** 93, 1-9.

126. Bosch, E.; Kochi, J. K., Catalytic Epoxidation of Hindered Olefins with Dioxygen. Fast Oxygen Atom Transfer to Olefin Cation Radicals from Nitrogen Oxides. *J. Am. Chem. Soc.* **1996,** 118, 1319-1329.

127. Martín, S. E.; Rossi, L. I., An efficient and selective aerobic oxidation of sulfides to sulfoxides catalyzed by $Fe(NO_3)_3$-$FeBr_3$. *Tetrahedron Letters* **2001,** 42, (41), 7147-7151.

128. Okun, N. M.; Ritorto, M. D.; Anderson, T. M.; Apkarian, R. P.; Hill, C. L., Polyoxometalates on Cationic Silica Nanoparticles. Physicochemical Properties of an Electrostatically Bound Multi-Iron Catalyst. *Chem Mater.* **2004,** 16, 2551-2558.

129. Okun, N. M.; Anderson, T. M.; Hill, C. L., Polyoxometalates on Cationic Silica. Highly Selective and Efficient O_2/Air-Based Oxidation of 2-Chloroethyl Ethyl Sulfide at Ambient Temperature. *J. Mol. Catal. A: Chem.* **2003,** 197, (1-2), 283-290.

130. Rossi, L. I.; Martin, S. E., Possible role of nitrate/nitrite redox cycles in catalytic and selective sulfoxidation reaction: Metallic nitrates and bromides as redox mediators: a comparative study. *Appl. Catal. A* **2003,** 250, (2), 271-278.

131. Bosch, E.; Kochi, J. K., Selective Catalysis of Thioether Oxidations with Dioxygen. Critical Role of Nitrosonium EDA Complexes in the Thermal and Photochemical Transfer of Oxygen Atom from Nitrogen Oxides to Sulfur Centers. *J. Org. Chem.* **1995,** 60, (10), 3172-3183.

132. Hill, C. L., STTR Phase II Proposal to the U.S. Army on CWA Detection. In U.S. Army: Emory University, 2004.

133. Mizuno, N.; Nozaki, C.; Kiyoto, I.; Misono, M., Highly efficient utilization of hydrogen peroxide for selective oxygenation of alkanes catalyzed by diiron-substituted polyoxometalate precursor. *J. Am. Chem. Soc.* **1998,** 120, 9267-9272.

134. Mizuno, N.; Nozaki, C.; Kiyoto, I.; Misono, M., Selective Oxidation of Alkenes Catalyzed by di-Iron-Substituted Silicotungstate with Highly Efficient Utilization of Hydrogen Peroxide. *J. Catal.* **1999,** 182, (1), 285-288.

135. Pettersson, L.; Andersson, I.; Selling, A.; Grate, G. H., Multicomponent Polyanions. 46. Characterization of the Isomeric Keggin Decamolybdodivanadophosphate Ions in Aqueous Solution by ^{31}P and ^{51}V NMR. *Inorg. Chem.* **1994,** 33, 982-993.

136. Takahashi, S.; Kuroyama, Y.; Sonogashira, K.; Hagihara, N., A Convenient Synthesis of Ethynylarenes and Diethynylarenes. *Synthsis* **1980**, 627-630.

137. Castellano, R. K.; Rebek, J. R., Jr., Formation of Discrete, Functional Assemblies and Informational Polymers through the Hydrogen-Bonding Preferences of Calixarene Aryl and Sulfonyl Tetraureas. *J. Am. Chem. Soc.* **1998,** 120, 3657-3663.

138. Zubieta, J., Clusters and Solid Phases of the Oxovanadium-Phosphate and - Organophosphonate Systems. *Comments Inorg. Chem.* **1994,** 16, (3), 153 - 183.

139. Hill, C. L.; Okun, N. M.; Hillesheim, D. A.; Geletii, Y. V., Catalysts for Aerobic Decontamination of Chemical Warfare Agents Under Ambient Conditions. In *Polymers and Materials for Anti-Terrorism and*

Homeland Defense, ACS Symposium Series, Third Ed., Reynolds, J. G.; Lawson, G. E., Eds. American Chemical Society: Washington, D.C., 2006.

140. Chmurzyski, L.; Kluczkowski, M.; Pilarczyk, M., Equilibria of copper(II) bromide in dimethyl sulphoxide solutions. *Electrochimica Acta* **1984,** 29, (3), 373-379.

141. Karipides, A. G.; Piper, T. S., Crystal Spectrum of Cs2CuBr4 *Inorg. Chem.* **1962,** 1, (4), 970-971.

142. Schläfer, H. L.; Opitz, H. P., *Z. Elektrochem.* **1961,** 62, 372.

143. Morosin, B.; Lingafelter, E. C., The Crystal Structure of Cesium Tetrabromocuprate(II) *Acta Cryst.* **1960,** 13, 807-809.

Understanding the Role of Nitrogen Oxides and Halide in the Aerobic Catalytic Oxidation of Sulfides: The NO_x/Br System

Published in part in:

J. Mol. Catal. A Chem. **2006**, 251, 234-238.

"Catalysts for Aerobic Decontamination of Chemical Warfare Agents Under Ambient Conditions," *Symposium on Polymers and Materials for Anti-terrorism and Homeland Defense*; American Chemical Society Symposium Series 980, Chapter 12, **2007**.

With:

Hill, C. L.; Geletii, Y. V.; Okun, N. O.; Tarr, J. C.; Zhang, L.; Hardcastle, K.;

Abstract

A series of catalytic systems were developed and explored in an attempt to determine the key intermediate in the rapid and selective catalytic aerobic oxidation of sulfides to sulfoxides by nitrogen oxides and bromide. Selective introduction of components to a base system was the method used to determine that the sources of nitrogen oxides and bromide anion were critical to catalysis. The catalytic activity of the system is dependent on the ratio of NO_x to Br^-. It was discovered that acid was required to facilitate conversion to the active species with certain nitrogen oxide sources. Transition metals potentially assist the conversion of the nitrogen oxide source to the active catalyst. The actual formula of the active catalyst in solution remains unknown and as such is referred to as "NO_x/Br".

Introduction

In 2006 the Hill group reported a highly efficient and selective catalyst for the aerobic oxidation of sulfides to sulfoxides (Equation 1).[1] The catalyst, $TBA_3H_2Fe^{III}[H(ONO_2)_2]PW_{11}O_{39}\bullet(HNO_3)$ (NO_xFePW_{11}), where TBA is tetrabutylammonium, was of particular interested because of its high turnover numbers and its selectivity; no evidence of the over oxidized sulfone product was detected. While several characterization methods were used to identify the active catalyst, and in particular, to confirm the location and nature of the NO_x species in the catalyst (FT-IR, Cyclic voltammetry, TGA, DSC, etc.), no disorder-free crystal structure had ever been achieved despite considerable effort toward this end. The strongest evidence for an active hydrogen dinitrate species stemmed from the IR spectrum where the characteristic stretches for $[H(ONO_2)_2]^-$ were detected. It was postulated that this species was crucial to catalytic activity. Furthermore, an interesting correlation between the presence of acid and catalytic activity was reported. When protons were added to the system the catalytic activity increased, when proton-specific bases were added, no sulfoxide was detected.[1]

$$R_2S + \tfrac{1}{2}\, O_2 \rightarrow R_2SO \quad (1)$$

Nitrogen oxides have long been reported to oxidize thioether substrates.[2-5] Nitric acid,[6] nitrous acid,[7] and sodium nitrite in the presence of hydrobromic acid, have been used in organic oxidation reactions,[8] though not specifically with sulfides. Nitric acid has been used as a stoichiometric oxidant for the conversion of sulfides to sulfoxides,[3, 9] and further studies have shown that transition-metal

halides catalyze this reaction.[10] Catalytic aerobic oxidations have been reported with nitrogen monoxide,[11] and nitrogen dioxide.[12]

The conversion of one type of nitrogen oxide species to another has been well reported. Bosch and Kochi established that NO_2, which is in equilibrium with N_2O_4 (bp 21 °C at 1 atm)[13], catalyzes aerobic sulfoxidation under mild conditions. NO also readily forms NO_2 under the reaction conditions via:

$$NO + ½\ O_2 \leftrightarrows 2\ NO_2 \leftrightarrows N_2O_4 \quad (2)$$

The conversion processes between various nitrogen oxides are facile and in dynamic equilibrium, particularly in the presence of halides, oxygen and acid,[14] which made the identification of the active catalyst in mixed systems, as was our goal, particularly difficult.

Experimental

Materials

All common reagents were purchased and used as delivered. $TBA_6\alpha$-$Mn^{II}SiW_{11}O_{39}$,[15] $TBA_6\alpha$-$Ni^{II}SiW_{11}O_{39}$,[15] $TBA_6\alpha$-$Co^{II}SiW_{11}O_{39}$,[15] $TBA_6\alpha$-$V^{V}SiW_{11}O_{40}$,[15] $TBA_6\alpha$-$Mn^{III}AlW_{11}O_{39}$,[16] and $TBA_7\alpha$-$Co^{II}AlW_{11}O_{39}$,[16] were synthesized according to literature procedures. Other than storing the $NOPF_6$ at -30 °C, no precautions were taken to keep materials away from air and moisture. We assumed that the acetonitrile contained some water.

Instrumentation

Transmission Infrared spectra (3–5 wt. % in KBr) were recorded on a Thermo Electron Corporation Nicolet 6700 FTIR spectrometer. Reflectance spectra of pure samples where recorded on the same instrument using a diamond attenuated total reflectance accessory. Catalytic reactions (reactant and product) were quantified using a Hewlett-Packard 5890 and 6890 GCs equipped with a HP-5 capillary column [poly(5% diphenyl/95% dimethylsiloxane)] and FID detectors. UV-Visible spectra of the materials and reactions were acquired using a Hewlett-Packard 8453 diode array spectrophotometer. Electrospray mass spectra were acquired on a Thermo Finnigan LTQ-FTMS in both positive and negative ion modes.

Catalysis

Normally stock solutions of the reagents to be combined to create a catalytic mixture were prepared in acetonitrile and mixed in the proper ratios to produce the required concentration in the 20 mL reaction vial equipped with a magnetic stir bar. Pure sulfide and internal standard (1,3-dichlorobenzene, DCB) were added via auto-pipette. When the reaction called for 1 atm O_2 atmosphere, the vial was flushed with oxygen before capping. Those vials were then equipped with a balloon filled with O_2 via a 25-gauge needle to maintain positive pressure and prevent air leaks. A thermostat-controlled water bath was used to maintain a constant temperature around the vials. Hamilton 7000 series μL syringes were used to deliver 0.1 μL of solvent to the GC inlet port. GC oven temperatures were adjusted to produce optimal peak separation in a minimal amount of time for

each sulfide tested. Retention time and peak area were entered into Excel for plotting.

Application to solid support

A stock solution of NO_X/Br catalyst was prepared from 5.0 mM $TBANO_2$, 10.0 mM TBABr and 10.0 mM *p*-TsOH and incubated with 0.5 g of NonoActive™ TiO_2, Al_2O_3, and SiO_2 each. The mixtures were filtered and the solid material was used as a catalyst under the normal conditions described above, with the exception that toluene was used instead of acetonitrile.

Synthesis of functionalized SiO_2

A 250 mL 2-neck round bottom flask was filled with 20 g of silica gel (particle size 0.040 – 0.063 mm, 230 - 400 mesh). An addition funnel was used to slowly add 7.7 g of chlorosulfonic acid over 1 hour. A large stir bar was used to agitate the solid. The second neck was equipped with a tube submersed in 150 mL of saturated Na_2CO_3 solution to neutralize the HCl gas byproduct of this reaction.[17]

Solid-Gas reactions

A small computer fan glued to a large stir bar was placed in the bottom of a 9 L glass desiccator. A magnetic stirrer caused the fan to rotate and circulate the gasses in the desiccator during reactions. The lid of the desiccator was equipped with a rubber stopper with a thermometer adaptor. The thermometer adaptor allowed for the replacement of disposable Teflon septa between each set of experiments. The solid catalyst was placed in a dish on a tray approximately 20

cm from the bottom of the desiccator. A gas tight syringe was used to withdraw 100 μL of gas for each GC analysis.

Results and Discussion

In order to clarify the role of nitrate, proton, and polyoxometalate (POM) in the catalytic aerobic oxidation of sulfides, we attempted to simplify a reference system, NO_xFePW_{11}. As common synthetic routes to organic soluble POMs often include the use of TBABr, we attempted to account for this in our system. We had previously observed $TBAFeBr_4$ as a co-catalyst in a separate set of highly catalytically systems (unpublished data). As such, we explored the possible effects of bromide on the catalytic activity systems containing NO_x. $TBANO_3$, TBABr and *p*-tolunesulfonic acid (*p*-TsOH) were used as sources of nitrate, bromide, and proton respectively, while $TBA_4Fe(H_2O)PW_{11}O_{39}$ ($FePW_{11}$) was used as a Fe-containing POM relevant to NO_xFePW_{11}. To address a role of the central heteroatom in Keggin-type POMs, $FePW_{11}$ was replaced with $TBA_5Fe(H_2O)SiW_{11}O_{39}$ ($FeSiW_{11}$). Then to address the role of the addendum transition metal, $FeSiW_{11}$ was replaced with $TBA_6Cu(H_2O)SiW_{11}O_{39}$ ($CuSiW_{11}$). As a control the $CuSiW_{11}$ was replaced with an equimolar amount of $Cu(ClO_4)_2$.

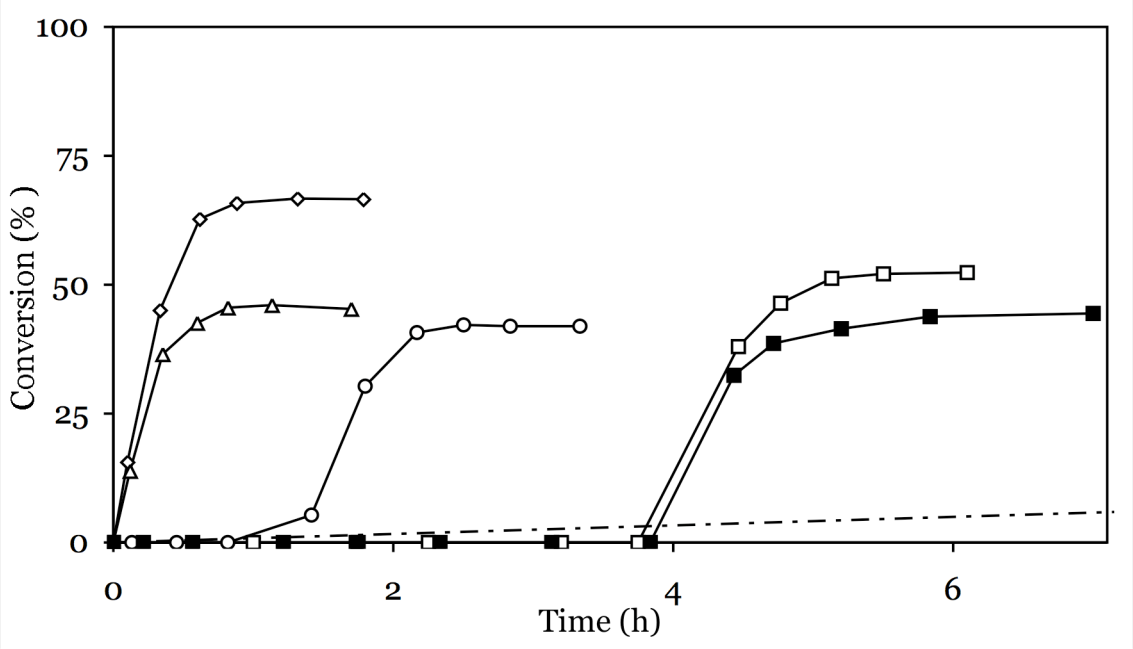

Figure 1. Oxidation of CEES (0.5 M) to CEESO catalyzed by nitrate (8 mM $TBANO_3$) / proton (42 mM *p*-TsOH) / bromide (8 mM TBABr) systems in acetonitrile at 30 °C and 1 atm O_2. Conversion (%) is calculated from the ratio of CEES to CEESO. The reactions when the following additional components are added to the reference catalytic system above (o) are shown: (■) plus 3.6 mM $TBA_4Fe(H_2O)PW_{11}O_{39}$, (□) plus $TBA_5Fe(H_2O)SiW_{11}O_{39}$, (◇) plus $TBA_6Cu(H_2O)SiW_{11}O_{39}$, (Δ) plus $CuClO_4$, (dashed line) reference system with no bromide, no POM.

Table 1. Homogeneous Air-Based Oxidation of CEES[a]

	Catalyst	[Catalyst], (mM)	Conversion, %[b]	TON[c]
1	NO_xFePW_{11}[d]	2.0	92.8	163
2	$TBA_4Fe(H_2O)PW_{11}O_{39}$[e]	2.0	~ 99	174
3	$TBANO_3$[f]	6.0	6	10.5
4	NO_xFePW_{11}[g]	5.0	0	0
5	$NOPF_6$	2.0	2.8	3.5
6	NO_2BF_4	2.0	2.5	4.4
7	$(NH_4)_2Ce^{IV}(NO_3)_6$	2.4	28.0	49
8	$Ti(NO_3)_4$	3.2	29.5	52

[a] General conditions: 0.35 M of 2-chloroethyl ethyl sulfide (CEES), catalyst (given in column 2), 1 atm of air, 1,3-dichlorobenzene (internal standard) in 2.3 mL of acetonitrile at 25 °C for 40 h in a 20-mL vial. [b] conversion = (mol of CEES consumed / mol of initial CEES) x 100; [c] turnover number = (moles of CEESO / moles of catalyst); [d] NO_xFePW_{11} = $[Fe^{III}[H(ONO_2)_2]PW_{11}O_{39}]^{5-}\bullet HNO_3$. [e] In the presence of 6.0 mM of $TBANO_3$ and 8.0 mM of *p*-TsOH (equivalent to concentrations in NO_xFePW_{11}). [f] In the presence of 8.0 mM of *p*-TsOH (equivalent to concentrations in $TBA_3H_2NO_xFePW_{11}$). [g] In the presence of 20 mM 2,6-di-*t*-butylpyridine.[18]

The catalytic system consisting only of nitrate and proton shows limited activity under both the conditions detailed in Table 1 (entry 3) and the minimally optimized conditions in Figure 1 (dashed line). In addition, bromide functions as a co-catalyst in the aerobic oxidation of 2-chloroethyl ethyl sulfide (CEES) by this simplified system. In the presence of TBABr, the reaction proceeds approximately two orders of magnitude faster but in a more complicated manner. A significant induction period is observed and the reaction terminates before reaching complete conversion (Figure 1). As in the reference system, the only detectable product is 2-chloroethyl ethyl sulfoxide (CEESO). Addition of $FePW_{11}$ to the nitrate / bromide / proton system does not affect the rate or the yield but considerably increases the induction period of the reaction. Substitution of $FeSiW_{11}$ for $FePW_{11}$ results in a modest but reproducible increase in yield. Significantly, replacement of $FePW_{11}$ with $CuSiW_{11}$ completely eliminates the induction period and increases both the reaction rate and product yield. Further simplification of the system by replacing the $CuSiW_{11}$ with $Cu(ClO_4)_2$ only removes induction period; the yield remains unchanged.[18]

We began performing reactions at elevated temperature to allow for more rapid scanning of conditions, catalysts, and targets to more quickly produce results that would help us identify the processes operating in this system. During the course of the research we quickly observed a dependence of the reaction rates on the partial pressure of oxygen. The reaction rate would slow dramatically accompanied by a decrease in the percent yield as the reaction proceeded and the

air atmosphere in the sealed vessel was depleted of O_2. A pure O_2 atmosphere gave us more consistent results and allowed us to perform analyses more quickly.

Simplified NO_x/Br System

In order to further explore the nature of the catalytic system we modified the precursor materials by eliminating any metals and POMs and carefully observed the subsequent changes in activity. Based on previous work we had observed that $NOPF_6$ alone was not an active catalyst,[1] however the addition of TBABr to the system yielded a highly active mixture (turnover frequency, TOF ~98 h^{-1}, Figure 2). Although the starting materials are colorless in solution, we immediately observed that the catalytic solution became yellow upon mixing. Variation of the ratio of NO^+ to Br^- showed a marked effect on catalytic activity and the spectral properties of the solution (see Figure 4 and related discussions later in this work). An optimized system suggested a mole ratio of NO^+ : Br^- of 1 : 1.5 would yield the best results. The experiments clearly demonstrated the deleterious effects of insufficient or excess bromide on the catalytic activity of the system (Figure 2). We often used a ratio of 1 : 2 when testing various additions to the NO_x/Br system to maintain a consistent basis for comparison.

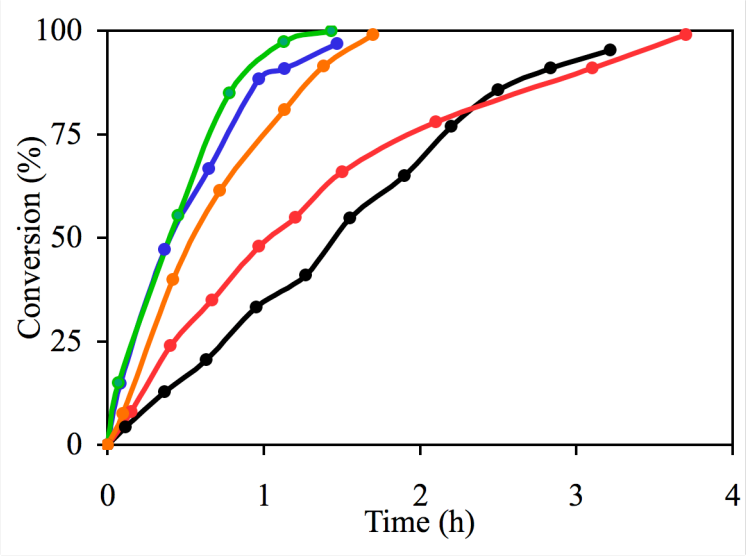

Figure 2. Oxidation of CEES to CEESO by NO_x/Br system with different initial ratios of nitrosonium to bromide. Conversion (%) is calculated from the ratio of CEES to CEESO. Red: 5.0 mM $NOPF_6$, 2.5 mM TBABr; Blue: 5.0 mM $NOPF_6$, 5.0 mM TBABr; Green: 5.0 mM $NOPF_6$, 7.5 mM TBABr; Orange: 5.0 mM $NOPF_6$, 10 mM TBABr; Black: 5.0 mM $NOPF_6$, 20 mM TBABr. Conditions: 3 mL acetonitrile, 30 °C, 1 atm O_2, 100 µL CEES (0.86 mmoles, 286 mM), 100 µL 1,3-dichlorobenzene (DCB, 0.88 mmoles, 292 mM, internal standard).

Initially we believed the color and activity observed to be a result of the formation of highly volatile nitrosyl bromide (Br-N=O or NOBr for simplicity) in acetonitrile solution, however we were only able to identify a UV-Visible absorption near 280 nm. This absorption does not strictly correspond to the values reported in the literature for this compound (a maximum at 210 nm with broad features from 200 to 740 nm).[19, 20] Additionally both positive and negative

ion mode electrospray ionization mass spectrometry revealed only the PF_6^+ and Br^- respectively. Some possible nitrogen-oxide containing species were identified, but their concentrations were so low as to make unequivocal mass assignments impossible. The extremely low concentrations of these fragments indicated that they were a result of the analysis process and were unlikely to be responsible for the catalytic activity observed under turnover conditions. In order to determine if a volatile species, such as NOBr, was responsible for the catalytic activity, freshly prepared catalytic solutions were allowed to "age" in solution in sealed vessels as well as evaporate to dryness. Upon evaporation a yellow-orange residual solid was collected. FT-IR analysis of this solid was inconclusive, showing no discernable nitrogen oxide stretches (the C-H absorptions from the TBA cations overwhelmed the NO_x region). The "aged solution" as well as the dissolved yellow solid showed remarkable catalytic activity (Figure 3) as well as similar characteristic peaks at 280 nm (Figure 4). In fact the "aged" solution showed a higher maximum turnover frequency. This result rules out NOBr as a possible reactive species.

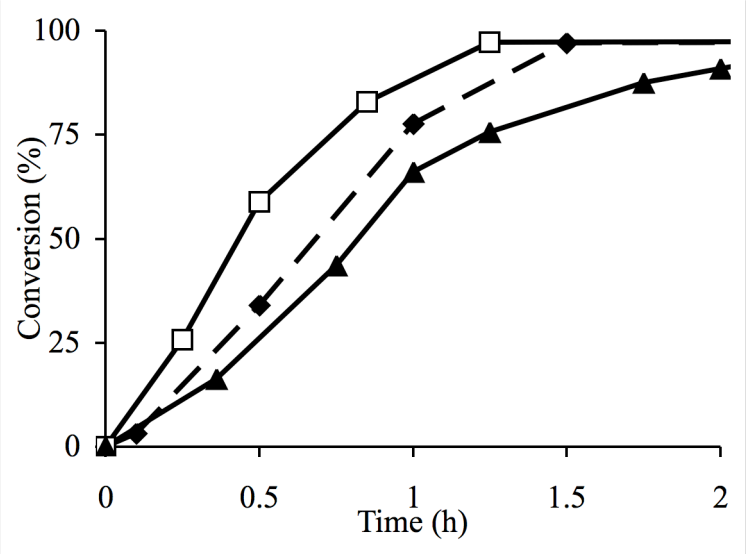

Figure 3. Effects of aging and drying on NO_x/Br system. Conversion (%) is calculated from the ratio of CEES to CEESO. (◆) Fresh 2.5 mM $NOPF_6$, 5.0 mM TBABr; (□) 2.5 mM $NOPF_6$, 5.0 mM TBABr aged in acetonitrile; (□) 2.5 mM $NOPF_6$, 5.0 mM TBABr dried then reconstituted. Conditions: 3 mL of acetonitrile, 30 °C, 1 atm O_2, 100 μL CEES (0.86 mmoles, 286 mM), 100 μL 1,3-dichlorobenzene (DCB, 0.88 mmoles, 292 mM, internal standard).

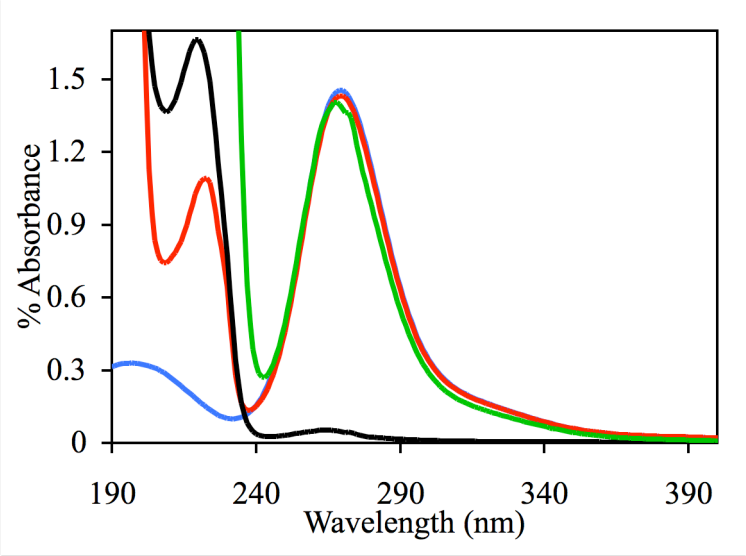

Figure 4. UV-Visible absorption spectra of various NO_x/Br systems. Blue: 0.05 mM $NOPF_6$, 0.1 mM TBABr; Red: 0.05 mM $TBANO_2$, 0.1 mM TBABr, 0.1 mM *p*-TsOH; Black: 0.05 mM $TBANO_3$, 0.1 mM TBABr, 0.1 mM *p*-TsOH, fresh; Green: 0.05 mM $TBANO_3$, 0.1 mM TBABr, 0.1 mM *p*-TsOH, aged.

The reaction mixture is colored (yellow-orange) under turnover conditions. The intensity of color correlates with reaction rates. The spectra of both NO_3^- and NO_2^- catalytic systems recorded in the course of catalytic process are very similar.

Kinetics of NO_x/Br

Unlike mixing $NOPF_6$ and TBABr, mixing of $TBANO_2$ and TBABr in acetonitrile does not result in any immediate color changes. The solution quickly turns dark yellow (absorbancy increases at 290-400 nm) upon addition of *p*-

TsOH. A build up of absorbancy seems to be exponential with typical reaction time < 1 min at 45 °C (under Ar). After absorbancy reaches a plateau, it remains almost constant (less than 10% drop after 1-2 hrs). The spectra of these solutions are the same as obtained by mixing $NOPF_6$ and TBABr. The kinetics of the reaction of this colored species with CEES was studied under Ar at 45 °C. CEES, $TBANO_2$ and TBABr were mixed in a thermostated UV-Vis cell, a solution of acid was injected to start the reaction. The reaction was followed by recording spectra at given time interval using the "kinetic mode" of a UV-Vis instrument. The results of this study showed that the formation of the color-producing species was indeed an exponential process.

The dependence of the sulfoxidation reaction rate on TBABr concentration has a bell-shape with a maximum at ~3 mM TBABr (NO_2^- : Br^- ~ 1 : 6), Figure 5. The initial rate in Figure 3 is ~ 500 mM/h (~0.5 M CEES, ~8 mM NO_x/Br at 30 °C). The kinetics data collected under argon suggest a rate (k[CEES][NO_x/Br]) of ~ 650 mM/h (for k =0.16 (1/mM.h) at 45 °C. There is good agreement between the stoichiometric and catalytic rates.

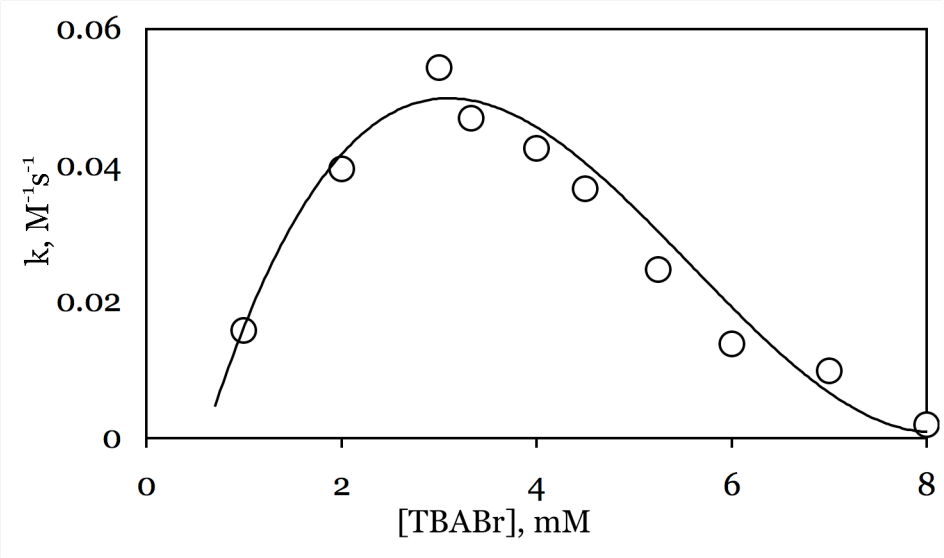

Figure 5. Dependence of stoichiometric reaction rate constant on TBABr concentration. Conditions: 0.5 mM $TBANO_2$; 4 mM *p*-TsOH; 202 mM CEES; 45 °C; Argon.

A mixing of nitrite, bromide and acid in the presence of CEES results in quick increases in absorbance (shown to be exponential, typical reaction times are shorter than 1 min). After reaching a maximum, the absorbance decreases with time. This decrease is also exponential. The apparent rate constants were obtained by fitting the kinetic curve to exponential law. The plot of this apparent rate constant versus [CEES] is a linear function (Figure 6). Thus, the reaction rate law follows Equation 4, where k = 0.044 $M^{-1}s^{-1}$ (~0.16 $mM^{-1}h^{-1}$):

$$-d[NO_x/Br] / dt = k[NO_x/Br][CEES] \quad \text{(Equation 3)}$$

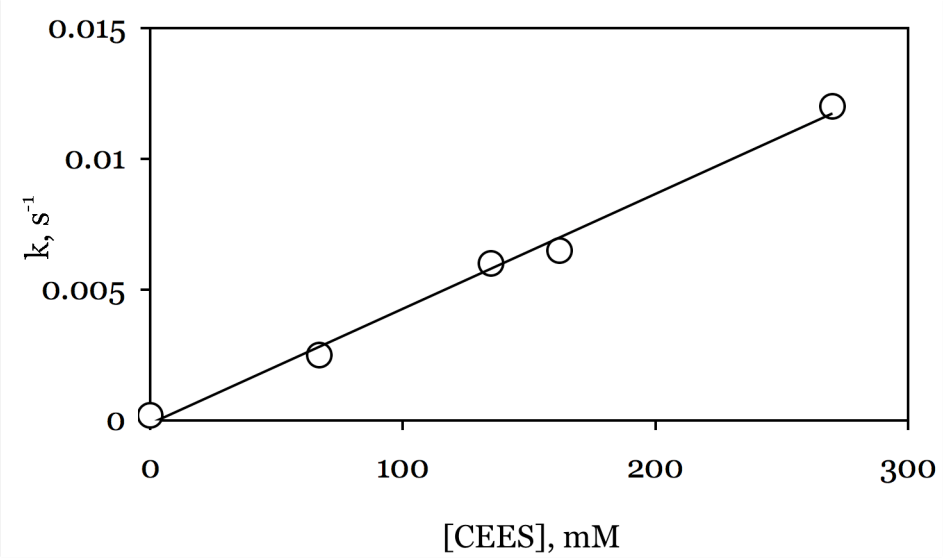

Figure 6. Apparent reaction rate constants for the reaction of NO_x/Br with CEES. Conditions: 0.5 mM $TBANO_2$; 2.0 mM TBABr; 2.0 mM *p*-TsOH; 45 °C; Argon.

Effects of proton on the catalytic system

To explore the effects of acid on the simplified system, we added two equivalents of an organic solvent soluble strong acid, *p*-toluenesulfonic acid. The results showed no appreciable effect (Figure 7). This was in marked contrast to the data reported for the POM systems where addition of acid increased reaction rates.[1, 21] We believe that acid was critical to the conversion of a charged unreactive NO_x species (NO_2^-, NO_3^-, etc) into the catalytically active species in the POM-based system. This hypothesized conversion process lead us to explore other nitrogen oxide sources.

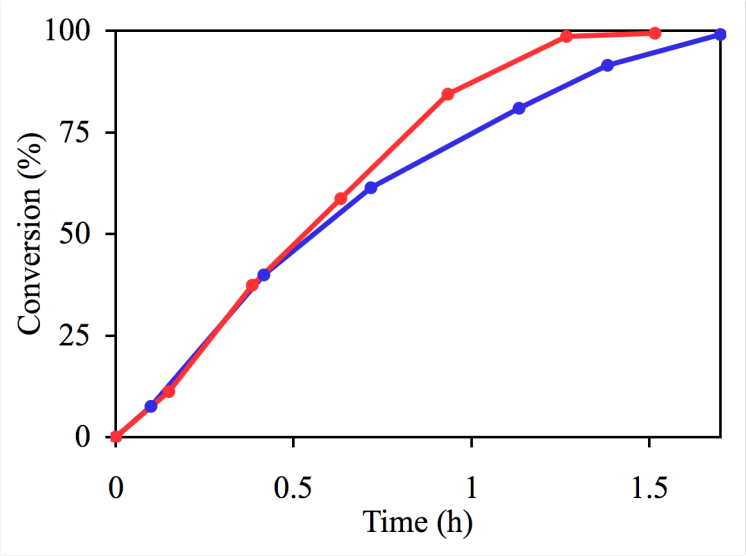

Figure 7. Effect of the addition of acid to $NOPF_6$ / TBABr system. Conversion (%) is calculated from the ratio of CEES to CEESO. Blue: 5.0 mM $NOPF_6$, 10 mM TBABr; Red: 5.0 mM $NOPF_6$, 10 mM TBABr, 10 mM *p*-TsOH. Conditions: 3 mL acetonitrile, room temperature, 1 atm O_2, 100µL CEES (0.86 mmoles, 286 mM), 100 µL DCB (0.88 mmoles, 292 mM).

For systems where $NOPF_6$ was replaced with $TBANO_2$ the rate constant *k* for the stoichiometric reaction decreases with $[RSO_3H]$ at low acid concentrations and then becomes independent at $[RSO_3H] > 2$ mM, Figure 8. Protons are important in facilitating the conversion of some nitrogen oxide species into the active catalyst but as can be seen from the results, only small concentrations are needed.

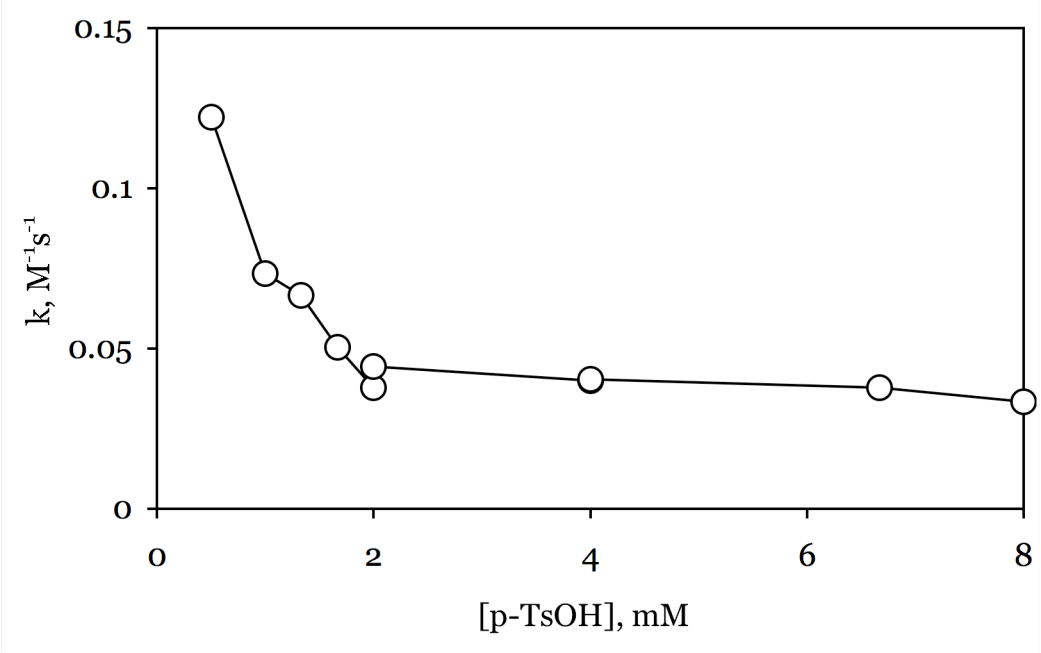

Figure 8. Dependence of reaction rate constant k for aerobic CEES oxidation on *p*-TsOH concentration. For each mole of acid added one mole of water was also introduced since the *p*-TsOH used was the monohydrate from. Conditions: 0.5 mM $TBANO_2$; 2.0 mM TBABr; 45 °C; Argon.

Sources of nitrogen oxides

In addition to $NOPF_6$ we explored other sources of "NO_x", including NO_2^-, in the preparation of a catalytically active system. Nitric oxide has been implicated in a variety of oxidative processes, including catalytic sulfoxidations[6, 8-12, 18, 22-25] leading us to choose this as a likely alternate source of "NO_x" to the hygroscopic and temperature sensitive $NOPF_6$.

The acetonitrile soluble salt, $TBANO_2$ was used to prepare the catalytically active solutions. We observed that neither NO_2^+ nor NO_2^- alone were catalytically active. Furthermore we found that acid must be present in addition to bromide to produce a catalytically active solution. The conversion of the almost clear $TBANO_2$ and TBABr solution to the characteristic yellow occurs immediately (< 5 seconds with mixing). While the non-acidified solutions show no reactivity in the conversion of thioethers to sulfoxides, the activity of the yellow acidified solutions were comparable to that of solutions prepared from $NOPF_6$ and TBABr (Figure 9). Nitrosyl bromide could be generated as an active catalyst in solution *via* the following process:

$$HNO_2 + HBr \rightarrow NOBr + H_2O \quad (4)$$

Our previous work eliminated the possibility of NOBr as a critical part of the reactive processes. To more rigorously quantify the observed correlation between the characteristic yellow color of a catalytic solution and its observed activity we analyzed the UV-Vis spectra of several solutions. The UV-Vis spectrum of a solution of NO_2^- and Br^- is similar to that of the fresh NO_3^- / Br^- / H^+ system. Upon addition of acid, the solution spectrum becomes very similar to that of the $NOPF_6$ / TBABr system (Figure 4). Clearly, despite the method used to produce a catalytically active system, the reactivity and spectral properties are virtually indistinguishable.

As indicated by the UV-Vis data, the use of $TBANO_3$ as a NO_x source was found to be particularly effective but its use resulted in an induction period.

Typically a mixture of $TBANO_3$, TBABr, and *p*-TsOH in acetonitrile was left to stand in overnight. The mixture changed colors from clear, to yellow (Figure 4). Solutions that were prepared without acid showed no color change and did not show catalytic activity. If the mixture was used fresh, that is, before color change occurred, a significant induction period was observed, and CEESO was not detected via GC until the solution had become pale yellow. If the aged solution was used, the solution that was already yellow, catalytic activity was immediate and comparable to solutions prepared from $NOPF_6$ (Figure 9).

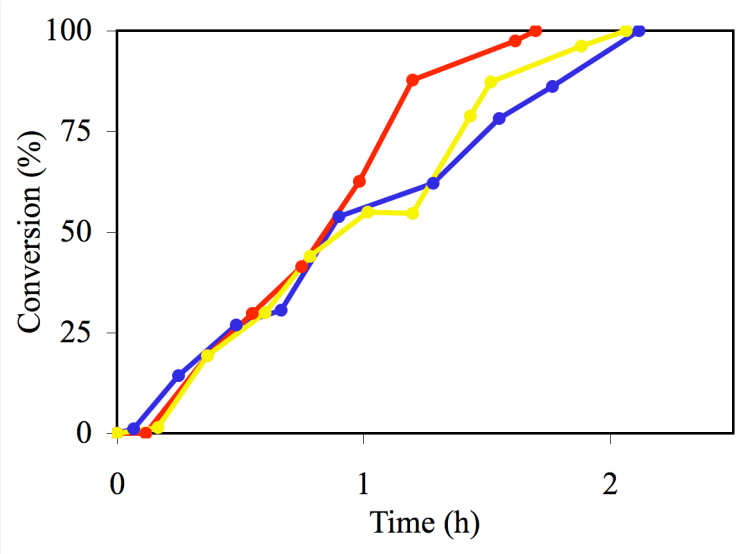

Figure 9. Effects of different nitrogen oxide sources on the catalytic conversion of CEES to CEESO by the NO_x/Br system. Yellow: 2.5 mM $NOPF_6$, 5.0 mM TBABr; Blue: 2.5 mM $TBANO_2$, 5.0 mM TBABr, 5.0 mM *p*-TsOH; Red: 2.5 mM $TBANO_3$, 5.0 mM TBABr, 5 mM *p*-TsOH aged 12 hours. Conditions: 3 mL acetonitrile, 40 °C, 1 atm O_2, 100 µL CEES (0.86 mmoles, 286 mM), 100 µL DCB (0.88 mmoles, 292 mM).

Sources of bromide

Having identified several NO_x sources, we made an effort to explore the effects of different bromide salts. We tested a variety of bromide salts, with both inorganic and organic cations. In order to simultaneously introduce a metal cation in the reactive mixture, we used $TBAFeBr_4$, $NiBr_2$, and $CuBr_2$ as bromide sources. We maintained a NO_x to Br^- ratio of 1 : 2 in all cases. In the initial experiments we used $NOPF_6$ as the NO_x source, but we also tested other previously identified sources of NO_x. The Fe and Ni systems showed no appreciable difference in catalytic activity from the $NOPF_6$ / TBABr system. The copper-based system shows a marked increase in activity (Figure 10). We delved deeper into the Cu-containing system by varying the NO_x source. A mixture of $TBANO_3$, $CuBr_2$, and *p*-TsOH in a 1 : 1 : 2 ratio also showed marked improvements in activity over the standard $NOPF_6$ / TBABr system.

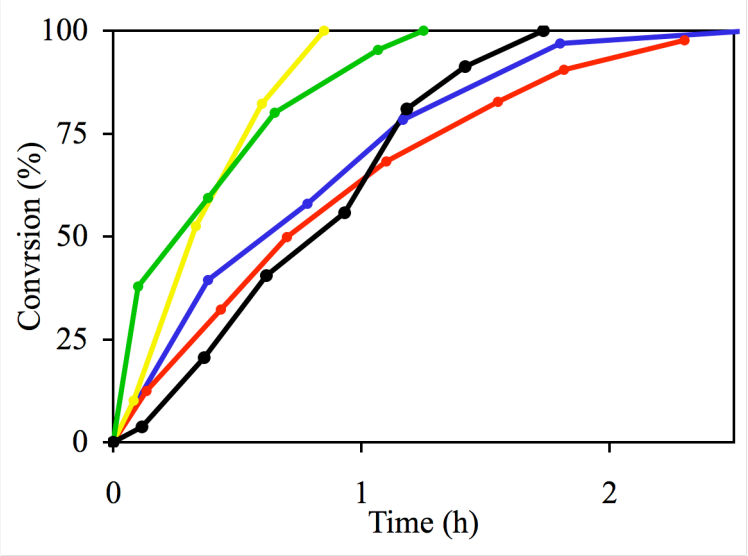

Figure 10. Effects of different transition-metal halides as sources of bromide on the catalytic conversion of CEES to CEESO by the NO_x/Br system. Conversion (%) is calculated from the ratio of CEES to CEESO. Yellow: 2.5 mM $TBANO_3$, 2.5 mM $CuBr_2$, 10 mM *p*-TsOH; Blue: 2.5mM $TBANO_3$, 2.5 mM $NiBr_2$, 5.0 mM *p*-TsOH; Red: 2.5 mM $NOPF_6$, 2.5 mM $NiBr_2$, 10 mM *p*-TsOH; Green: 2.5 mM $TBANO_2$, 2.5 mM $CuBr_2$, 10 mM *p*-TsOH; Black: 2.5 mM $TBANO_3$, 1.3 mM $TBAFeBr_4$, 10 mM *p*-TsOH. Conditions: 3 mL acetonitrile, 100 µL CEES (0.86 mmoles, 286 mM), 100 µL DCB (0.88 mmoles, 292 mM), 1 atm O_2, room temperature.

Effects of transition-metal cations

Since we had already observed that the addition of Cu^{2+} or Fe^{3+} to the NO_x/Br system generally enhances the catalytic activity, we decided to explore the possibility more rigorously. Catalytic mixtures were prepared with copper

and iron salts serving as the sources of nitrate and bromide. Those systems containing $Cu(NO_3)_2$ and $TBAFeBr_4$ showed the greatest turnover frequency. A catalytic system produced by combining these two compounds as the NO_x and Br^- source respectively, achieved the most active system. As expected acid was a critical component, though systems that lacked it still showed some catalytic activity. Those mixed-metal non-acidified systems, while active, did not compare favorably to those systems with acid.

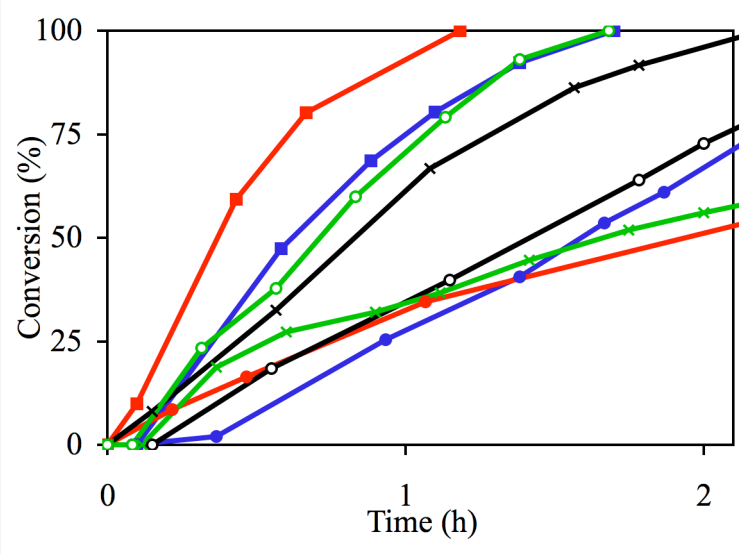

Figure 11. Effects of different transition-metal halide combinations as sources of bromide on the catalytic conversion of CEES to CEESO by the NO_x/Br system. (Red ■): 1.0 mM $Cu(NO_3)_2$, 1.0 mM $TBAFeBr_4$, 2.0 mM, *p*-TsOH; (Blue ■): 0.67 mM $Fe(NO_3)_3$, 1.0 mM $CuBr_2$, 2.0 mM *p*-TsOH; (Red □): 1.0 mM $Cu(NO_3)_2$, 1.0 mM $TBAFeBr_4$; (Blue □): 0.67 mM $Fe(NO_3)_3$, 2.0 mM $CuBr_2$; Black x: 2.0 mM $TBANO_3$, 1.0 $TBAFeBr_4$, 2.0 mM *p*-TsOH; (Black ○): 0.67 $Fe(NO_2)_3$, 4.0 mM TBABr, 2.0 mM *p*-TsOH; (Green x): 2.0 mM $TBANO_3$, 2.0 $CuBr_2$, 2.0 mM *p*-TsOH; (Green ○): 1.0 mM $Cu(NO_3)_2$, 4.0 mM TBABr, 2.0 mM *p*-TsOH. Conditions: 3 mL acetonitrile, 1 atm O_2, 40 °C, 50 µL tetrahydrothiophene (THT, 0.57 mmoles, 189 mM), 50 µL DCB (0.38 mmoles, 128 mM).

Color changes in copper containing systems

While developing the various Cu^{2+} containing systems, we observed a series of color changes. The initial color of the $NOPF_6$ / $CuBr_2$ system was dark green, the same color as an equally concentrated solution of $CuBr_2$. Over the course of 5 minutes the solution turned yellow, almost identical to the color of the $NOPF_6$ / TBABr system. Upon addition of CEES the solution immediately turned to a very dark green, almost black color. As the reaction progressed the color faded until it was again pale yellow. The return of the pale yellow color coincided with the total conversion of CEES to CEESO. When a catalytic system is prepared from $TBANO_3$, $CuBr_2$, and *p*-TsOH in a 1 : 1 : 2 ratio, the initial green color persists for about 20 minutes. The color change is nearly instantaneous if a small portion of $TBANO_2$ is added to the solution. Once the yellow color has formed the addition of CEES effects a rapid change to very dark green or black. This color is only persistent as long as there is CEES in the system. As with the $NOPF_6$ / $CuBr_2$ system, the yellow color returns when all the CEES is consumed, as detected by GC. While the intense black and green colors overwhelmed any attempts to identify the indicative absorption at 280 nm, we were able to identify this peak in the yellow solutions.

Effects of bromide replacement

Having focused strictly on sources of bromide, attempts were made to replace Br^- with another anion. The results in Table 2 show that, of the anions tested, only bromide leads to active systems. Particularly interesting was the fact that Cl^- showed very little activity. Based on the literature we had expected to see

some catalytic activity from the NO_x/Cl system. Evidently the system we created is not the same as those previously used for nitrosation and other oxidative reactions.[26, 27]

Table 2. Conversion of CEES to CEESO by catalytic systems with varying NO^+ counterions

	Catalyst[a]	*Conversion (%)*[b]	*TON*[c]
1	TBACN	0	0.0
2	TBACl	4	0.2
3	LiBr	45	2.6
4	KBr	100	5.8
5	NH_4Br	100	5.8
6	THABr[d]	100	5.8
7	*p*-TsOH	2	0.1
8	TBASCN	3	0.2
9	TBAI	0	0.0
10	Domiphen Bromide[e]	50	2.9
11	$NiBr_2$	100	5.8
12	$CuBr_2$	100	5.8
13	$TBAFeBr_4$	100	5.8

[a] 5 mM $NOPF_6$, 10 mM X^-, 3 mL acetonitrile, 1 atm O_2, room temperature, 100 μL CEES; [b] percent of sulfide converted to sulfoxide after 1 hour; [c] turnover number = (moles of sulfide / moles of catalyst); [d] tetraheptylammonium; [e] (dodecyldimethyl-2-phenoxyethyl)ammonium.

Solid-supported NO_x/Br systems

Efforts to develop a NO_x/Br-type system on various solid supports for heterogeneous catalysis have met with little to no success. Initially we added solid $K_5SiW_{12}O_{40}$ to a solution of $NOPF_6$ and TBABr, prepared using the standard procedure that was confirmed to be catalytically active. We tested the POM added system for activity in the aerobic oxidation of CEES, however after 24 hours we detected no oxidation product (CEESO). We also tested the effects of $Na_5AlW_{12}O_{40}$ and $Na_3PMo_{12}O_{40}$. Surprisingly, both POMs resulted in a dramatic reduction of activity, to the point where only trace amounts of sulfoxide were detected after 24 hours at 40 °C under 1 atm O_2.

We proceeded to screen several polyoxometalate systems for activity. $TBA_6Mn^{II}SiW_{11}O_{39}$, $TBA_6Ni^{II}SiW_{11}O_{39}$, $TBA_6Co^{II}SiW_{11}O_{39}$, $TBA_6V^{V}SiW_{11}O_{40}$, $TBA_6Mn^{III}AlW_{11}O_{39}$, and $TBA_7Co^{II}AlW_{11}O_{39}$ all showed a decrease in activity from the base $NOPF_6$/TBABr system. It was apparent that any additive in the form of a POM eliminated any activity of the NO_x/Br system with respect to sulfide oxidation.

We explored the possibility of depositing or adsorbing a catalyst mixture onto various materials due to the failure of the POM based supports. Catalytic solutions were incubated with potential support materials TiO_2, Al_2O_3 and SiO_2. The suspensions were filtered. The TiO_2 and Al_2O_3-containing samples remained white powders, but the SiO_{23}-containing sample changed from white to a faintly

yellow color. The solids were suspended in toluene and sulfide (CEES) was introduced. After 24 hours the titania and alumina systems showed no evidence of sulfoxide. The silica system, however, showed complete conversion after 2 hours. We observed leaching of the yellow color from the SiO_2 solid into the toluene solution. We tested the filtrates of the TiO_2 and Al_2O_3 systems and observed these to be very active. We concluded that the NO_x/Br catalyst did not adsorb on TiO_2 and Al_2O_3 but did adsorb slightly on SiO_2. Unfortunately leaching of the NO_x/Br precluded realization of a heterogeneous catalyst system.

Based on our positive observations of some binding of the NO_x/Br catalyst to the silica, we attempted to use functionalized silica gel as a solid support. Previously Zolfigol and co-workers had reported a system for the heterogeneous oxidation of pyridines and disulfides using sulfuric acid-modified silica and $NaNO_2$.[17, 28, 29] We used sulfuric acid-modified silica as the acid source when preparing solutions of catalyst from $TBANO_2$ and $TBANO_3$ with TBABr. The solutions turned yellow as we had observed when using *p*-TsOH as the acid, and in acetonitrile solvent the conversion of sulfide to sulfoxide proceeded similarly to the reaction under the standard catalytic solutions. However, as with our previous experiences with SiO_2 we were unable to produce a solid supported catalyst that did not display obvious leeching of the chromophoric catalytically active components in reactions where toluene or hexane was the solvent. Clearly the source of the yellow color, which is directly related to the active catalyst species, does not strongly bind to any to silica we tested, and the observed reactions were not truly solid-liquid heterogeneous reactions.

Exploring heterogeneous catalytic systems

Based on the observed leeching in the attempted heterogeneous systems, catalytic solutions were prepared and shown to be active in solvents far less polar than acetonitrile (hexane, toluene). As the solid-liquid heterogeneous catalytic systems failed, we developed a method for testing solid-gas heterogeneous systems for activity. The catalyst was prepared in solution and then allowed to evaporate on a glass dish to form a yellow solid. This dish was placed in the gas reactor and liquid samples of dimethyl sulfide or propane thiol were aspirated into the sealed chamber. Because the oxidized products are far less volatile, we were only able to monitor the consumption of sulfide or thiol relative to an internal standard. Rinsing the inside of the chamber with acetonitrile and then analyzing the solution via gas chromatography detected some products. Experiments showed only limited activity in the conversion of dimethyl sulfide to dimethyl sulfoxide. We attribute this primarily to the very low surface area of the solid catalyst. These supported catalysts from depositing the heterogeneous NO_x/Br system on a variety of materials showed no activity in the gas reactor. Solid silica, alumina and titania were all tested as potential supports for the NO_x/Br catalyst. These composite materials failed to show any activity for the conversion of thiol to disulfide in a gas-solid heterogeneous system. As stated above only the NO_x/Br-silica material showed any activity for the conversion of thiol to disulfide in a liquid-solid system. We postulate that the application of the NO_x/Br on the surface of these supports either destroys the active catalyst, or prevents any process that might lead to formation of the active catalyst. Leeching of the NO_x/Br from the silica material and the subsequent activity observed in

this system supports the hypothesis that a solid support sequesters the active catalyst in the NO_x/Br system and prevents any catalytic activity.

Conclusion

The NO_x/Br system developed is a highly active oxidation catalyst for the conversion of sulfides to sulfoxides under mild conditions. The catalyst is selective as no detectable sulfone is produced. Over-oxidation of thioethers, i.e. conversion of the initial sulfoxide to the sulfone, is often a competing reaction,[30-32] and is best avoided due to the toxicity of the sulfone ($CEESO_2$ in particular).[33, 34] It was established that the catalytic activity is highly dependent on the presence of bromide ion. Furthermore the ratio of bromide to NO_x was shown to be critical for optimal activity; this phenomenon has not been documented previously.

By studying the $NOPF_6$ / TBABr system we were able to rule out an acid dependence of the actual catalytic reaction, since addition of acid had no appreciable affect on catalytic activity. When studying systems that did not use $NOPF_6$ as the NO_x source, however, acid was proven to be critical in facilitating conversion of the initial nitrogen oxide (nitrate, nitrite) into the catalytically active species. We have determined that HNO_2 and HNO_3 do not catalyze sulfoxidations under our experimental conditions in the absence of bromide. Because of the observed acid independence of the $NOPF_6$ / TBABr system, we have shown that acid allows for the transformation of either NO_2^- or NO_3^- into a species that can then react with bromide to form the active catalyst in solution.

In order to explain the observed catalytic activity of NO_xFePW_{11}, it is possible that under turnover conditions, hydrogen dinitrate is the nitrogen oxide source, bromide could be present from the salts used to synthesize the POM, and the acidity of the POM itself could facilitate production of the active catalyst.

When proposing possible active intermediates for our systems we eliminated the possibility that a volatile compound, namely NOBr, is the active catalyst based on spectroscopic data and by demonstrating that the aged and dried catalytic solutions retain active when solvent is subsequently re-introduced. Figure 12 shows the intermediate proposed by Bosch and Kochi wherein N_2O_4 disproportionates in the presence of sulfide:

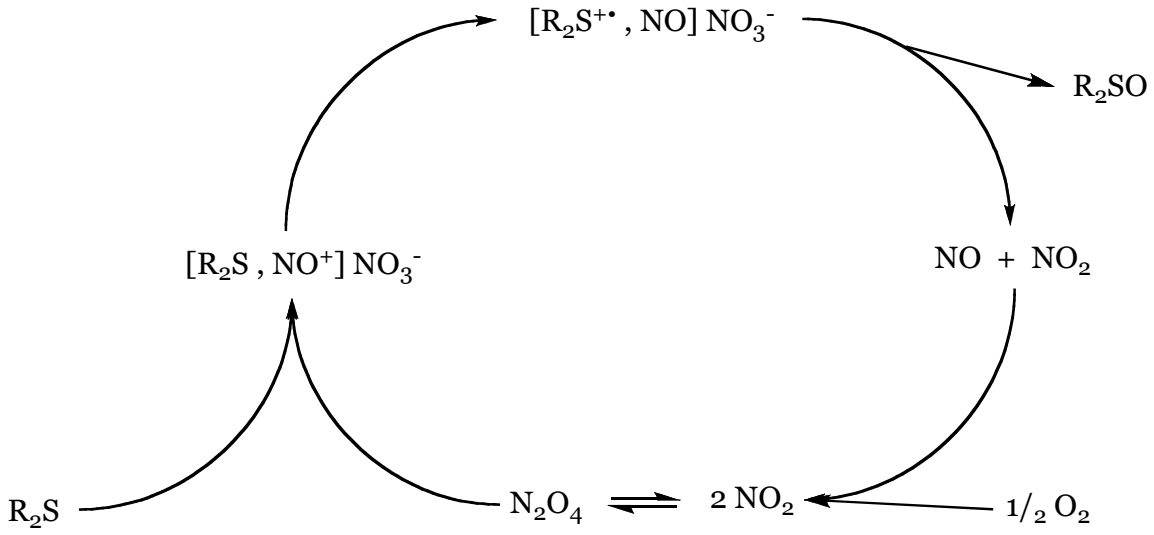

Figure 12. Proposed catalytic cycle for the conversion of sulfides to sulfoxides by N_2O_4.[12]

The intermediate is proposed to decompose to a thioether cation radical followed the oxidation of NO by molecular oxygen.[12] While these components are present in our system, we never directly add NO_2. Furthermore, as both NO_2 and N_2O_4 are gases at room temperature, it is difficult to explain why our materials do not show significant decreases in activity upon standing or drying and upon re-dissolving the residual dried yellow material. Lastly, this scheme fails to explain the key role of bromide that we have observed. Nitryl bromide ($BrNO_2$) is an extremely reactive species and as been implicated in high altitude atmospheric oxidation of dimethylsulfide. However $BrNO_2$ is not stable at room temperature under 1 atmosphere of pressure and rapidly decomposes to molecular bromine and nitrogen dioxide[35], suggesting that this compound is not responsible for the catalysis we observe.

While studying the kinetics of the nitric acid oxidation of sulfides, Ogata and Kamei observed that the system behaved differently under N_2 atmosphere than when molecular oxygen was present. They further observed an induction period, which could be eliminated by the addition of nitrite. They found the kinetics of the reaction is first order in nitrous acid. They postulated that the reactive species N_2O_2 exists in equilibrium according to Equation 5. Dinitrogen dioxide reacts with acid to produce $HN_2O_2^+$ which then transfers an oxygen atom to the sulfide.[9]

Scheme 1

$$4\,H^+ + HNO_3 + HNO_2 \leftrightarrows N_2O_2 + H_2O$$

$$N_2O_2 + H^+ \leftrightarrows HN_2O_2^+$$

$$2H_2O + R_2S + HN_2O_2^+ \rightarrow R_2SO + N_2O_3 + 5\,H^+$$

$$N_2O_3 + H_2O \leftrightarrows 2\,HNO_2$$

While Scheme 1 could certainly help explain some of the complex reactions likely to be occurring in our solutions, it does not account for the clear bromide dependence we observe.

While we have not conclusively identified the reactive intermediate, we continue to explore the NO_x/Br system in an attempt to discover the nature of the catalyst.

References

1. Okun, N. M.; Tarr, J. C.; A., H. D.; Zhang, L.; Hardcastle, K. I.; Hill, C. L., Highly Reactive Catalysts for Aerobic Thioether Oxidation. The Fe-substituted Polyoxometalate/hydrogen Dinitrate System. *J. Mol. Catal. A. Chem.* **2006,** 246, 11-17.
2. Pummerer, R., *Chemische Berichte* **1910,** 136, 75.
3. Goheen, D. W.; Bennett, C. F., *J. Org. Chem.* **1961,** 26, 1331.
4. Robert Louw; Hans P. W. Vermeeren; Asten, J. J. A. v.; Ultée, W. J., Reaction of sulphides with acyl nitrates; a simple and rapid method for preparing sulphoxides. *J. Chem. Soc., Chem. Commun.* **1976,** 13, 496 - 497.
5. George A. Olah, B. G. B. G., Subhash C. Narang, Onium ions. 20. Ambident reactivity of the nitronium ion. Nitration vs. oxidation of heteroorganic (sulfur, selenium, phosphorus, arsenic, antimony) compounds. Preparation and NMR spectroscopic (carbon-13, nitrogen-15, phosphorus-31) study of nitro and nitrito onium ions. *J. Am. Chem. Soc.* **1979,** 110, (18), 5317-5322.
6. Ogata, Y.; Tezuka, H.; Sawaki, Y., Kinetics of the nitric acid oxidation of benzaldehydes to benzoic acid. *Tetrahedron* **1967,** 23, (2), 1007-1014.
7. Park, J. R.; Williams, D. L. H., Kinetics of the reactions of nitrous acid with olefins. Kinetic identification of probable nitrosating agents. *J. Chem. Soc., Perkin Trans. 2* **1972,** 14, 2158-2163.

8. Naik, R.; Pasha, M. A., DMSO/$NaNO_2$/49% HBr: A Novel and Powerful Oxidant for the Direct Conversion of Primary Benzylamines to Benzoic Acids. *Synth. Commun.* **2006,** 36, 165-168.

9. Ogata, Y.; Kamei, T., Kinetics of the nitric acid oxidation of sulfides to sulfoxides. *Tetrahedron* **1970,** 26, (24), 5667-5674.

10. Rossi, L. I.; Suárez, Á. R., Transition metal halides as catalysts in the oxidation reaction of sulfides into sulfoxides. *Sulful Letters* **2002,** 25, (4), 123-127.

11. Bosch, E.; Kochi, J. K., Catalytic oxidation of chlorpromazine and related phenothiazines. Cation radicals as the reactive intermediates in sulfoxide formation. *J. Chem. Soc., Perkin Trans. 1* **1995,** 8, 1057-1064.

12. Bosch, E.; Kochi, J. K., Selective Catalysis of Thioether Oxidations with Dioxygen. Critical Role of Nitrosonium EDA Complexes in the Thermal and Photochemical Transfer of Oxygen Atom from Nitrogen Oxides to Sulfur Centers. *J. Org. Chem.* **1995,** 60, (10), 3172-3183.

13. Lide, D. R., *CRC Handbook of Chemistry and Physics*. 81 ed.; CRC Press: Boca Raton, FL, 2000.

14. Lengyel, I.; Nagy, I.; Bazsa, G., Kinetic Study of the Autocatalytic Nitric Acid-Bromide Reaction and Its Reverse, the Nitrous Acid-Bromine Reaction. *J. Phys. Chem.* **1989,** 93, 2801-2807.

15. Tézé, A.; Hervé, G., α-, β-, and γ-Dodecatungstosilicic Acids: Isomers and related Lacunary Compounds. In *Inorganic Syntheses*, Ginsberg, A. P., Ed. John Wiley and Sons: New York, 1990; Vol. 27, pp 85-96.

16. Zonnevijlle, F.; Tourné, C. M.; Tourné, G. F., Preparation and Characterization of Heteropolytungstates Containing group 3A Elements. *Inorg. Chem.* **1982,** 21, (7), 2742-2750.

17. Zolfigol, M. A., Silica sulfuric acid/NaNO2 as a novel heterogeneous system for production of thionitrites and disulfides under mild conditions. *Tetrahedron* **2001,** 57, (46), 9509-9511.

18. Hill, C. L.; Okun, N. M.; Hillesheim, D. A.; Geletii, Y. V., Catalysts for Aerobic Decontamination of Chemical Warfare Agents Under Ambient Conditions. In *Polymers and Materials for Anti-Terrorism and Homeland Defense, ACS Symposium Series, Third Ed.*, Reynolds, J. G.; Lawson, G. E., Eds. American Chemical Society: Washington, D.C., 2006.

19. Houel, N.; Bergh, H. V. d., Bromine nitrogen oxide (BrNO) : thermodynamic properties, the ultraviolet/vis spectrum, and the kinetics of its formation. *International Journal of Chemical Kinetics* **1977,** 9, (6), 867-874.

20. Loock, H.-P.; Qian, C. X. W., Photodissociation studies on nitrosyl bromide: I. Photofragment spectroscopy and electronic structure. *J. Chem. Phys.* **1998,** 108, (8), 3178-3186.

21. Hill, C. L.; Anderson, T. M.; Han, J.; Hillesheim, D. A.; Geletii, Y. V.; Okun, N. M.; Cao, R.; Botar, B.; Musaev, D. G.; Morokuma, K., New complexes and materials for O_2-based oxidations. *J. Mol. Catal. A: Chem.* **2006,** 251, 234-238.

22. Geletii, Y. V.; Musaev, D. G.; Khavrutskii, L.; Hill, C. L., Peroxynitrite Reactions with Dimethylsulfide and Dimethylselenide: An Experimental Study. *J. Phys. Chem. A* **2004,** 108, 289-294.

23. Shafirovich, V.; Lymar, S. V., Nitroxyl and its anion in aqueous solutions: Spin states, protic equilibria, and reactivities toward oxygen and nitric oxide. *PNAS* **2002,** 99, (11), 7340-7345.

24. Crookes, M. J.; Roy, P.; Williams, D. L. H., Nitrosation of acetylacetone (pentane-2,4-dione) and some of its fluorinated derivatives. *J. Chem. Soc., Perkin Trans. 2* **1989,** 8, 1015-1019.

25. Masashi Hojo, T. U., Chihiro Daike, Fumiko Takezaki, Yumi Furuya, Kiyomi Miyamoto, Akio Narutaki and Ryosuke Kato, Great Enhancement in the Oxidation Ability of Dilute Nitric Acid in Nanoscale Water-Droplets of Reverse Micelle Systems. *Bulletin of the Chemical Society of Japan* **2006,** 76, (8), 1215-1222.

26. Williams, D. L. H., Indirect method for the determination of the reactivity of amines and other compounds towards nitrosyl chloride. *Chemical Communications* **1974,** 9, 324-325.

27. Gowenlock, B. G.; Richter-Addo, G. B., Preparations of C-Nitroso Compounds. *Chem. Rev.* **2004,** 104, 3315-3340.

28. Zolfigol, M. A.; Shirini, F.; Choghamarani, A. G.; Mohammadpoor-Baltork, I., Silica modified sulfuric acid/NaNO2 as a novel heterogeneous system for the oxidation of 1,4-dihydropyridines under mild conditions. *Green Chemistry* **2002,** 4, (6), 562-564.

29. Zolfigol, M. A.; Torabi, M.; Mallakpour, S. E., Silica chloride/NaNO2 as a novel heterogeneous system for the oxidation of urazoles under mild conditions. *Tetrahedron* **2001,** 57, (39), 8381-8384.

30. Drabowics, J.; Kielbasinski, P.; Mikolajczyk, M., In *The Chemistry of Sulphones and Sulphoxides*, Patai, S.; Rappoport, Z.; Stirling, C. J. M., Eds. John Wiley: New York, 1988.

31. Capozzi, G.; Drabowicz, J.; Kielbasinski, P.; Menichetti, S.; Mikolajczyk, M.; Nativi, C.; Schank, K.; Schott, N.; Zoller, U., *The Syntheses of Sulphones, Sulphoxides and Cyclic Sulphides: Updates from the Chemistry of Functional Groups*. John Wiley & Sons: Chichester, 1994; p 720.

32. Drabowicz, J.; Kielbasinski, P.; Mikolajczyk, M., Synthesis of sulphoxides. In *Syntheses of Sulphones, Sulphoxides and Cyclic Sulphides*, Patai, S.; Rappoport, Z., Eds. John Wiley & Sons: Chichester, 1994; pp 529-648.

33. Anslow, J., W. P.; Karnofsky, D. A.; Val Jager, B.; Smith, H. W., *J. Pharmacol. Exp. Ther.* **1948,** 93, 1-9.

34. Hirade, J.; Ninomiya, A., Effects of the Oxidation of Vesicants on Their Blistering Capacity. *J. Biochem. (Tokyo)* **1950,** 37, 19-26.

35. Scheffler, D.; Grothe, H.; Willner, H.; Frenzel, A.; Zetzsch, C., Properties of Pure Nitryl Bromide. Thermal Behavior, UV/Vis and FTIR Spectra, and Photoisomerization to trans-BrONO in an Argon Matrix. *Inorg. Chem.* **1997,** 36, (3).

Decomposition of γ-$[(SiO_4)W_{10}O_{28}(OH)_4]^{4-}$ as a Pathway to an Active Catalyst in Hydrogen Peroxide-based Homogeneous Epoxidations

Abstract

The selective, green, catalytic epoxidation of alkenes is highly desirable because epoxides are key for manufacture of resins, adhesives, coatings, and pharmaceutical intermediates. The organic-solvent-soluble tetra-*n*-butylammonium salt of $[\gamma\text{-}SiW_{10}O_{32}(OH)_4]^{4-}$ (**1**) was shown to be the precursor of an active species that catalyzes oxygen transfer from aqueous H_2O_2 to olefins. Complex **1** transforms under the reaction conditions to a stable diperoxo species $[\gamma\text{-}SiW_{10}O_{32}(O_2)_2]^{4-}$, which has been isolated and shown to be inactive toward oxygen transfer. As infrared spectroscopy was inconclusive in distinguishing the various POM species, UV-Visible spectroscopy was used to monitor changes in POM speciation. An acid dependent H_2O_2-based reaction is believed to generate the active catalyst in solution *via* decomposition. A catalyst assembled in situ from monomeric components (TBA_2WO_4, $HClO_4$) exhibits a similar rate but a slightly different epoxidation regioselectivity relative to **1**.

Introduction

The epoxidation of olefins is an important large-scale industrial technology used in the production of a variety of materials from resins and coatings to pharmaceutical intermediates.[1, 2] The principle processes currently used to transform olefins remain non-catalytic, such as the chlorohydrin process, or employ non-green oxidants, such as organic peroxides in the Halcon-Arco process.[3-5] Catalytic systems that proceed in high selectivity at high conversion using a green oxidant continue to be of considerable intellectual and practical interest. Hydrogen peroxide is an ideal oxidant because it is inexpensive, easily handled, has high oxygen content, and only produces water as a byproduct. These are common traits for all green oxidants; atom efficient, high percentage of active oxygen, produce only water (or nothing in the case of dioxygenase stoichiometries with O_2). Publications addressing many types of catalysts for hydrogen peroxide and O_2 based epoxidations are plentiful.[1, 6-12] Mizuno, *et. al.* reported the selective and efficient H_2O_2-based epoxidation of olefins catalyzed by the polyoxometalate (POM), $[\gamma\text{–}SiW_{10}O_{36}]^{8-}$.[13]

In a subsequent paper Mizuno, *et. al.* reported that a stable diperoxo species, $TBA_4[\gamma\text{-}SiW_{10}O_{34}(O_2)_2]$, is produced under reaction turnover conditions. They state this compound is activated by acid and peroxide (with peroxide potentially serving as an acid) to form the active species that catalyzes oxygen transfer.[14] Herein, we attempt to determine more accurately the nature of the active species, and the pathway by which it forms.

Experimental

Instrumentation

Transmission infrared spectra (3–5 wt. % in KBr) were recorded on a Thermo Electron Corporation Nicolet 6700 FTIR spectrometer. Catalytic reactions were monitored with a Hewlett-Packard 5890 GC equipped with a HP-5 capillary column (poly(5% diphenyl/95% dimethylsiloxane) and an FID detector. Single and time dependent UV-Vis spectra were acquired using a Hewlett-Packard 8452A diode array spectrophotometer. Aqueous pH measurements were performed using an Orion 230 Aplus pH and ISE meter equipped with an Orion Ross Combination pH electrode. Solution ^{1}H NMR spectroscopic measurements were made on a Varian INOVA 400 MHz spectrometer and resonance signals were referenced to residual solvent signals. Solution ^{29}Si NMR spectroscopic measurements were made on a Varian INOVA 400 MHz spectrometer with AutoProbe pre-shimmed using a ^{29}Si standard. Thermogravimetric measurements were performed on an ISI TGA-1000. Electrospray mass spectra were acquired on a Thermo Finnigan LTQ-FTMS in both positive and negative ion modes.

Materials

All chemicals were reagent grade and used as received from commercial sources unless otherwise specified. Concentrations of H_2O_2 in aqueous stock solutions were determined by UV-Vis spectroscopy, using $\varepsilon_{254} = 19.6 \pm 0.3\ M^{-1}cm^{-1}$ [this value was found at www.h2o2.com, a site maintained by US Peroxide]. A column with neutral AlO_3 was used to purify olefins before use in reactions.

Synthesis of $K_8[\beta_2\text{-}SiW_{11}O_{39}]$

Based on the literature procedure,[15] an aqueous solution of Na_2SiO_3 (11g, 50 mmol) was added to an acidified aqueous solution (470 mL of 1.4 M HCl) of Na_2WO_4 (182 g, 550 mmol). The pH was adjusted to 5.5 and maintained for 90 minutes by addition of 4 M HCl. The precipitate, collected by addition of excess KCl, was redissolved and the solution filtered to remove solids. Excess KCl was again added and the resulting precipitate collected and dried under suction to yield 77.25 g of solid (47.5% yield). Molecular weight of $K_8[\beta_2\text{-}SiW_{11}O_{39}]\bullet 14H_2O$: 3239.3 g/mol. FT-IR (KBr): 991.15, 948.66, 876.05 (very strong), 855.91 (very strong), 806.75, 722.86, 868.16 (weak, shoulder), 620 (very broad, shoulder), 530 cm^{-1}.

Synthesis of $K_8[\gamma\text{-}SiW_{10}O_{36}]$

Based on the literature procedure,[15] 10 g $K_8[\beta_2\text{-}SiW_{11}O_{39}]$ (3.1 mmol) was dissolved in water and the solution filtered. The pH was adjusted to 9.1 was maintained for 15 minutes by addition of aqueous K_2CO_3. Addition of an excess of KCl followed by filtration and air-drying yielded 6.73 g of white solid (68.8% yield). Molecular weight of $K_8[\gamma\text{-}SiW_{10}O_{36}]\bullet 12H_2O$: 3155.3 g/mol. FT-IR (KBr) : 987.52, 941.82 (strong), 902.86, 863.10 (very strong), 816.71 (strong), 738.38 (very strong), 660 (broad), 558.61 (weak), 529.8 (broad), 480 (weak) cm^{-1}.

*Synthesis of $TBA_4[\gamma\text{-}SiW_{10}O_{32}(OH)_4]$ (**1**)*

Closely following the procedure in Mizuno *et. al.*,[1] an organic soluble form of $[\gamma\text{-}SiW_{10}O_{36}]^{8-}$ was synthesized. The potassium salt (7 g, 2.2 mmol) was initially dissolved in 25 mL of deionized water, the solution acidified to pH 2 with

dilute nitric acid and stirred for 15 minutes. A solution of TBABr (14 g, 44 mmol) in 10 mL of water was quickly added, and the resulting precipitate collected via suction filtration (5 g, 66 % yield). Purification was performed by slow addition of water to a concentrated acetonitrile solution of **1**, followed by isolation of the solid by suction filtration. TGA analysis showed no weakly associated water molecules (Figure S1). Molecular weight of $[(C_4H_9)_4N]_4[\gamma\text{-}SiW_{10}O_{32}(OH)_4]$: 3416.4 g/mol. $TBA_3SiW_{10}O_{34}^{1-}$ was identified in the mass spectrum. FT-IR (KBr): 1152 (weak), 1107 (weak), 1060 (weak), 1025 (shoulder), 1003.07 (weak), 962.7 (strong), 924 (shoulder), 906.99 (very strong), 876.79 (shoulder), 786.44 (very strong), 738.80, 687.51 (strong), 564.35 (shoulder), 545.6 (broad) cm^{-1}.

*Synthesis of $TBA_4[\gamma\text{-}SiW_{10}O_{32}(O_2)_2]$ (**2**)*

Closely following the procedure in Mizuno *et. al.*,[1] isolation of the diperoxo species was performed by addition of 50% H_2O_2 (225 μL, 3 mmol) to a cold solution of **1** (0.5 g, .15 mmol) in 10 mL of acetonitrile. The mixture was stirred for 2 hours at 0 °C. Addition of 40 mL of diethyl ether produced immediate precipitation of a while solid that was collected via suction filtration (0.49 g, 98% yield). TGA analysis showed no weakly associated water molecules (Figure S2). Molecular weight of $[(C_4H_9)_4N]_4[\gamma\text{-}SiW_{10}O_{32}(O_2)_2]$: 3412.3 g/mol. FT-IR (KBr): 1150 (weak), 1107 (weak), 1086.2, 1060 (weak), 1026 (shoulder), 1005.6, 965.91 (strong), 919 (shoulder), 907.91 (very strong), 883 (shoulder), 799 (strong, broad), 740 (broad, shoulder), 667.9 (broad), 550 (board) cm^{-1}.

Synthesis of TBA_2WO_4

Based on the literature procedure,[16] solid $WO_3 \cdot H_2O$ (13 g, 51 mmol) was added in ~2 g increments to an 80 °C solution of 285 mL aqueous TBAOH (0.35 M). The reaction was stirred continuously for about 30 minutes. After cooling to room temperature and filtering, the solution was dried on a rotary evaporator to produce a slurry which was subsequently dried in a vacuum oven to afford a white hygroscopic solid (30 g, 80% yield). Molecular weight of $[(C_4H_9)_4N]_2WO_4$: 732.77 g/mol. FT-IR (KBr): 1152.11, 1106 (weak), 1059 (broad), 1029, 1007 (weak), 883.44, 794.58 (very strong), 740.20 cm^{-1}.

*Oxidation with hydrogen peroxide catalyzed by **1***

Typically a 28 mL glass vial was equipped with a magnetic stir bar, charged with solid prescribed amounts of **1**, alkene, 50% aqueous H_2O_2, and decane as internal standard and brought to ~3 mL volume with acetonitrile. The vial was then sealed with a septum cap and placed in a water bath maintained at 40.5 ± 1 °C. Aliquots are withdrawn with a syringe at given intervals and assayed via gas chromatography. In the case of the R-(+)-limonene reaction, the ratio of 8,9-epoxide to total epoxides (1,2-epoxide and 8,9-epoxide) was determined from integrated peak areas on the GC traces.

Determination of oxygen equivalents

An iodometric method was used to quantify the oxygen oxidizing equivalents. A mixture of 1 mL of TBAI (10 mM in acetonitrile), 1 mL of acid (0.15 M $HClO_4$ in glacial acetic acid), and 1 ml of **2** (2.2 mM in acetonitrile) were combined in a quartz UV-Vis cuvette. The absorbance at 450 or 470 nm was

recorded and compared to a standardization curve produced with known concentrations of aqueous hydrogen peroxide. Hydrogen peroxide concentration in reaction solutions was determined in a similar fashion. A small aliquot of reaction solution, usually 0.05 mL, was withdrawn at the desired reaction time and mixed with 2 mL of TBAI (10 mM in acetonitrile). The absorbencies at 450 or 470 nm were recorded immediately after addition of 1 ml of 0.15 M $HClO_4$ in glacial acetic acid.

pH titrations

The probe was calibrated with standard solutions prior to measurement. Values were recorded in both mV and pH units.

Results and Discussion

When compound **1** is exposed to hydrogen peroxide under catalytic conditions compound **2** forms. It is reported that the conversion is nearly complete in less than 10 minutes. Mizuno *et. al.* suggest that the peroxide unit is formed at the position labeled **a** in Figure 1.[14] Based on the considerable literature in this area, transition metal peroxo species are generally of three structural types: $M(O_2)$ $(\eta_2)\}$,[3, 17-21] M-O-O-M,[6, 22-24] and M-O-OH.[25, 26] A potential pathway for the formation of **2** is shown in Scheme 1. It was reported that the isolated **2** was inactive with respect to oxygen transfer to olefins. As such, a further activation step was postulated, an acid-base equilibrium step leading to an activated oxygen species.[14] Our Scheme 1 shows two potential pathways involving aqueous acid.

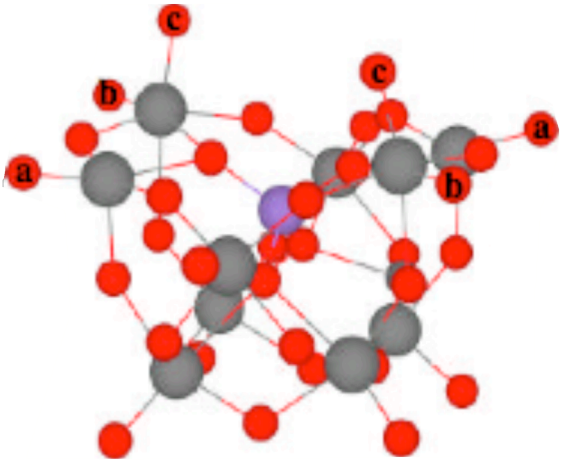

Figure 1. Ball and stick model of $[\gamma\text{-}SiW_{10}O_{34}]^{4-}$. Tungsten in grey, oxygen in red, silicon in purple.

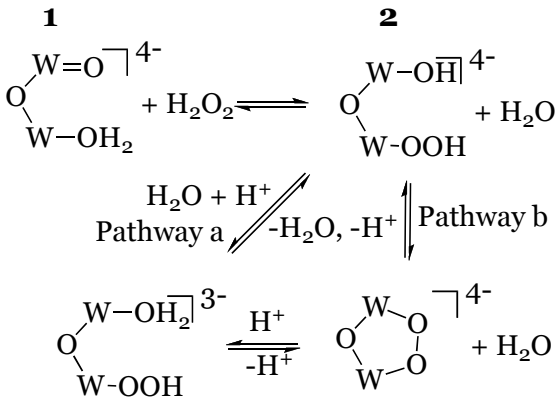

Scheme 1. Reaction of hydrogen peroxide with **1** to form **2**. Two potential acid-base equilibrium pathways.

*Aqueous Titration of $K_8[\gamma\text{-}SiW_{10}O_{36}]$ & Acidity of **1** in acetonitrile*

Given the demonstrated importance of acidity in the catalytic reactions of **1** we decided to further investigate the role of acid in the synthesis of **1**. During the synthesis of the catalyst precursor **1**, an aqueous solution of $K_8[\gamma\text{-}SiW_{10}O_{36}]$ is acidified before precipitation by TBABr. Previous studies have shown that the catalytic activity of **1** reaches a maximum when the pH of the precipitating solution is 2.[13, 27] The inset in Figure 2 shows the reversible protonation of aqueous $[\gamma\text{-}SiW_{10}O_{36}]^{8-}$; approximately 4 protons are taken up, consistent with the formulation $[\gamma\text{-}SiW_{10}O_{32}(OH)_4]^{4-}$; the first pk_a is 4.7. The primary curve in Figure 2 shows a similar plot, but the pH of the solution was adjusted to 2, as

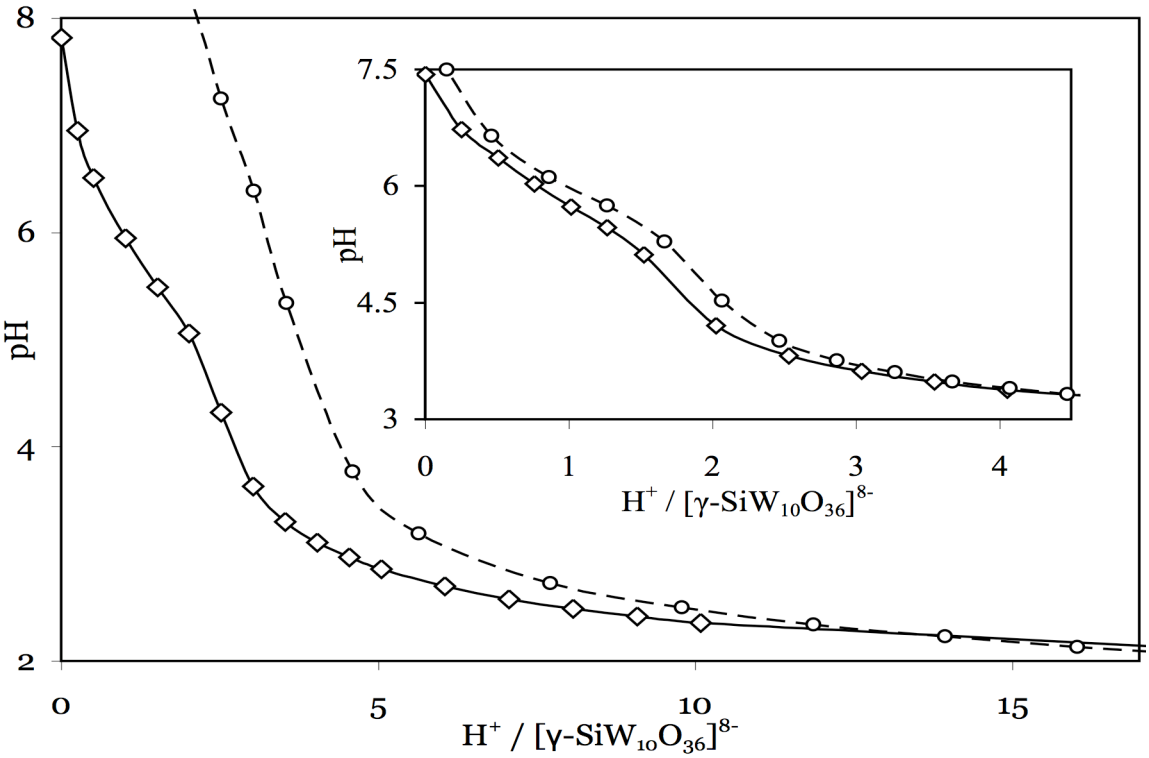

Figure 2. Aqueous titration of $[\gamma\text{-}SiW_{10}O_{36}]^{8-}$. The inset curves show reversibility, while the larger curve, obtained by extended exposure to acidic conditions, does not.

specified for the synthesis of the most catalytically active form of **1**.[13, 27] At this point the ratio of H^+ to $[\gamma\text{-}SiW_{10}O_{36}]^{8-}$ is approximately 25 to 1. In this case the reverse curve, obtained by addition of strong base, is not consistent with reversible deprotonation of $[\gamma\text{-}SiW_{10}O_{32}(OH)_4]^{4-}$. We conclude that another species is formed under these conditions. It is reported that $[\gamma\text{-}SiW_{10}O_{36}]^{8-}$ is unstable under very acidic conditions, converting into $[\beta_2\text{-}SiW_{12}O_{40}]^{4-}$ via decomposition.[15, 28-30]

Similar titration curves were produced for monomeric WO_4^{2-} in water (Figure S3). The monomer showed uptake of 2 equivalents of H^+ near pH 5. As with the over acidified titration shown in figure 2, there was no reversibility of this protonation-induced chemistry upon addition of base.

In order to determine the acidity of **1** in acetonitrile, a solution of the POM containing *p*-nitrophenol as an indicator was titrated with TBAOH. End point calculations revealed that the unpurified product contained 0.6 equivalents of labile proton per $[\gamma\text{-}SiW_{10}O_{32}(OH)_4]^{4-}$ moiety. After two recrystallizations the procedure was repeated and the material was found to have 0.5 labile protons per molecule. As the pKa of *p*-nitrophenol is 7.15[31] **1** is deprotonated by the strong base before the indicator.

To further determine the acidity of the **1**, the indicator Methyl Orange (pK_a 3.46 in water[31]) was dissolved in acetonitrile. Upon addition of solid **1** (approximately 10 mg, 3 mmol) the solution changed color from pale yellow to red-orange, signifying a protonation of the indicator dye. Furthermore dilute

perchloric acid was slowly added to a solution of Crystal Violet (pK_a 1.5 in water[31]) in acetonitrile until the color of the solution was pale green, indicating both protonated and unprotonated dye were present. When solid **1** (approximately 10 mg, 3 mmol) was added to the solution, the color immediately changed to pale yellow, indicating the dye was protonated by the POM.

Compound **1** is very acidic in acetonitrile and is quickly converted to the diperoxo species under reaction conditions. Mizuno *et. al.* propose a mechanism that calls for an acid to serve as the proton donor. They suggest hydrogen peroxide serves the role of acid.[14] Given the acidity of **1** and its structural similarity to **2**, it is difficult to justify protonation of the diperoxo species by a weak acid such as hydrogen peroxide as postulated by Mizuno *et. al.*[14] Another mechanism for activation of **2** to form a catalytic species seems likely.

Limonene Oxidation Selectivity

R-(+)-limonene, a terpene containing two alkene groups with differing steric and electronic properties, was used to assess the selectivity of the various catalytic systems. The relative amounts of 1,2 and 8,9 epoxides were compared by GC analysis of the peak surface areas as labeled in Figure 3. To assess the ratio of *cis* to *trans* epoxide at the 1,2 position we first analyzed a commercial sample of (+)-*cis*/*trans*-limonene oxide via GC and then by ^{1}H NMR. By analyzing the splitting pattern based on the Karplus equation[32] we determined the peak at 2.996 ppm corresponds to the epoxide proton in the *trans* isomer while the doublet centered at 2.937 ppm originates from the *cis* isomer. The cis :

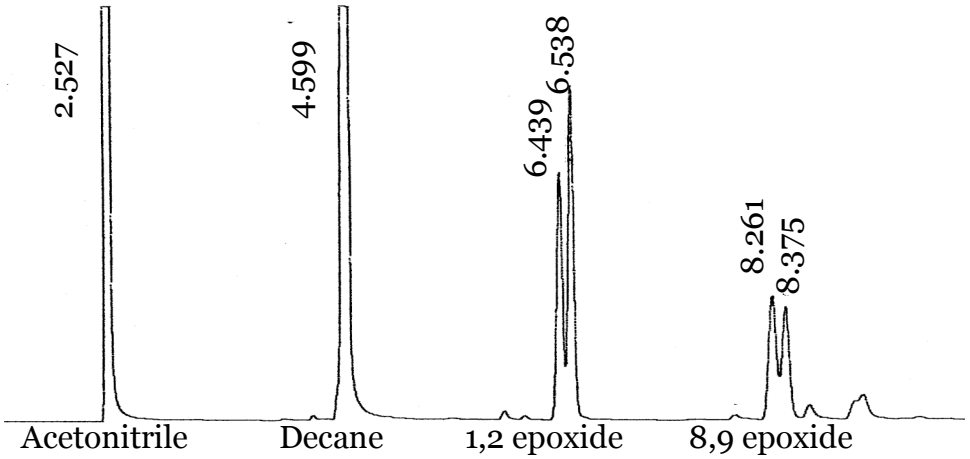

Figure 3. Typical gas chromatography trace. The *cis* and *trans* isomers of limonene oxide were distinguishable for both expoxide locations. Retention times in minutes are given for the respective peaks.

trans ratio as determined by NMR for the epoxide produced by reaction with **1** is 1.24 : 1. The ratio as determined by GC is 1.16 : 1.

Effects of tungstate monomer

To probe the possibility that **1** decomposes under the catalytic reaction conditions, and these byproducts were in some way affecting the catalysis of oxygen transfer, we synthesized TBA_2WO_4 and used it as a catalyst in the absence and in the presence of acid ($HClO_4$). A mixture of TBA_2WO_4 and $HClO_4$ showed an extremely high catalytic activity (Figure 4). At only 6 mol% tungsten, the monomer catalyzes oxygen transfer at a similar rate to **1**. Furthermore, the monomeric system showed no evidence of an induction period.

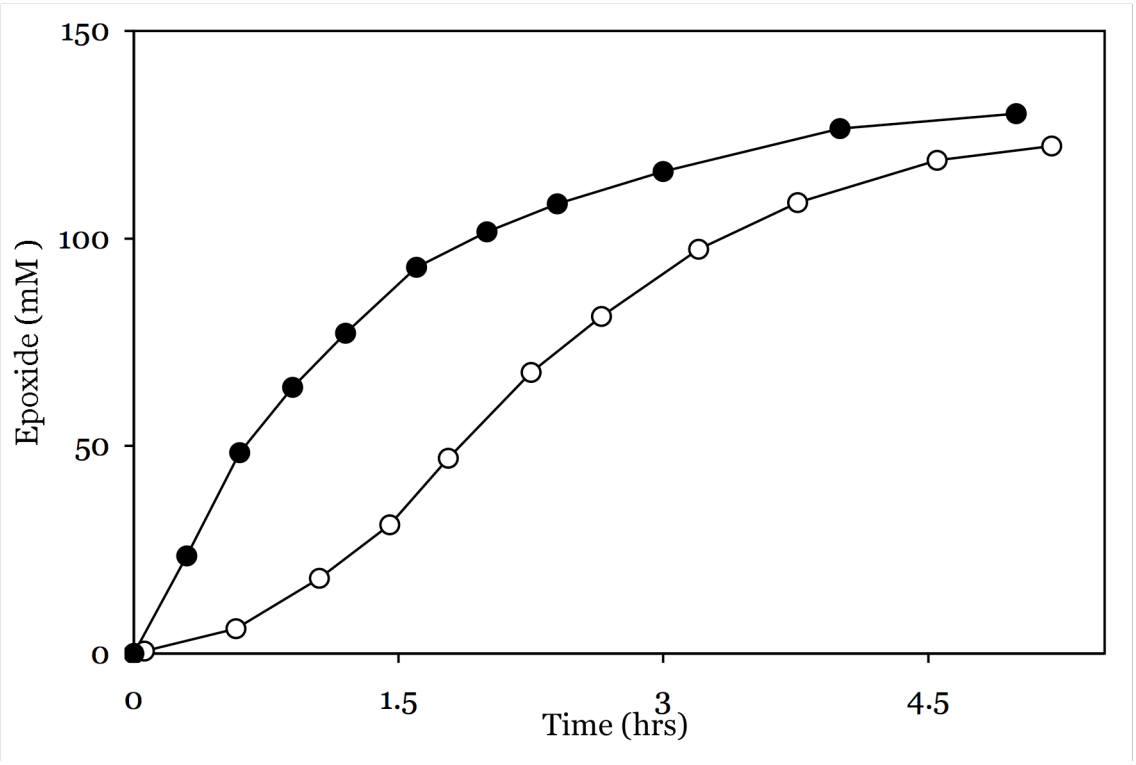

Figure 4. Kinetics of cis-cyclooctene epoxidation by hydrogen peroxide catalyzed by different tungsten-containing species: (○) 1.4 mM **1**; (●) 0.84 mM TBA_2WO_4 and 2.2 mM $HClO_4$. Conditions: 365 mM *cis*-cyclooctene, 135 mM H_2O_2, ca. 0.25 M H_2O, 40.5 °C, acetonitrile.

To further analyze the differences between the monomeric system and **1**, we determined the intermolecular regioselectivity in epoxidation of the two different double bonds in (R)-(+)-limonene. The 8,9-epoxide/(total epoxide) ratio in the reaction catalyzed by **1** was 0.33±0.03, which is in good agreement with a number reported by Mizuno, 0.38. This ratio varied widely in the $TBA_2WO_4/HClO_4$ system when the concentration was changed, showing that different active oxygen species are formed different concentrations. The active

species in the monomeric systems are likely different from the species formed in the reactions catalyzed by **1**.

To determine whether the decomposition of a small percentage of **1**, in the presence of acid and peroxide, is a possible reaction pathway to an active catalyst, we studied the effects of addition of TBA_2WO_4 and $HClO_4$ to the catalytic system comprising **1**. It is known that sterically bulky oxidizing agents exhibit selectivity toward the least hindered ene site, as are more electron rich oxidants.[33] As seen

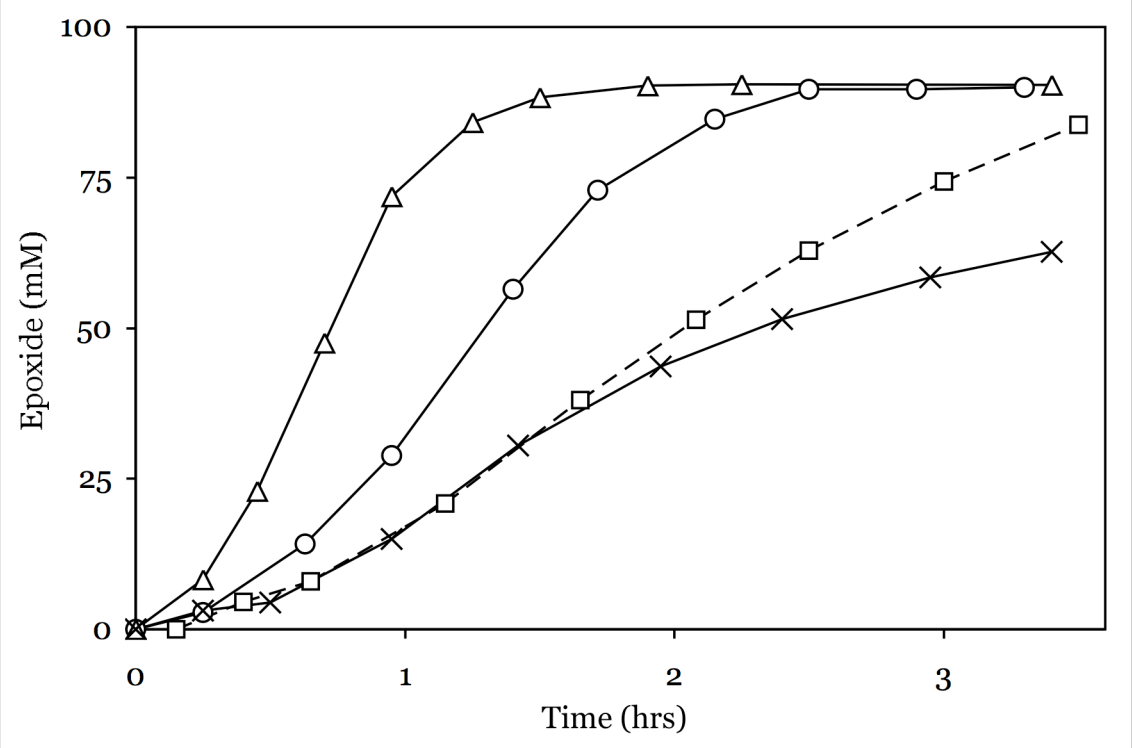

Figure 5. Effects of addition of monomeric tungstate and acid on the activity of **1**: (o) no additions; (Δ) with both 0.24 mM TBA_2WO_4 and 0.4 mM $HClO_4$; (x) with 0.4 mM $HClO_4$; (□) with 0.24 mM TBA_2WO_4 only. Conditions: 365 mM *cis*-cyclooctene, 90 mM H_2O_2, 1.2 mM **1**, ca. 0.15 M H_2O, 40.5 °C, CH_3CN.

in Figure 5, addition of monomeric tungstate and acid to **1** almost doubled the rate of *cis*-cyclooctene epoxidation while nearly eliminating the induction period. Individually, TBA_2WO_4 and $HClO_4$ did not have positive effects on either the rate or the induction period. Our results show the active catalyst in solution is selective toward the less hindered alkene moiety. By quantifying the ratio of 8,9-epoxide to total epoxide we were able to determine that the regioselectivity of the **1**/TBA_2WO_4/$HClO_4$ mixture and **1** by itself is nearly the same. It is possible that the same active species is formed in both cases. Our attempts to use IR-spectroscopy to observe such a species were unsuccessful.

FT-IR studies

The synthesis and purification of **1**, as well as the conversion to the diperoxo compound **2** was monitored by FT-IR. Figure S4 shows the spectral

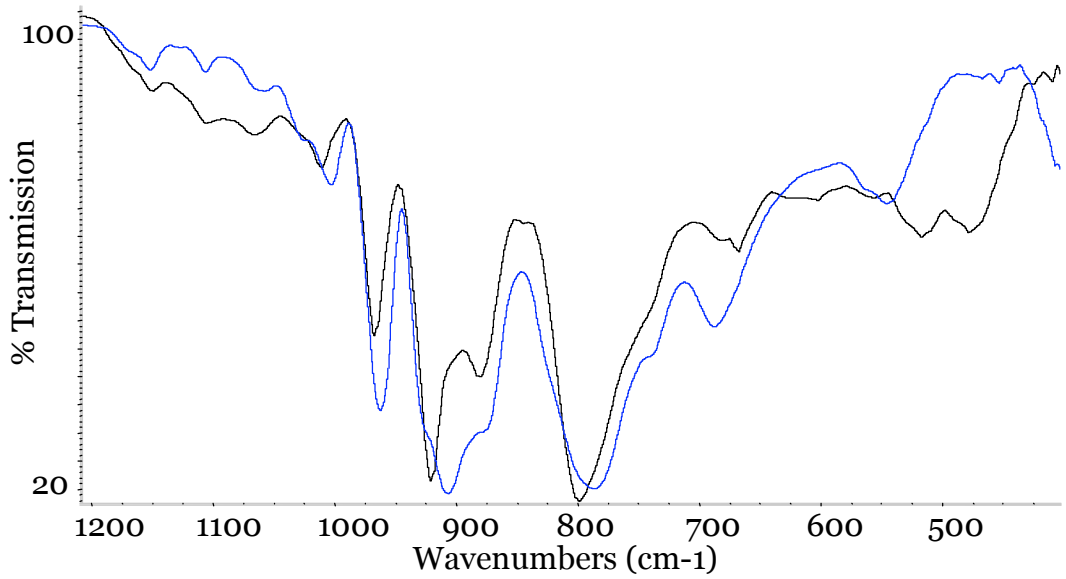

Figure 6. FT-IR of materials recovered after *cis*-cyclooctene epoxidation. **1** (blue); **1**/TBA_2WO_4/$HClO_4$ (black).

changes as the unprotonated $[\gamma\text{-}SiW_{10}O_{36}]^{8-}$ is converted to the organic soluble form of **1** at pH 2. Three peaks in the spectrum of the unpurified compound **1** decrease dramatically upon subsequent recrystallizations, as marked in Figure S5. Strikingly, conversion of **1** to **2** does not produce a distinct change in the IR spectrum (Figure S6). Figure 6 compares the spectra of **1** with the spectrum of the material collected from the vacuum drying of a reaction solution containing **1** plus TBA_2WO_4 and $HClO_4$. The spectral changes are not significant enough to make any determinations.

UV-Visible studies

Since the FT-IR data was not specific enough to make any determinations about the active catalytic species, UV-visible spectroscopy was used to analyze the catalyst under reaction conditions. As the reaction proceeded, a small aliquot was withdrawn from the reaction vessel, diluted and the absorbance spectrum recorded. Figure 7 clearly shows the appearance of a peak near 260 nm, which increases over the course of the reaction. Neither cyclooctene nor the epoxide

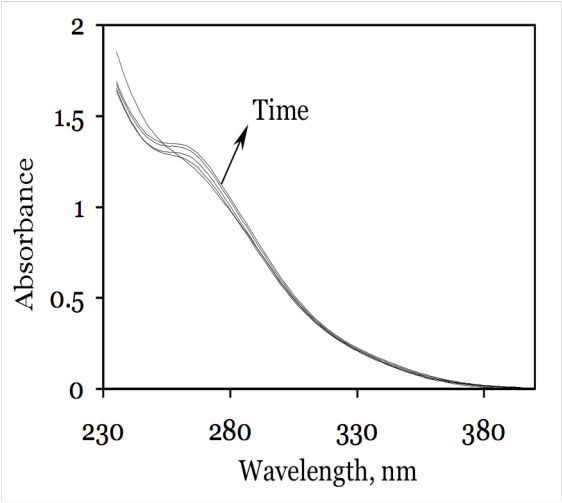

Figure 7. Changes in UV-vis spectra of a catalytic solution under reaction conditions. Conditions: 365 mM *cis*-cyclooctene, 90 mM H_2O_2, 1.2 mM 1, ca. 0.15 M H_2O, 40.5 °C, CH_3CN, 0.1 mL solution were withdrawn and added to 3 mL CH_3CN. Reaction time: 0, 2, 3, 4 and 6 hrs.

absorbs in this region. The changes are therefore attributed to a polytungstate species formed under reaction conditions. Further work is ongoing to identify this species.

Conclusion

We undertook this research because determining the species that is the active catalyst and the correct epoxidation mechanism could not only lead to optimization of this system but also clarify mechanistic issue associated with other heavily investigated and effective POM epoxidation catalysts (V_2SiW_{10}, Fe_2SiW_{10}, peroxotungstates).[12, 34, 35] We conclude that **1** is a catalyst precursor in the epoxidation of alkenes by hydrogen peroxide. We postulate that after the rapid formation of **2** under reaction conditions, another species forms. Our data indicate that this species is likely formed by the reaction of **2** with monomeric tungstate. The source of this tungstate is the acid dependant H_2O_2-based degeneration of the POM **1** under the reaction conditions.

References

1. Sheldon, R. A.; Kochi, J. K., *Metal-Catalyzed Oxidations of Organic Compounds*. Academic Press: New York, 1981; p Chapter 5.
2. Hill, C. L., *Advances in Oxygenated Processes*. JAI: London, 1988; Vol. 1.
3. Mimoun, H.; Mignard, M.; Brechot, P.; Saussine, L., Selective epoxidation of olefins by oxo[N-(2-oxidophenyl)salicylidenaminato]vanadium(V) alkylperoxides. On the mechanism of the Halcon epoxidation process. *J. Am. Chem. Soc.* **1986,** 108, (13), 3711-3718.
4. Jørgensen, K. A., Transition-Metal-Catalyzed Epoxidations. *Chem. Rev.* **1989,** 89, 431-458.
5. Brégeault, J.-M., Transition-metal complexes for liquid-phase catalytic oxidation: some aspects of industrial reactions and of emerging technologies. *Dalton Transactions* **2003**, (17), 3289-3302.
6. Salles, L.; Piquemal, J.-Y.; Thouvenot, R.; Minot, C.; Bregeault, J.-M., Catalytic epoxidation by heteropolyoxoperoxo complexes: from novel precursors or catalysts to a mechanistic approach. *J. Mol. Catal. A: Chem.* **1997,** 117, (1-3), 375-387.
7. Sheldon, R. A.; van Santen, R. A., *Catalytic Oxidation: Principles and Applications*. World Sci: Singapore, 1995; p 381.
8. Lane, B. S.; Burgess, K., Metal-Catalyzed Epoxidations of Alkenes with Hydrogen Peroxide. *Chem. Rev.* **2003,** 103, (7), 2457-2473.
9. Witte, P. T.; Alsters, P. L.; Jary, W.; Mullner, R.; Pochlauer, P.; Sloboda-Rozner, D.; Neumann, R., Self-Assembled $Na_{12}[WZn_3(ZnW_9O_{34})_2]$ as an Industrially Attractive Multi-Purpose Catalyst for Oxidations with

Aqueous Hydrogen Peroxide. *Organic Process Research & Development* **2004,** 8, (3), 524-531.

10. Mizuno, N.; Yamaguchi, K.; Kamata, K., Epoxidation of olefins with hydrogen peroxide catalyzed by polyoxometalates. *Coord. Chem. Rev.* **2005,** 249, 1944-1956.

11. Brégeault, J.-M.; Vennat, M.; Salles, L.; Piquemal, J.-Y.; Mahha, Y.; Briot, E.; Bakala, P. C.; Atlamsani, A.; Thouvenot, R., From polyoxometalates to polyoxoperoxometalates and back again; potential applications. *J. Mol. Catal. A: Chem.* **2006,** 250, 177-189.

12. Kamata, K.; Kuzuya, S.; Uehara, K.; Yamaguchi, S.; Mizuno, N., μ- η ^{1}: η ^{1}-Peroxo-Bridged Dinuclear Peroxotungstate Catalytically Active for Epoxidation of Olefins. *Inorg. Chem.* **2007,** 46, 3768-3774.

13. Kamata, K.; Yonehara, K.; Sumida, Y.; Yamaguchi, K.; Hikichi, S.; Mizuno, N., Efficient Epoxidation of Olefins with >99% Selectivity and Use of Hydrogen Peroxide. *Science* **2003,** 300, (5621), 964-966.

14. Kamata, K.; Kotani, M.; Yamaguchi, K.; Hikichi, S.; Mizuno, N., Olefin Epoxidation with Hydrogen Peroxide Catalyzed by Lacunary Polyoxometalate [γ-$SiW_{10}O_{34}(H_2O)_2]^{4-}$. *Chem. Eur. J.* **2007,** 13, (2), 639-648.

15. Tézé, A.; Hervé, G., α-, β-, and γ-Dodecatungstosilicic Acids: Isomers and related Lacunary Compounds. In *Inorganic Syntheses*, Ginsberg, A. P., Ed. John Wiley and Sons: New York, 1990; Vol. 27, pp 85-96.

16. Che, T. M.; Day, V. W.; Francesconi, L. C.; Fredrich, M. F.; Klemperer, W. G.; Shum, W., Synthesis and Structure of the $[n\text{-}^5C_5H_5)Ti(Mo_5O_{18})]^{3-}$ and $[(n\text{-}^5C_5H_5)Ti(W_5O_{18})]^{3-}$ Anions. *Inorg. Chem.* **1985,** 24, (24), 4055-4062.

17. Mimoun, H., Oxygen Transfer from Inorganic and Organic Peroxides to Organic Substrates: A Common Mechanism? *Angew. Chem. Int. Ed. Engl.* **1982,** 21, 734-750.

18. Chong, A. O.; Oshima, K.; Sharpless, K. B., Synthesis of dioxobis(tert-alkylimido)osmium(VIII) and oxotris(tert-alkylimido)osmium(VIII) complexes. Stereospecific vicinal diamination of olefins. *J. Am. Chem. Soc.* **1977,** 99, (10), 3420-3426.

19. Sharpless, K. B.; Townsend, J. M.; Williams, D. R., Mechanism of epoxidation of olefins by covalent peroxides of molybdenum(VI). *J. Am. Chem. Soc.* **1972,** 94, (1), 295-296.

20. Herrmann, W. A.; Fischer, R. W.; Scherer, W.; Rauch, M. U., Methyltrioxorhenium(VII) as Catalyst for Epoxidations: Structure of the Active Species and Mechanism of Catalysis. *Angew. Chem. Int. Ed.* **1993,** 32, (8), 1157-1160.

21. Amato, G.; Arcoria, A.; Ballistreri, F. P.; Tomaselli, G. A.; Bortolini, O.; Conte, V.; Difuria, F.; Modena, G.; Valle, G., Oxidations with peroxotungsten Complexes: Rates and mechanism of stoichiometric olefin epoxidations. *J. Mol. Catal.* **1986,** 37, (2-3), 165-175.

22. Dengel, A. C.; Griffith, W. P.; Parkin, B. C., Studies on polyoxo- and polyperoxo-metalates. 1. Tetrameric heteropolyperoxotungstates and

heteropolyperoxomolybdates. *J. Chem. Soc., Dalton Trans.* **1993**, (18), 2683-2688.

23. Salles, L.; Aubry, C.; Thouvenot, R.; Robert, F.; Dorémieux-Morin, C.; Chottard, G.; Ledon, H.; Jeannin, Y.; Brégeault, J.-M., ^{31}P and ^{183}W NMR Spectroscopic Evidence for Novel Peroxo Species in the "$H_3[PW_{12}O_{40}]\cdot yH_2O/H_2O_2$" System. Synthesis and X-ray Structure of Tetrabutylammonium (μ-Hydrogen phosphato)bis(μ-peroxo)bis(oxoperoxotungstate)(2-): A Catalyst of Olefin Epoxidation in a Biphase Medium. *Inorg. Chem.* **1994,** 33, 871-878.

24. Gresley, N. M.; Griffith, W. P.; Parkin, B. C.; White, A. J. P.; Williams, D. J., Studies on polyoxo- and polyperoxometalates. Part 4. The crystal structures of $[NMe_4][(Me_2AsO_2)\{MoO(O_2)_2\}_2]$, $[NMe_4][(Ph_2PO_2)\{MoO(O_2)_2\}_2]$, $[NBun_4][(Ph_2PO_2)\{WO(O_2)_2\}_2]$ and $[NH_4][(Ph_2PO_2)\{MoO(O_2)_2(H_2O)\}]$ and their use as catalytic oxidants. *J. Chem. Soc., Dalton Trans.* **1996**, (10), 2039-2045.

25. Ledon, H. J.; Varescon, F., Role of peroxo vs. alkylperoxo titanium porphyrin complexes in the epoxidation of olefins. *Inorganic Chemistry* **1984,** 23, (18), 2735-2737.

26. Wahl, G.; Kleinhenz, D.; Schorm, A.; Sundermeyer, J.; Stowasser, R.; Rummey, C.; Bringmann, G.; Fickert, C.; Kiefer, W., Peroxomolybdenum Complexes as Epoxidation Catalysts in Biphasic Hydrogen Peroxide Activation: Raman Spectroscopic Studies and Density Functional Calculations. *Chem. Eur. J.* **1999,** 5, (11), 3237-3251.

27. Kamata, K.; Nakagawa, Y.; Yamaguchi, K.; Mizuno, N., Efficient, regioselective epoxidation of dienes with hydrogen peroxide catalyzed by $[\gamma\text{-}SiW_{10}O_{34}(H_2O)_2]^{4-}$. *J. Catal.* **2004,** 224, (1), 224-228.

28. Tézé, A.; Cadot, E.; Béreau, V.; Hervé, G., About the Keggin Isomers: Crystal Structure of $[N(C_4H_9)_4]_4\text{-}\gamma\text{-}[SiW_{12}O_{40}]$, the γ-Isomer of the Keggin Ion. Synthesis and ^{183}W NMR Characterization of the Mixed γ-$[SiMo_2W_{10}O_{40}]^{n-}$ (n = 4 or 6). *Inorg. Chem.* **2001,** 40, (9), 2000-2004.

29. Tézé, A.; Canny, J.; Gurban, L.; Thouvenot, R.; Hervé, G., Synthesis, structural characterization, and oxidation-reduction behavior of the γ-isomer of the dodecatungstosilicate anion. *Inorg. Chem.* **1996,** 35, (4), 1001-1005.

30. Canny, J.; Tézé, A.; Thouvenot, R.; Hervé, G., Disubstituted Tungstosilicates. 1. Synthesis, stability, and structure of the lacunary precursor polyanion $\gamma\text{-}SiW_{10}O_{36}^{8-}$. *Inorg. Chem.* **1986,** 25, (13), 2114-2119.

31. Lide, D. R., *CRC Handbook of Chemistry and Physics*. 81 ed.; CRC Press: Boca Raton, FL, 2000.

32. Lambert, J. B.; Shurvell, H. F.; Lightner, D. A.; Cooks, R. G., *Organic structural spectroscopy*. Prentice-Hall, Inc.: Upper Saddle River, New Jersey, 1998; p 568.

33. Carey, F. A.; Sundberg, R. J., *Advanced organic chemistry part b: reactions and synthesis*. Kluwer Academic/Plenum Publishers: New York, 2000; p 965.

34. Mizuno, N.; Nozaki, C.; Kiyoto, I.; Misono, M., Highly efficient utilization of hydrogen peroxide for selective oxygenation of alkanes catalyzed by diiron-substituted polyoxometalate precursor. *J. Am. Chem. Soc.* **1998,** 120, 9267-9272.

35. Botar, B.; Geletii, Y. V.; Kögerler, P.; Musaev, D. G.; Morokuma, K.; Weinstock, I. A.; Hill, C. L., The True Nature of the Di-iron(III) γ-Keggin Structure in Water: Catalytic Aerobic Oxidation and Chemistry of an Unsymmetrical Trimer. *J. Am. Chem. Soc.* **2006,** 128, 11268-11277.

Supplemental Information

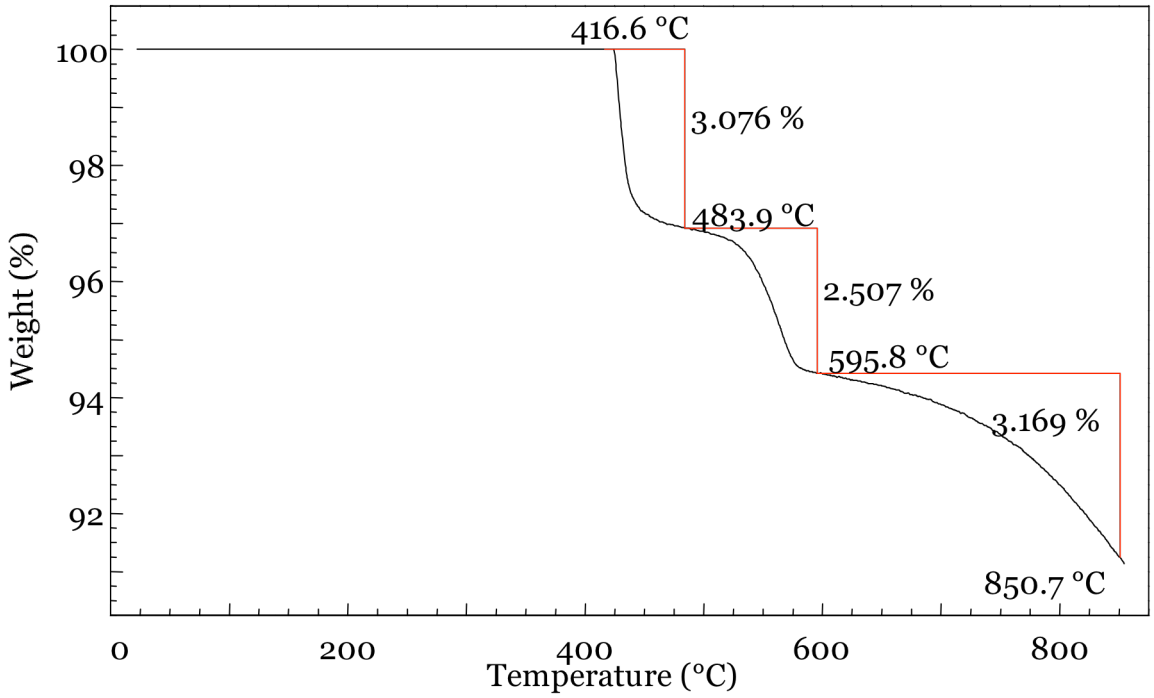

Figure S1 TGA plot of **1**. No loosely bound water molecules were observed.

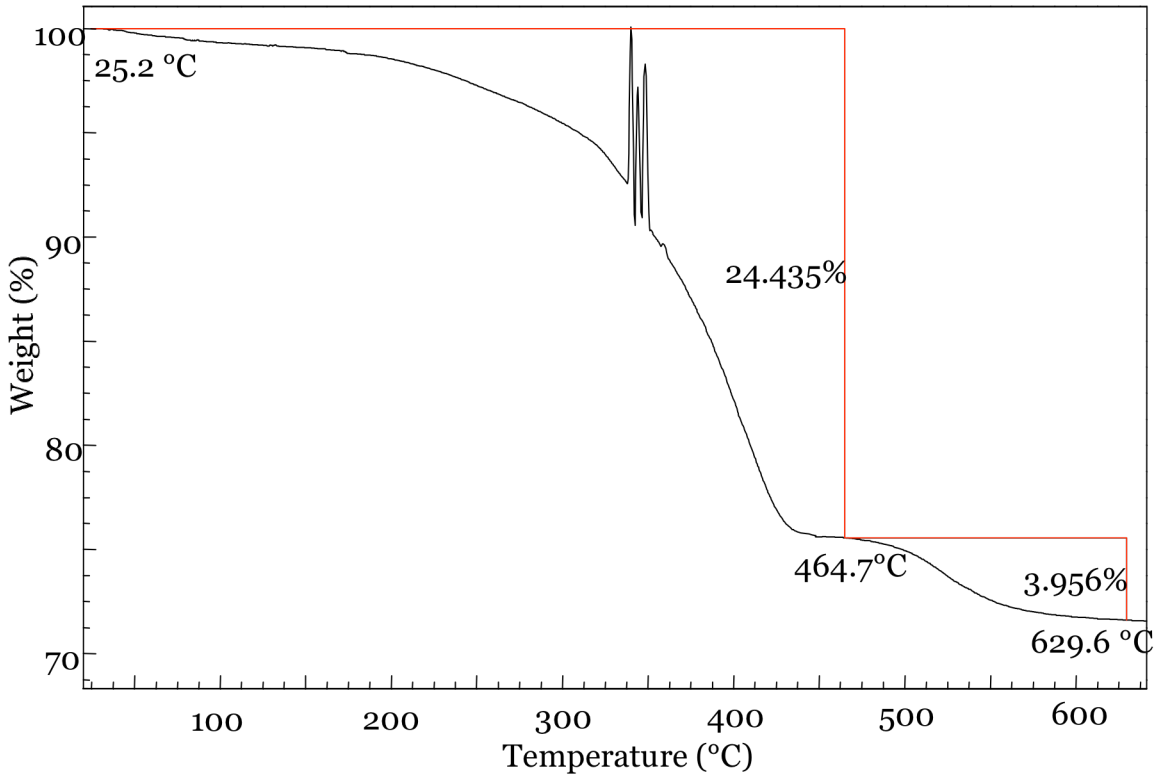

Figure S2. TGA plot of 1. No loosely bound water molecules were observed. The anomaly at ~340 °C is attributed to explosive decomposition of the peroxide.

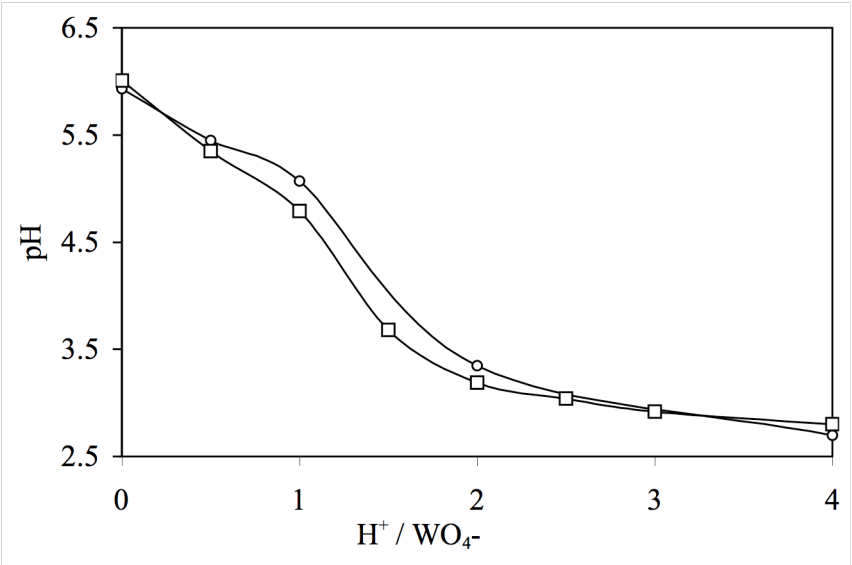

Figure S3. Acidification of monmeric tungstate. (o) TBA_2WO_4; (□) Na_2WO_4. No reversibility of the protonation was observed upon addition of base.

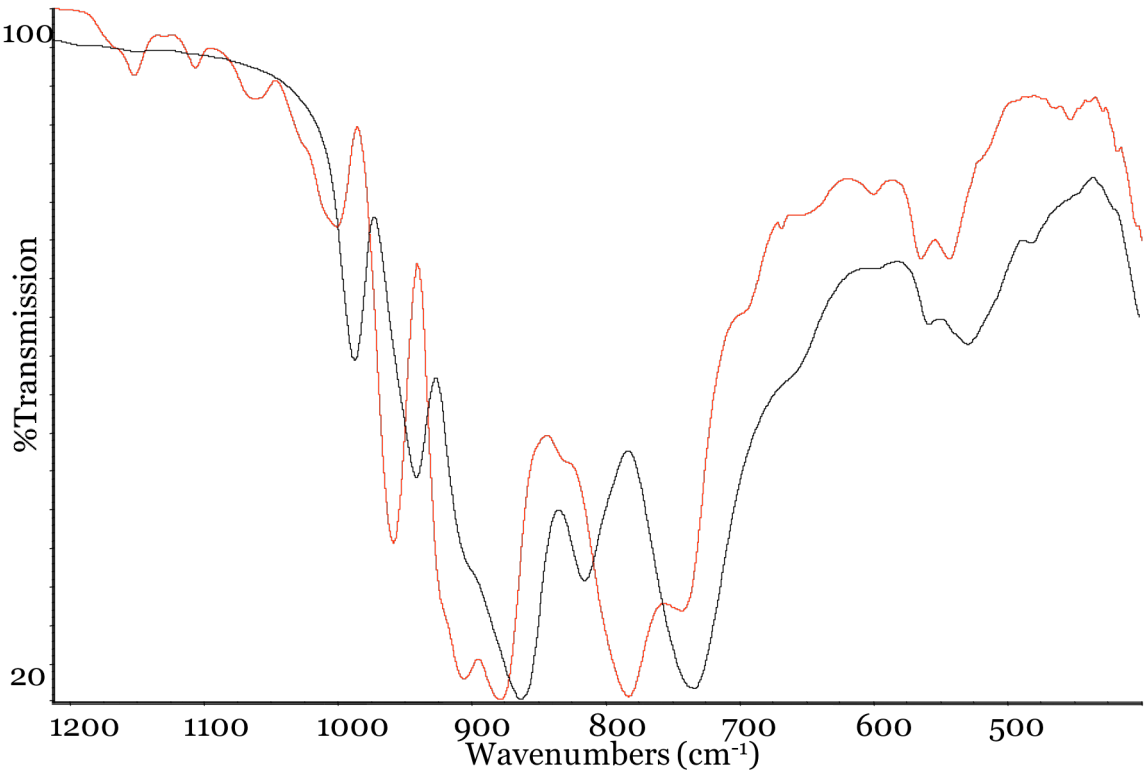

Figure S4. FT-IR spectra of $K_8[\gamma\text{-}SiW_{10}O_{36}]$ (black) and **1** (red) as isolated without recrystallization.

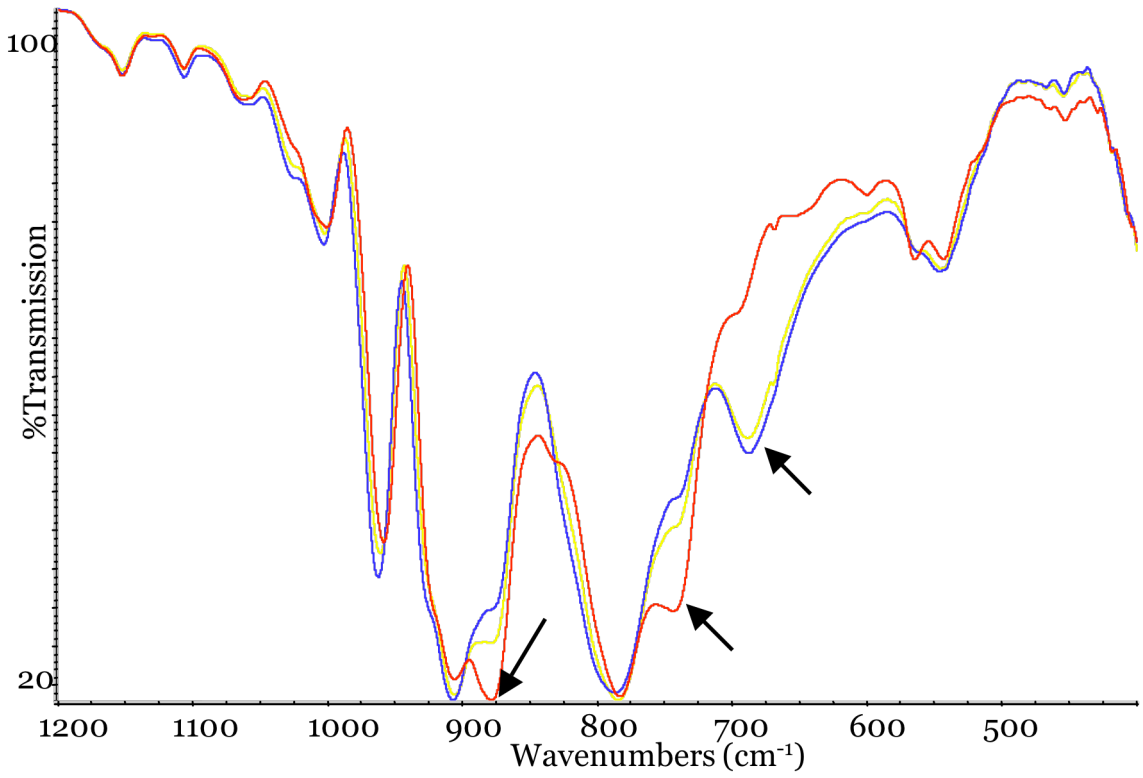

Figure S5. FT-IR spectra of **1** as isolated without recrystalization (red), **1** after one recrystalization (yellow), and **1** after two recrystalizations (blue). The black arrows indicate areas of most significant change.

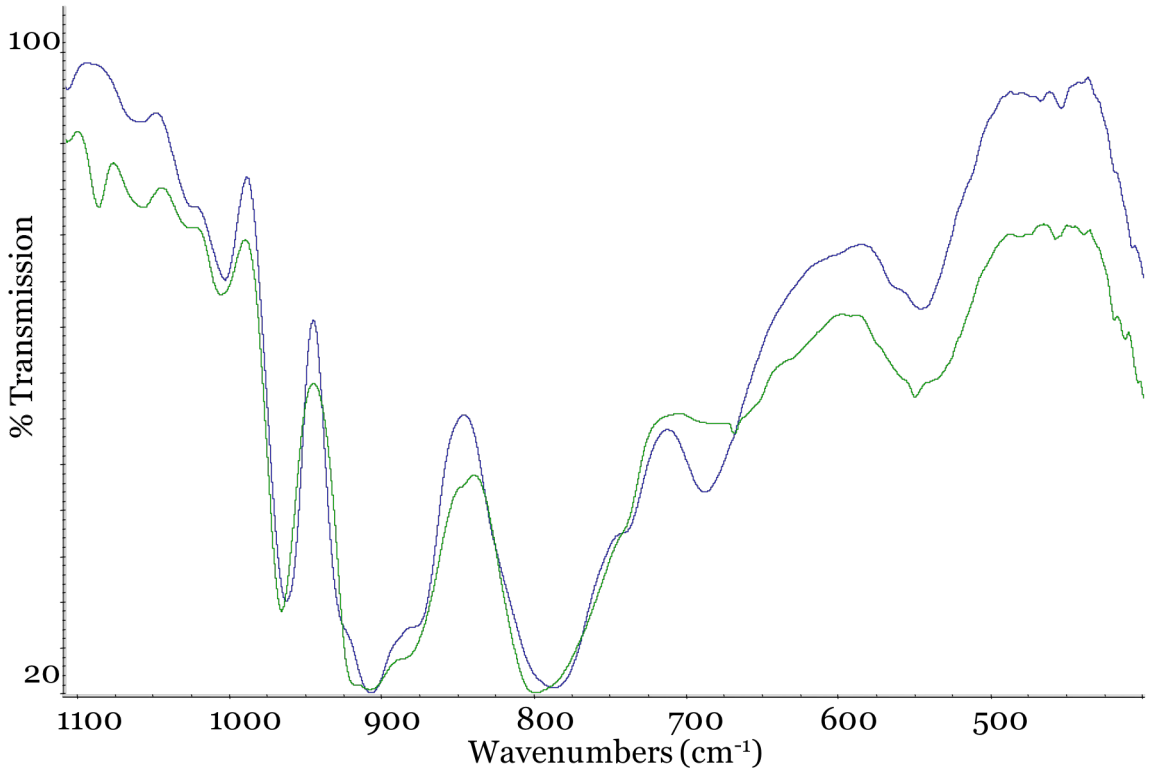

Figure S6. FT-IR spectra of **1** after two recrystalizations (blue) and **2** as isolated from the reaction vessel by precipitation (green).

Disorder-Free Palladium and Platinum Oxo Complexes

Published in part in:

Angew. Chem. Int. Ed., **2008**, *47*, 9380-9382.

With:

Cao, R.; Anderson, T. A.; Kögerler, P.; Hardcastle, K. I.; Hill, C. L.

Abstract

Palladium and platinum are two of the most commonly used catalysts in modern industrial and chemical applications. Work to understand the intricate mechanisms and transformations that occur on the surface of these elemental materials and the related metal-oxide supported counterparts has been a particular focus of the scientific community. The work presented herein continues the pursuit to isolate and characterize palladium and platinum-oxo units stabilized by polyoxometalate ligands. These compounds can function as tractable molecular models, amenable to structural, spectroscopic, and chemical characterization, for the common heterogeneous catalytic materials whose analogous properties are not amenable to facile characterization.

Introduction

Noble metal catalysts are abundant in modern society, from vehicle catalytic convertors to reactive catalysts for air-based oxidations.[1-7] Although a great deal of research has been conducted on these heterogeneous catalysts, many of their physical and chemical properties at the molecular level remain unclear because they are very hard to investigate and unequivocally establish. The availability of effective molecular and soluble representations of metal and supported metal catalyst surfaces would greatly facilitate investigation and establishment of these properties.

Late-transition metal-oxo (LTMO) complexes, that is terminal oxo complexes of the transition metal elements to the right of column 8,in the periodic table, have been suggested for O_2 activation at platinum surfaces in catalytic converters,[4] fuel cells,[1] and industrial catalysis.[2] Work to stabilize LTMO complexes has been pursued for many years[8-16] but despite this considerable and long-term effort only one such complex was known prior to 2004, an oxo-Ir^V complex.[17] In 2004 Anderson and co-workers published a platium-oxo stabilized by polyoxometalate ligands.[18] Metal oxygen multiple bonds are common in the high oxidation states of the early transition metals, but the terminal metal-oxo moiety becomes increasingly unstable in metals with high d-electron counts.[18-28] It has been shown that the POMs can stabilize a LTMO bond. POMs have long been know to be good elctron acceptors[29, 30] and the large diffuse metal-based orbitals of the POM are postulated to withdraw electron density and therefore stabilize the metal-oxo bond.[18, 21, 22, 29] The work herein

details the work toward the synthesis and characterization of disorder-free crystal structures of Pd(IV)- and Pt(IV)-oxo comples.

Experimental

Instrumentation

Transmission infrared spectra (3–5 wt. % in KBr) were recorded on a Thermo Electron Corporation Nicolet 6700 FT-IR spectrometer. Single UV-Vis spectra were acquired using a Hewlett-Packard 8452A diode array spectrophotometer. Aqueous pH measurements were performed using an Orion 230 Aplus pH and ISE meter equipped with an Orion Ross Combination pH electrode. Solution ^{1}H NMR spectroscopic measurements were made on a Varian INOVA 400 MHz spectrometer and resonance signals were referenced to residual solvent signals. Solution ^{29}Si NMR spectroscopic measurements were made on a Varian INOVA 400 MHz spectrometer with AutoProbe pre-shimmed using a ^{29}Si standard. Solution ^{31}P NMR spectroscopic measurements were made on a Varian UNITY 400 MHz spectrometer and resonance signals were referenced to 85% H_3PO_4 in water. Elemental analyses were performed by Atlantic Microlabs Atlanta, GA (carbon, hydrogen, and nitrogen) and Kontilabs, Quebec, Canada (all elements). Thermogravimetric measurements were performed on an ISI TGA-1000.

Materials

All chemicals were reagent grade and used as received from commercial sources unless otherwise specified. The POMs $Na_9[A\text{-}\alpha\text{-}PW_9W_{34}]$ (hereafter

{PW_9})[31], $K_8[\gamma\text{-}SiW_{10}O_{36}]$[32], $K_8[\alpha\text{-}SiW_{11}O_{39}]$[32], $K_4[\alpha\text{-}SiW_{12}O_{40}]$[32] were prepared by literature procedures.

Synthesis of "*$(CH_6N_3)_8[\alpha\text{-}Pt_2SiW_{10}O_{40}]$" (**{$Pt_2SiW_{10}$}**)*

$K_2Pt(OH)_6$[33] (0.2 g, 0.58 mmol) and $K_8[\alpha\text{-}SiW_{11}O_{39}]\bullet 13H_2O$ (hereafter {αSiW_{11}})[32] (2.8 g, 0.90 mmol) were dissolved in 50 ml of water. The pH of the pale yellow/orange slurry was 9.5. The pH was adjusted to 11.5 by the addition of KOH (~0.5 mL of 3.0 M), upon which all the solid dissolved. Returning the solution to neutral pH with HNO_3 (~0.5 mL of 3.0 M) caused clouding in the solution. The mixture was then concentrated to 30 mL via a boiling water bath. Addition of guanidinium hydrochloride (0.3 g, 0.31 mmol) produced 0.7 g of a fine white powder. FT-IR (KBr pellet) 1664 (vs), 1576 (w sh), 992, 941, 866 (vs), 793 (s), 724 (s, br), 538, 519 cm^{-1}. Addition of excess guanidinium hydrochloride gave 1.55 g of a yellow-orange powder. FT-IR (KBr pellet) 1668 (vs), 1653 (vs, sh), 991, 941, 868 (s), 794, 727 (br, s), 539 (br).

Guanidinium salts of the POMs:

All guanidinium salts were prepared in a similar manner. The potassium salt of the POM (500 mg) was dissolved in 10 mL of water. To this was added 0.3 mL of saturated guanidinium hydrochloride in water. The resulting precipitate was collected via suction filtration and washed with 20 mL of cold water in two equal portions and allowed to air dry. All yields were >95%

Synthesis of $(CH_6N_3)_xK_{8-x}[\gamma\text{-}SiW_{10}O_{36}]$

FT-IR (KBr pellet) 1659 (br, vs), 1579, 1384 w, 1243 (br, w), 984 (w), 937, 891 (sh), 863 (s), 770 (s), 740 (br), 570 (br) cm^{-1}.

Synthesis of $(CH_6N_3)_xK_{8-x}[\alpha\text{-}SiW_{11}O_{39}]$

FT-IR (KBr pellet) 1663 (br, vs), 1575 (w, sh), 992(s), 940(s), 868 (br, vs), 794 (s), 725 (br, s), 538 (br), 520 (br, s), 476 (sh), 419 (w) cm^{-1}.

Synthesis of $(CH_6N_3)_xK_{4-x}[\alpha\text{-}SiW_{12}O_{40}]$

FT-IR (KBr pellet) 1665(vs), 1572 (w), 1561 (w, sh), 1015, 996(w, sh), 970 (s), 920 (vs), 883, 789 (br, vs), 531 (br), 481 (sh), 420 (w) cm^{-1}.

*Synthesis of $K_{16}O{=}Pd(OH_2)(A\text{-}\alpha\text{-}PW_9O_{34})_2{\bullet}XH_2O$ (**{O=PdP₂W₁₈}**)*

Water (25 mL) in an ice bath was acidified with 0.4 mL of 0.5 M H_2SO_4 (0.2 mmoles, 1 eq H^+). To this solution, 100 mg of $PdSO_4$ (0.4 mmol) was added and the resulting mixture allowed to stir for 5 minutes which produced a brown suspension (pH 2.2). Rapid addition of 2.2 g of $Na_9[A\text{-}\alpha\text{-}PW_9W_{34}]$ (0.84 mmoles, 2.1 eq) afforded a mixture that contained a yellow suspension and reached pH 6.5 after 2 minutes. The slurry was transferred from the beaker to a centrifuge tube and the liquid separated from the solid (small pellet ~0.2 g). The decanted solution was transferred to a beaker in an ice bath with 8.5 g of KCl and stirred for 5 minutes. The yellow-white solid was isolated from the pale yellow solution via centrifugation and redissolved in ~40 mL of water at 45 °C. The solution slowly darkened as it was heated for 1 hour (pH 7.1) then filtered through fine paper. Dark red crystals formed within 2 hours. These were allowed to grow

overnight and then collected. FT-IR (KBr pellet) 1072 (s), 1018, 961 (sh), 940 (s), 889 (w), 830 (s), 743 (br s), 704 (w sh), 612 (br), 512 (w), 430 (w) cm^{-1}.

*Synthesis of $K_{10}P_2W_{20}O_{70}•24H_2O$ (**{P_2W_{20}}**)*

This synthesis was adapted and optimized from the published preparation by Contant.[34] Rapid addition of 10 mL of 1.0 M phosphoric acid to a solution of 100 mL of 1.0 M potassium tungstate results in a slightly cloudy mixture of pH 8.7. The mixture is heated to 60 °C and 51 mL of 3.0 M hydrochloric acid are added drop-wise under vigorous stirring. Localized clouding is observed at the point of acid addition. When the mixture reaches pH 3.0 it becomes completely clear and addition of acid should be halted to prevent formation of $[PW_{12}O_{40}]^{3-}$ byproduct (identified by IR). The solution is filtered through fine filter paper into a crystallizing dish. A white solid is collected after 2 days, dried, weighed, and re-dissolved in ~1 mL of 50 °C water per gram of solid. Large, colorless prisms are collected after 4 days. Yield 10.7 g (~38% with respect to the polyanion). FT-IR (KBr pellet) 1086 9(s), 1077 (s), 1019, 954 (s), 922 (s), 857, 767 (sh), 749 (br), 659, 593(br, sh), 520, 468 (w), 446 (w), 424(w) cm^{-1}. ^{31}P NMR -12.3 ppm.

*Synthesis of $K_{10}O{=}Pt^{IV}(OH_2)P_2W_{20}O_{70}•XH_2O$ (**{$O{=}PtP_2W_{20}$}**)*

{P_2W_{20}} (0.6 g, 0.1 mmol, 1 eq) was dissolved in 30 mL H_2O, and the pH was adjusted to 7 by addition of 5M $NaHCO_3$. Solid K_2PtCl_4 (0.1 g, 0.2 mmoles, 2 eq) was dissolved in minimal amount of water and added drop wise to the stirring P_2W_{20} solution. The yellow-red solution was headed to 70 °C for 45 minutes at which time a dramatic color change to dark green was observed. The pH of the dark green solution was 6.9. The solution was cooled to ambient temperature,

filtered on a medium porosity frit, and allowed to evaporate in dish to produce 0.12 g of dark green powder. FT-IR (KBr pellet) 1078, 1019 (w), 941, 925 (sh), 887 (br), 850, 796 (sh), 740 (br), 694 (br), 668 (sh), 596 (w), 518, 461 (w), 420 (w) cm^{-1}.

*Synthesis of $Rb_5K_6C_6H_5SnP_2W_{19}O_{69}•16H_2O$ (**{$PhSnP_2W_{19}$}**)*

To a beaker filled with 180 mL of water, 0.333 mL of phenyltin trichloride (2.0 mmoles, 1.15 eq) is quickly added followed immediately by 10.0 g of $K_{10}[P_2W_{20}O_{70}]$ (1.7 mmoles, 1 eq). The solution is stirred for 10 minutes followed by drop-wise addition of 1M KOH to adjust the pH to 5.0 (~7 mL). RbCl (180 drops of 5.0 M solution) are added and the solution is gravity filtered through fine filter paper. Crystals of the pure product are harvested after 2 days. Yield 6.33 g (~68% with respect to the polyanion). FT-IR (KBr pellet) 1083 (s), 1072 (s sh), 1023, 949 (s), 930 (sh), 890 (w), 849, 786, 746 (w), 708, 593, 517, 443, 418 cm^{-1}. ^{31}P NMR -10.3 ppm. Elemental composition: theoretical: C 1.22%, H 0.87%, Rb 7.21%, W 58.89%, Sn 2.00%, O 24.81%, P 1.04%, K 3.96%. Elemental composition: experimental: C 1.22%, H 0.58%.

*Synthesis of $((CH_3)_2NH_2)Rb_3K_3Pd^{II}C_6H_5SnP_2W_{19}O_{69}•16H_2O$ (**{$PdPhSnP_2W_{19}$}**)*

A solution of 25 mg $Pd(NO_3)_2•XH_2O$ (~0.09 mmol) in 10 mL of water was left to stir and dissolve for 30 minutes then filtered on a 0.20 μm syringe filter to yield a yellow-orange solution at pH 2.16. To this solution 0.5 g of {$PhSnP_2W_{19}$} (~0.1 mmol) was rapidly added as a solid. The solution became dark brown-black and opaque upon stirring for 10 minutes and the final pH was 2.65. The dark solution was filtered on fine filter paper and 3 drops of 1.0 M

dimethylammonium chloride (DMACl) were added to the resulting red-brown solution. Large dark red-brown prism-shaped crystals formed overnight. Yield 0.11 g (~20% with respect to the polyanion). FT-IR (KBr pellet) 1084 (s), 1062, 953 (s), 931, 899 (sh), 775 (br s), 700 (br w), 583 (w), 520 (w), 445, 414 cm^{-1}. ^{31}P NMR -12.87 ppm.

*Synthesis of $Rb_4K_7O{=}Pd(OH_2)C_6H_5SnP_2W_{19}O_{69}{\bullet}XH_2O$ (**$\{O{=}PdPhSnP_2W_{19}\}$**)*

A mixture of 25 mg $Pd(NO_3)_2{\bullet}XH_2O$ (~0.09 mmoles) in 10 mL of water was left to stir and dissolve for 30 minutes then filtered through a 0.20 μm syringe filter to yield a yellow-orange solution at pH 2.16. To this solution 0.5 g of PHSn19 (~0.1 mmol) were rapidly added as a solid. The solution became dark brown-black and opaque upon stirring for 10 minutes, and the final pH was 2.65. The dark solution was filtered through a fine filter paper and 3 drops of 5.0 M RbCl were added to the resulting red-brown solution. Large dark red-brown prism-shaped crystals formed overnight. FT-IR (KBr pellet) 1084 (s), 1062, 953 (s), 931, 899 (sh), 775 (br s), 700 (br w), 583 (w), 520 (w), 445, 414 cm^{-1}. ^{31}P NMR -13.04 ppm.

Results and Discussion

Kortz and coworkers questioned the validity of the initially published crystal structure of Pd-oxo, while dismissing several other lines of evidence. An updated structure was aquired and the involving the palladium and tungsten sites in the belt were well modeled.[21] Nonetheless, Kortz continued to question the work. In order to quell the controversy and respond to disparaging remarks about the original work in a subsequent paper,[35] we initially re-investigated the

claim of an LTMO (a di-Pt-oxo complex) reporeted by U. Lee and coworkers that Kortz and Lee had noted in the aforementioned 2008 paper.

Debunking {Pt_2SiW_{10}}

The compound in question was reported to be an α -Keggin silicotungstate with two of the tungsten atoms replaced with oxo-Pd^{IV}, "[α-$SiPt^{IV}_2W_{10}O_{40}]^{8-}$" (henceforth {$Pt_2SiW_{10}$}). Two aspects of the published synthesis were inconsistent with our observations of other oxo-Pt^{IV} POMs, the starting material $K_2Pt(OH)_6$ and the basic pH adjustments. The Pt^{IV} source is far less reactive to substitution than a Pt^{II} compound. The other reported oxo-Pt makes use of an oxidation reaction after the more reactive Pt^{II} binds to the POM ligand. The synthesis calls for the addition of KOH to adjust the pH to 11.5. It is known that the {αSiW_{11}} is stable between pH 4.5 and 7, but decomposes under very basic conditions.[32]

When we attempted to reproduce the compound {Pt_2SiW_{10}} we isolated a pale-yellow powder. The IR spectrum of this material is identical to the guanidinium salt of {SiW_{11}}. We also compared the IR spectrum to that of $(guanidinium)_4[\alpha\text{-}SiW_{12}O_{40}]$. The spectra are quite, yet we would expect them to be similar given the comparable symmetry and therefore related vibrational spectra (see Figure 1). When examining the elemental analysis data published for {Pt_2SiW_{10}}, the values calculated for $(guanidinium)_8[SiW_{11}O_{39}]\cdot 2H_2O$ are closer than those calculated for $(guanidinium)_8[SiPt_2W_{10}O_{40}]\cdot 2H_2O$. Furthermore, when following the synthesis procedure published by of Lee et al.[36] exact the compounds isolated is a pale yellow. The other literature LTMO complexes are

all darkly colored due to electronic transitions with large extinction coefficients.[18, 21, 22]

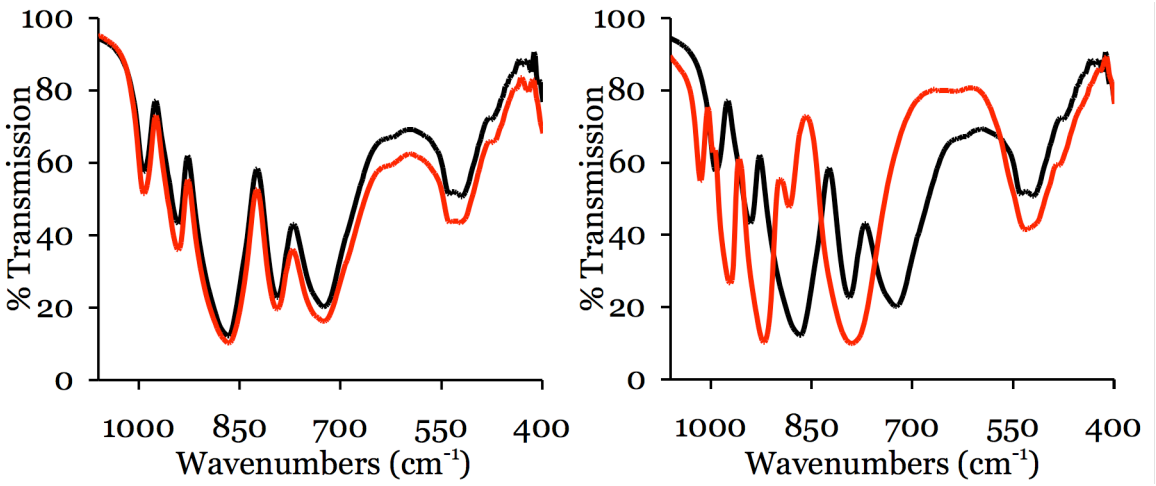

Figure 1. Comparison of the infrared spectra of "(guanidinium)$_8$[SiPt$_2$W$_{10}$O$_{40}$]•2H$_2$O" ({SiPt$_2$W$_{10}$}; red spectrum), (guanidinium)$_8$[α-SiW$_{11}$O$_{39}$] ({SiW$_{11}$}; black spectrum on left), and (guanidinium)$_4$[α-SiW$_{12}$O$_{40}$] ({SiW$_{12}$}; black spectrum on right) in the spectral range relevant to metal oxygen vibrational modes.

Palladium-oxo stabilized by {PW$_9$}

To further lay any of Kortz's concerns to rest we undertook the synthesis of a disorder free Pd=O stabilized by POM ligands. Our attempts began by replicating the synthesis for the Pt-oxo compound,[18] but changing the transition metal salt from PtCl$_4$ to Pd(SO$_4$). We were only able to observe decomposed tungstate salts following this procedure. In order to slow the decomposition of the POM reactant, {PW$_9$}, we cooled the Pd suspension in an ice bath before

rapid addition of the POM. Again, we only observed decomposed tungstates as a product.

In order to avoid the insoluble slurry observed when using sulfate salt of Pd^{2+}, the more soluble nitrate salt was used. The ratio of $\{PW_9\}$ to Pd^{2+} (2:1) was more carefully controlled with this method. Variability in the pH of the initial $Pd(NO_3)_2$ solution was accompanied by variability in the color of the solution. Unfortunately, we observed no correlation between initial pH (ranging from 1.8 to 2.3) and any reactivity. Under these conditions we were able to isolate crystals that nominally represented mixtures of $\{O{=}PdP_2W_{18}\}$ and the all tungsten complex, $[P_2W_{19}O_{69}]^{14-}$.[37] Figure 2 shows the X-ray crystal structure determination of the compound isolated. The overlapping atoms of tungsten and palladium (co-crystallization of the W-oxo and Pd-oxo units in the central position) render this structure unsuitable for unequivocal determination of the distances in this central unit. The ^{31}P NMR of this compound shows 3 peaks when freshly prepared (~2 min in solution). Ostensibly these peaks would be $\{O{=}PdP_2W_{18}\}$, $\{P_2W_{19}\}$, and some decomposition product. When the solution is allowed to age, the peak at approximately -11 ppm is the only one detected. This peak corresponds to $[PW_{11}O_{39}]^{8-}$ and this assignment was confirmed by comparison of the FT-IR spectrum to literature values.[34] Attempts at recrystallization yielded one of several results: (1) decomposition to a powder; (2) isolation of the previously characterized oxo $[(O{=}Pd)_2P_2W_{19}]^{6-}$[38]; (3) reisolation of the mixed $\{O{=}PdP_2W_{18}\}$ / $[P_2W_{19}O_{69}]^{14-}$ mixed crystals. We attributed the

decomposition to the long reaction times used (more than 20 minutes) to ensure clear solutions and satisfactory recrystallization to obtain large crystals.

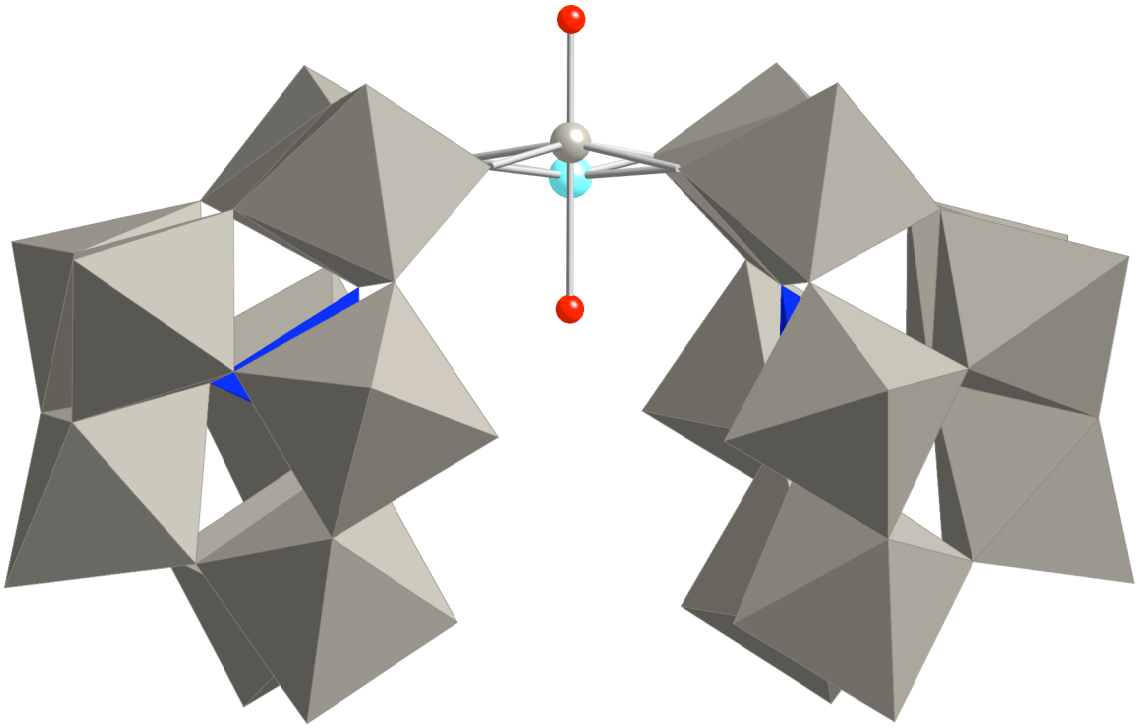

Figure 2. Polyhedral representation of $\{O{=}PdP_2W_{18}\}$. The belt tungsten atoms are shown in ball-and-stick mode to accentuate the overlap of Pd and W (~20% Pd, 80% W present, as determined by X-ray crystallography). Tungsten octahedra in grey, phosphorus tetrahedra in blue, and palladium in light blue. Bound waters omitted for clarity.

We explored the possibility of preacidification of the solution. We had previously seen that Pd^{2+} was not soluble above pH 5. When adding $\{PW_9\}$ to the acidic Pd^{2+} solutions we always observed increases in solution pH, even passing neutral to become basic solutions. We postulated that these conditions prevented the incorporation of Pd^{2+} into a POM structure. We assumed that the insoluble

Pd material was a result of condensation. By increasing the acidity of the solution before addition of Pd^{2+} we prevented condensation and further improved the solubility of the $\{PW_9\}$, which we had observed to be more soluble in slightly acidic solutions.

Based on the available evidence, the thermodynamic product of a mixture of $\{PW_9\}$ and Pd^{2+} (either as monomers or in some combined compound) in the pH regime of acetate buffer and slightly higher (~4.2 to 5.5) is $[(O=Pd)_2P_2W_{19}]^{6-}$. We obtain this product either by allowing for crystallization of 2:1 mixtures of $\{PW_9\}$ and Pd^{2+} and by redissolving $\{O=PdP_2W_{18}\}$ followed by acidification of the solution to the proper pH range. Crystallographic, FT-IR and ^{31}P NMR evidence indicates that the kinetic product of the reaction of $\{PW_9\}$ and Pd^{2+} in this pH range is the mono-substituted $\{O=PdP_2W_{18}\}$, thus rapid reaction times and precipitation of the product are critical to prevent the thermodynamic $[(O=Pd)_2P_2W_{19}]^{6-}$ from forming.

The final breakthrough for isolation of $\{O=PdP_2W_{18}\}$ came by shortening the reaction times to avoid the double incorporation of palladium. This was accomplished by rapid precipitation by addition of excess KCl. While we were able to overcome the issue of decomposition of starting material to $\{PW_{11}\}$ and the formation of $[(O=Pd)_2P_2W_{19}]^{6-}$ we were unable to prevent the formation of the all-tungsten $\{P_2W_{19}\}$. Efforts are ongoing to separate the unstable, but scientifically interesting $\{O=PdP_2W_{18}\}$.

Palladium substituted {$PhSnP_2W_{19}$}

In order to circumvent the decomposition issues presented by {PW_9} in aqueous solution, we attempted to incorporate Pd^{2+} into the phosphotungstate {$PhSnP_2W_{19}$}.[39] This compound is stable in the pH range of 2.5 to 6. We hoped that the substitution of the phenyl-Sn in the belt of the POM would further decrease the symmetry of any complexes containing Pd ions and allow for a disorder-free compound to crystallize. The synthesis of {$PhSnP_2W_{19}$} was optimized first by adjusting the ratio of $PhSnCl_3$ to {P_2W_{20}}. It was observed that upon addition to water the $PhSnCl_3$ produced a small amount of white solid determined to be ~10% by weight of the starting material, thus the compensation using excess $PhSnCl_3$ in the reaction mixture. Upon addition of base to reaction mixture, the compound(s) in solution transform to {$PhSnP_2W_{19}$}. The reaction can be easily followed by pH probe because of a buffering effect in the pH range of 2.3 to 5.0. Rubidium cations were found to be the best counterion for producing crystals of {$PhSnP_2W_{19}$} in a reasonable time frame yet a soluble complex (molar concentrations).

The facile synthesis and good yields of {$PhSnP_2W_{19}$} allowed us to produce this ligand in bulk and perform a series of reactions with $Pd(NO_3)_2$. Crystals of {$Pd^{II}PhSnP_2W_{19}$} were isolated when dimethylammonium was used as a counterion, while {$O{=}Pd^{IV}PhSnP_2W_{19}$} was isolated with rubidium chloride. The IR spectra of these compounds are nearly identical, but they can be distinguished by the ^{31}P NMR chemical shift (-12.87 for the square planar Pd^{II} species, -13.04 for the oxo-Pd^{IV} species). Fresh solutions of the {$PdPhSnP_2W_{19}$} complex showed

two ^{31}P NMR peaks, one corresponding to the Pd^{II} complex and one corresponding to the oxo-Pd^{IV} complex. Based on ^{31}P NMR, the addition of base results in the disappearance of the oxo-Pd^{IV} peak. We postulate that the base deprotonates the ammonium counterions and the resulting amine reduces the Pd^{IV} species. This hypothesis is further confirmed by the isolation of $\{O{=}PdPhSnP_2W_{19}\}$ from solutions that contain no reducing agents.

We were able to isolate diffraction quality crystals of both the Pd^{II} (Figure 3) and the oxo-Pd^{IV} complexes, however there were issues with the crystallography of the later (Figure 4). The complex $\{PdPhSnP_2W_{19}\}$ crystallizes in monoclinic *C2/c* space group (V = 18695(3) Å^3, Z = 8). The Pd-O(W) bond distances (1.979(11) - 2.009(12) Å, 1.992 Å by average), and bond valance sum (2.33) are all consistent with a d^8 Pd^{II} center.

The crystallographic analysis of complex $\{O{=}PdPhSnP_2W_{19}\}$ is more difficult. While the phenyl-Sn group breaks down the D_{3h} symmetry of the complex, a crystallographically imposed C_2 axis was observed. The carbon atoms in the phenyl ring were in line with the crystallographically imposed C_2 axis (Figure 4 shows an idealized structure). The complex $\{O{=}PdPhSnP_2W_{19}\}$ crystallizes in monoclinic $P_{2/n}$ space group (V = 9986.4(11) Å3, Z = 4). Furthermore there was 2-fold disorder in the W and Pd sites.

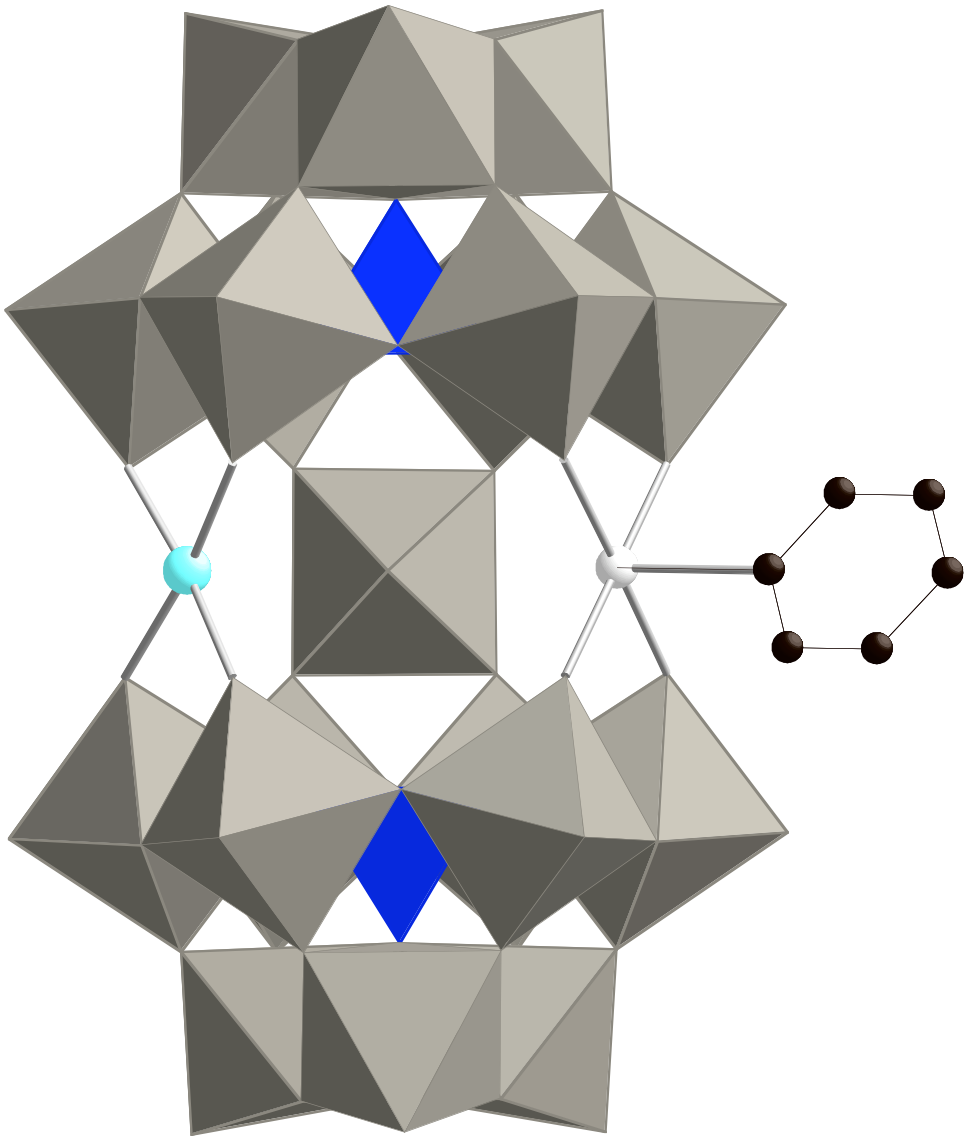

Figure 3. Polyhedral representation of {$PdPhSnP_2W_{19}$}. Some atoms in the belt are shown in ball-and-stick mode to clarify positions. Tungsten octahedra are in grey, phosphorus tetrahedral are in blue, tin is a white sphere, and palladium is an aquamarine sphere. Bound waters, including one trans to the phenyl ring on the tin, are atom omitted for clarity.

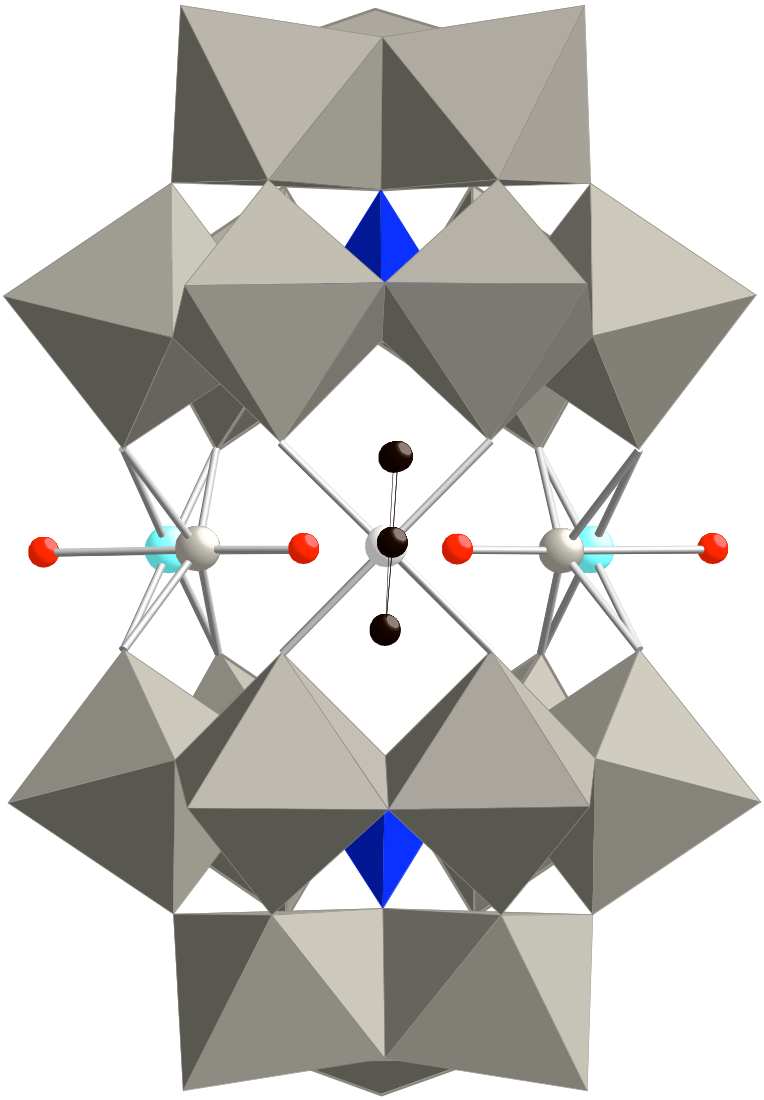

Figure 4. Polyhedral representation of {O=PdPhSnP_2W_{19}} as seen from the crystallographically imposed C_2 axis. Some atoms in the belt are shown in ball-and-stick mode to clarify positions and accentuate the Pd/W positional disorder. Tungsten octahedra are in grey, phosphorus tetrahedral are in blue, the tin is a white sphere, and the palladium is an aquamarine sphere. Bound waters including one trans to the phenyl ring on the tin are atom hidden for clarity.

{P_2W_{20}} as ligand for platinum

Based on previous results, we hoped to see oxidation of Pd^{II} to oxo-Pd^{IV} after binding to a POM ligand.[22] When {P_2W_{20}} was reacted with K_2PtCl_4 and heated, the reaction exhibited a dramatic color-change characteristic of the conversion of Pt^{II} to POM-stabilized Pt^{IV}. IR evidence showed that the stating material {P_2W_{20}} was consumed and a green/black powder was isolated. Various cations were used to produce diffraction quality crystals; however, no crystals were ever observed. A majority of crystallization attempts resulted in the decomposition of {$O=PtP_2W_{20}$} to platinum oxide and unidentifiable tungstates. This was almost always the case when protonated ammonium salts were used. While work on the Pd-oxo species has recently overshadowed this effort, future work will return to the task of isolating and unequivocally identifying these unprecedented compounds.

Conclusions

We were able to show that the first LTMO stabilized by POMs was indeed the {$O=PtP_2W_{18}$} published by Anderson *et. al.*[18] the putative {Pt_2SiW_{10}} of Lee et. al. was shown to be {SiW_{11}}, which was 12-fold disordered in the X-ray crystal structure determination by that group.[36] While great progress has been made on isolation and identification of the palladium analog of {$O=PtP_2W_{18}$}, challenges still remain in isolating a pure compound. The possibilities presented by the {$PhSnP_2W_{19}$} ligand cannot be understated.

References

1. Appleby, A. J.; Foulkes, F. R., *Fuel cell handbook*. Krieger Publising Company, Malabar, Florida: 1993; p 762.
2. Somorjai, G. A., *Introduction to surface chemistry and catalysis*. Wiley: New York, 1994; p 667.
3. Wesendrup, R.; Schröder, D.; Schwarz, H., Catalytic Pt+-Mediated Oxidation of Methane by Molecular Oxygen in the Gas Phase. *Angew. Chem. Int. Ed.* **1994,** 33, (11), 1174-1176.
4. Shelef, M., Selective catalytic reduction of NO_x with N-free reductants. *Chem. Rev.* **1995,** 95, (1), 209-225.
5. Labinger, J. A.; Bercaw, J. E., Understanding and exploiting C-H bond activation. *Nature* **2002,** 417, (6888), 507-514.
6. Thomas, J. M.; Thomas, W. J., *Principles and Practice of Heterogeneous Catalysis*. VCH: Weinheim, 2005.
7. Santen, R. A. v.; Neurock, M., *Molecular Heterogeneous Catalysis*. Wiley-VCH: Weinheim, 2006.
8. Glueck, D. S.; Wu, J.; Hollander, F. J.; Bergman, R. G., Monomeric (Pentamethylcyclopentadienyl)iridium Imido Compounds: Synthesis, Structure, and Reactivity. *J. Am. Chem. Soc.* **1991,** 113, 2041-2054.
9. Andrews, M. A.; Gould, G. L.; Voss, E. J., Evidence for Platinum(II) Oxo Intermediates in Reactions of (Diphosphine)platinum(II) Carbonate Complexes. *Inorg. Chem.* **1996,** 35, 5740-5742.
10. Vicic, D. A.; Jones, W. D., Evidence for the Existence of a Late-Metal Terminal Sulfido Complex. *J. Am. Chem. Soc.* **1999,** 21, 4070-4071.

11. Mindiola, D. J.; Hillhouse, G. L., Terminal Amido and Imido Complexes of Three-Coordinate Nickel. *J. Am. Chem. Soc.* **2001,** 123, 4623-4624.

12. Melenkivitz, R.; Mindiola, D. J.; Hillhouse, G. L., Monomeric Phosphido and Phosphinidene Complexes of Nickel. *J. Am. Chem. Soc.* **2002,** 124, 3846-3847.

13. Mindiola, D. J.; Hillhouse, G. L., Synthesis, Structure, and Reactions of a Three-Coordinate Nickel-Carbene Complex, {1,2-Bis(di-tert-butylphosphino)ethane}Ni=CPh_2. *J. Am. Chem. Soc.* **2002,** 124, 9976-9977.

14. Thyagarajan, S.; Shay, D. T.; Incarvito, C. D.; Rheingold, A. L.; Theopold, K. H., Intramolecular C-H Activation by Inferred Terminal Cobalt Imido Intermediates. *J. Am. Chem. Soc.* **2003,** 125, 4440-4441.

15. Kogut, E.; Zeller, A.; Warren, T. H.; Strassner, T., Structure and Dynamics of Neutral β-H Agostic Nickel Alkyls: A Combined Experimental and Theoretical Study. *J. Am. Chem. Soc.* **2004,** 126, 11984-11994.

16. MacBeth, C. E.; Thomas, J. C.; Betley, T. A.; Peters, J. C., The Coordination Chemistry of "[BP_3]NiX" Platforms: Targeting Low-Valent Nickel Sources as Promising Candidates to L_3Ni=E and L_3Ni(E) Linkages. *J. Inorg. Chem.* **2004,** 43, (15), 4645-4662.

17. Hay-Motherwell, R. S.; Wilkinson, G.; Hussain-Bates, B.; Hursthouse, M. B., Synthesis and X-ray Crystal-Structure of Oxotrimesityliridium(V). *Polyhedron* **1993,** 12, (16), 2009-2012.

18. Anderson, T. M.; Neiwert, W. A.; Kirk, M. L.; Piccoli, P. M. B.; Schultz, A. J.; Koetzle, T., F.; Musaev, D. G.; Morokuma, K.; Cao, R.; Hill, C. L., A

Late-Transition Metal Oxo Complex: $K_7Na_9[O=Pt^{IV}(H_2O)L_2]$, $L=[PW_9O_{34}]^{9-}$. *Science* **2004,** 306, 2074-2077.

19. Nugent, W. A.; Mayer, J. M., *Metal-Ligand Multiple Bonds*. John Wiley & Sons, Inc.: New York, 1988.

20. Holm, R. H., Metal-centered oxygen atom transfer reactions. *Chem. Rev.* **1987,** 87, (6), 1401-1449.

21. Anderson, T. M.; Cao, R.; Slonkina, E.; Hedman, B.; Hodgson, K. O.; Hardcastle, K. I.; Neiwert, W. A.; Wu, S.; Kirk, M. L.; Knottenbelt, S.; Depperman, E. C.; Keita, B.; Nadjo, L.; Musaev, D. G.; Morokuma, K.; Hill, C. L., A Palladium-Oxo Complex. Stabilization of This Proposed Catalytic Intermediate by an Encapsulating Polytungstate Ligand. *J. Am. Chem. Soc.* **2005,** 127, 11948-11949.

22. Cao, R.; Anderson, T. M.; Piccoli, P. M. B.; Schultz, A. J.; Koetzle, T. F.; Geletii, Y. V.; Slonkina, E.; Hedman, B.; Hodgson, K. O.; Hardcastle, K. I.; Fang, X.; Kirk, M. L.; Knottenbelt, S.; Kögerler, P.; Musaev, D. G.; Morokuma, K.; Takahashi, M.; Hill, C. L., Terminal Gold-oxo Complexes. *J. Am. Chem. Soc.* **2007,** 129, (36), 11118-11133.

23. MacBeth, C. E.; Gupta, R.; Mitchell-Koch, K. R.; Victor G. Young, J.; Lushington, G. H.; Thompson, W. H.; Hendrich, M. P.; Borovik, A. S., Utilization of Hydrogen Bonds To Stabilize M-O(H) Units: Synthesis and Properties of Monomeric Iron and Manganese Complexes with Terminal Oxo and Hydroxo Ligands. *J. Am. Chem. Soc.* **2004,** 126, 2556-2567.

24. Poverenov, E.; Efremenko, I.; Frenkel, A. I.; Ben-David, Y.; Shimon, L. J. W.; Leitus, G.; Konstantinovski, L.; Martin, J. M. L.; Milstein, D., Evidence

for a terminal Pt(iv)-oxo complex exhibiting diverse reactivity. *Nature* **2008,** 455, (7216), 1093-1096.

25. Morris, R. J.; Girolami, G. S., A Square-Planar 0xo-Alkyl of Manganese(III). Synthesis and X-ray Crystal Structure of $\{Li_2[MnOMe_3] . 2Li_2(Meacac).tmed\}_2$. *Polyhedron* **1988,** 7, (19/20), 200-2008.
26. Parkin, G., Terminal Chalcogenido Complexes of the Transition Metals. In *Prog. Inorg. Chem.*, Karlin, K. D., Ed. Wiley: New York, 1998; Vol. 47, pp 1-165.
27. Green, M. T.; Dawson, J. H.; Gray, H. B., Oxoiron(IV) in Chloroperoxidase Compound II Is Basic: Implications for P450 Chemistry. *Science* **2004,** 304, (11 JUNE 2004), 1653-1656.
28. Rohde, J.-U.; In, J.-H.; Lim, M. H.; Brennessel, W. W.; Bukowski, M. R.; Stubna, A.; Münck, E.; Nam, W.; Que Jr., L., Crystallographic and Spectroscopic Characterization of a Nonheme Fe(IV)=O Complex. *Science* **2003,** 299, 1037-1039.
29. Rong, C.; Pope, M. T., Lacunary Polyoxometalate Anions Are .Ir-Acceptor Ligands. Characterization of Some Tungstoruthenate(II,III,IV,V)Heteropolyanions and Their Atom-Transfer Reactivity. *J. Am. Chem. Soc.* **1992,** 114, 2932-2938.
30. Weinstock, I. A., Homogeneous-Phase Electron-Transfer Reactions of Polyoxometalates. *Chem. Rev.* **1998,** 98, (1), 113-170.
31. Domaille, P. J., Vanadium (V) Substituted Dodecatungstophosphates. In *Inorganic Syntheses*, Ginsberg, A. P., Ed. John Wiley and Sons: New York, **1990**; Vol. 27, pp 96-104.

32. Tézé, A.; Hervé, G., α-, β-, and γ-Dodecatungstosilicic Acids: Isomers and related Lacunary Compounds. In *Inorganic Syntheses*, Ginsberg, A. P., Ed. John Wiley and Sons: New York, **1990**; Vol. 27, pp 85-96.

33. Lee, U.; Kobayashi, A.; Sasaki, Y., Structure of Pentasodium Trihydrogenhexatungstoplatinate(IV) Icosahydrate, $Na_5[H_3PtW_6O_{24}].20H_2O$. *Acta Cryst.* **1983,** C39, 817-819.

34. Contant, R., Relation between tungstophosphates related to the phosphorus tungsten oxide anion ($PW_{12}O_{40}^{3-}$). Synthesis and properties of a new lacunary potassium polyoxotungstophosphate (K10P2W20O70.24H2O). *Can. J. Chem.* **1987,** 65, (3), 568-573.

35. Lee, U.; Joo, H.-C.; Park, K.-M.; Mal, S. S.; Kortz, U.; Keita, B.; Nadjo, L., Facile Incorporation of Platinum(IV) into Polyoxometalate Frameworks: Preparation of $[H_2Pt^{IV}V_9O_{28}]^{5-}$ and Characterization by ^{195}Pt NMR Spectroscopy. *Angew. Chem. Int. Ed.* **2008,** 47, (4), 793-796.

36. Lee, U.; Joo, H.-C.; Park, K.-M.; Ozeki, T., Synchrotron structure determination of an α-Keggin doubly Pt^{IV}-substituted silicotungstate, $(CH_6N_3)_8[\alpha\text{-}SiPt_2\text{-}W_{10}O_{40}]\cdot 6H_2O$. *Acta Cryst.* **2003,** 59, 152-155.

37. Tourné, C. M.; Tourné, G. F., Aquanonadecatungstodiphosphate(14-) polyanion, $[P_2W_{19}O_{69}(OH_2)]^{14-}$: x-ray crystallographic structure of its potassium salt, chemical relationships in the tungstophosphate system, and conversion into the diaquaeicosatungstodiphosphate [P2W20O70(OH2)2]10-. *J. Chem. Soc., Dalton Trans.* **1988**, 2411-2420.

38. Cao, R.; O'Halloran, K. P.; Hill, C. L., *J. Am. Chem. Soc.* **2009,** in press.

39. The detailed synthesis and characterization of this complex is the subject of an upcoming publication with Rui Cao, Kevin P. O'Halloran, Kenneth I. Hardcastle, and Craig L. Hill, but is not described in this dissertation.

Supplemental Information

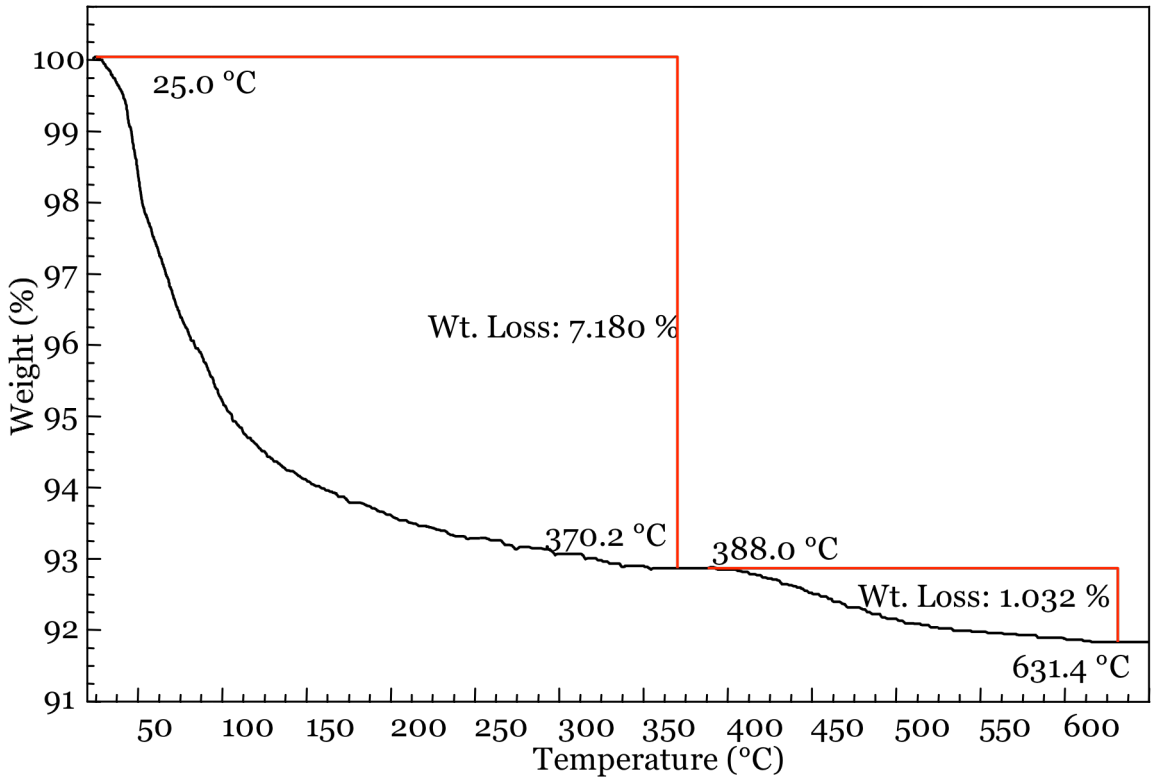

Figure S1. Thermogravimetric plot of $\{PhSnP_2W_{19}\}$. The first weight drop corresponds to ~23 water molecules which is supported by X-ray data. The second weight drop could be a phenyl group, but only accounts for ~40% phenyl per molecule. Data gathered under inert atmosphere.

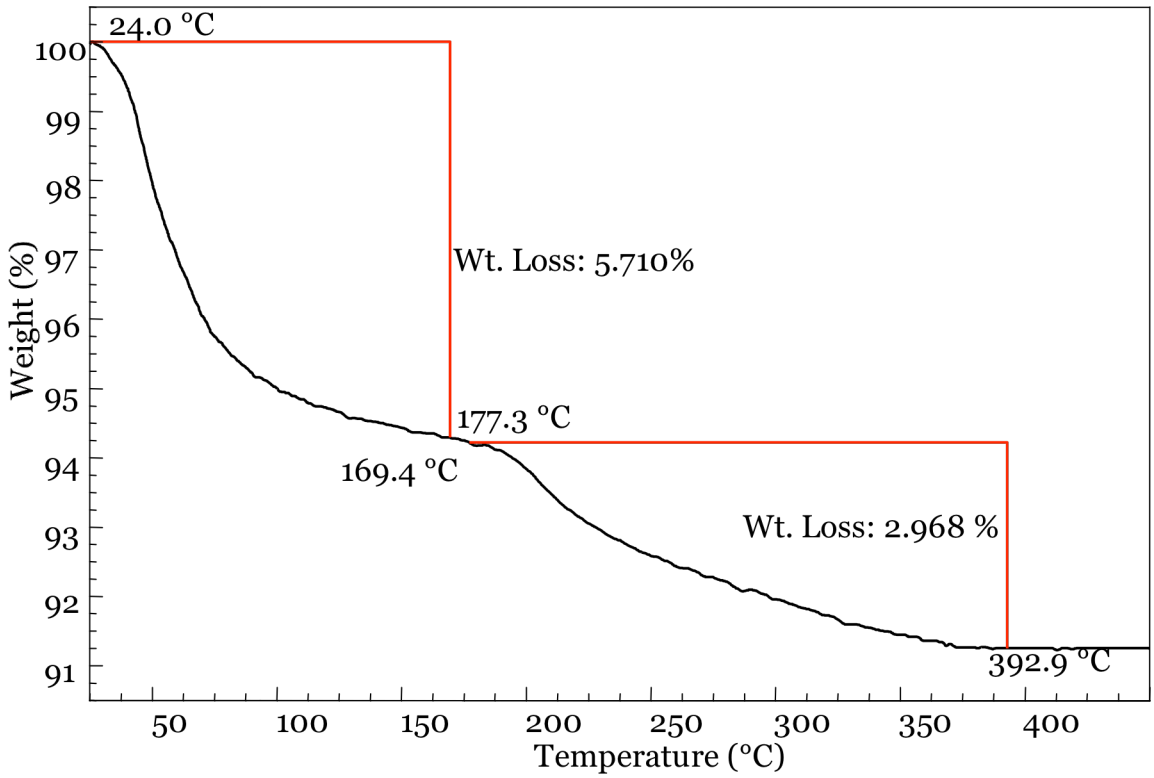

Figure S2. Thermogravimetric plot of {$PdPhSnP_2W_{19}$}. The first weight drop corresponds to ~16 water molecules which is supported by X-ray data. The second weight drop is likely to be elimination of P_2O_5,. Data gathered under inert atmosphere.

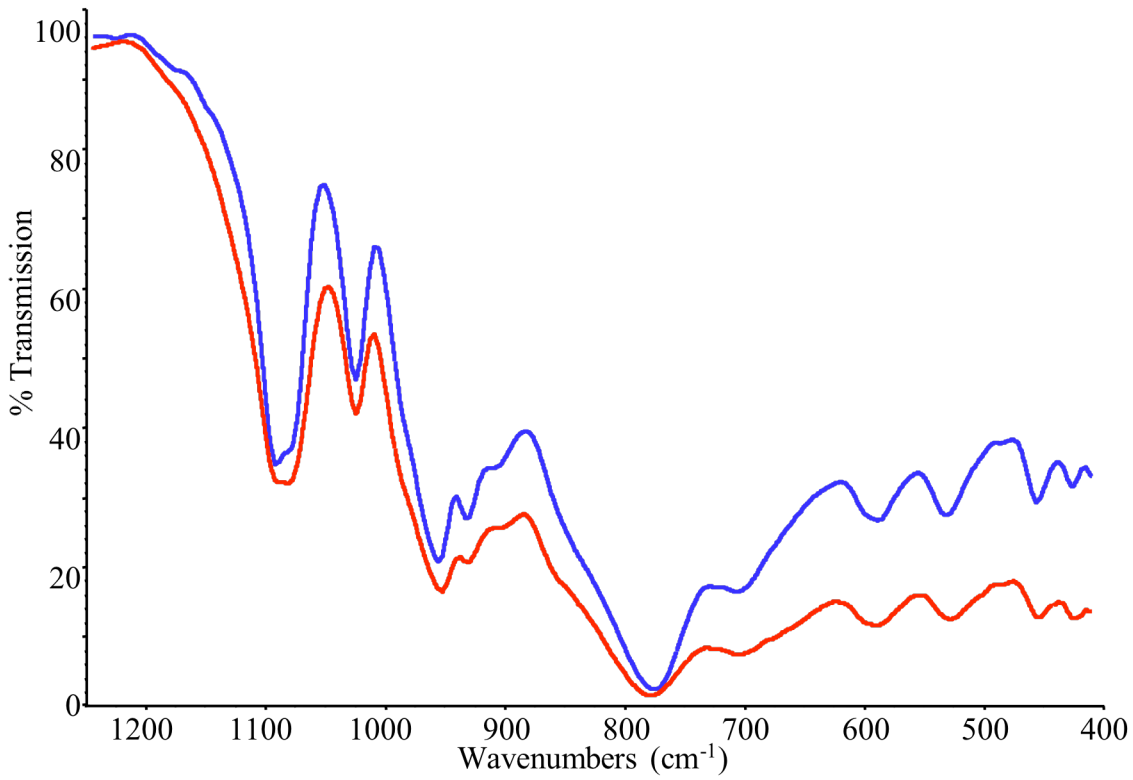

Figure S3. FT-IR spectra of {O=PdPhSnP_2W_{19}} in red and {PdPhSnP_2W_{19}} in blue.